Tissue-to-Analysis Framework Enables Multiscale Mapping of the Architectural and Cellular Organization in the Human Dorsal Root Ganglion

Matthew Adam Hunt[1]*, Sven David Arvidsson[1]*, Gustaf Wängberg[1]*, Zhening Zhang[1], Zerina Kurtović[1], Emerson Krock[2], Lisbet Haglund[3], Camilla I Svensson[1#]

[1]Department of Physiology and Pharmacology, Centre for Molecular Medicine, Karolinska Institutet, Stockholm, Sweden,

[2]Faculty of Dental Medicine and Oral Health Sciences, Alan Edwards Centre for Research on Pain, McGill University, Montreal, QC, Canada,

[3]Division of Orthopaedic Surgery, Department of Surgery, McGill University, Montreal, QC, Canada,

*contributed equally to this manuscript.

[#]Corresponding author: Address: Biomedicum 5B, Karolinska Institutet, Solnavagen 9, 17165 Solna, Sweden. Tel.: +1 46 8 524 87948. E-mail address: camilla.svensson@ki.se (C. I. Svensson)

Introduction

The dorsal root ganglia (DRG) house the cell bodies of the primary sensory neurons responsible for signaling pain, touch, temperature, and itch from the periphery to the central nervous system. Dysfunction of the DRG is considered a major contributor to chronic pain and sensory disorders. Despite its critical role, direct investigation of human DRG (hDRG) biology has historically been limited by access to tissue and technical challenges. Foundational insights into somatosensory neuron diversity emerged from electrophysiological and anatomical studies that characterized A-beta, A-delta and C-fibers[1–3] and later studies that identified their relationship with neuronal soma size[4,5]. Advances in single-cell (sc) and single-nucleus (sn) RNA sequencing (RNAseq) have refined this framework, identifying between 13-22 transcriptionally distinct sensory neuron subtypes in rodent and human DRGs[6–12]. These transcriptomic atlases have transformed our understanding of sensory neuron diversity and provided an essential molecular foundation/resource for the field.

However, transcriptomic identity alone is insufficient to fully capture the functional and organizational complexity of the hDRG. While neuronal subtypes in rodent models display discrete and mutually exclusive expression of canonical markers[13], those in the hDRG exhibit a broader expression profile[8,14–16]. Moreover, relationships between molecular identity, soma size, and spatial organization are less clearly defined in hDRGs[6,7,10,17], making direct translation of animal models to the human system challenging.

In parallel, nociception is shaped not only by neurons, but also the environmental niche of the DRG and complex interactions with surrounding cell types. The DRG is highly vascularized[18,19] and contains a diverse population of satellite glial cells (SGC), immune cells, endothelial cells and stromal cells[9,18,20–23] that can act on neuronal somata. Rodent studies have shown that SGCs[24–26] and macrophages[27–31] can modulate neuronal excitability and pain-like behaviors. And recent studies using hDRGs have further revealed distinct species-specific differences in immune organization, including the presence of CX3CR1-expressing perineuronal macrophages that are largely absent in rodents[18,21]. Despite their abundance and strategic localization, systematic protein-level and spatial characterization of non-neuronal cell populations in hDRG remains limited.

A major barrier to progress is the lack of standardized methodologies for protein-level and spatial analysis of hDRG tissue. Most hDRG samples are obtained post-mortem from organ donors, often without clinical pre-selection, and exhibit substantial biological and technical variability. Tissue quality and antigen preservation are highly sensitive to collection, fixation and processing protocols[32–35]. Donor-to-donor variability has hindered the development of high-throughput technologies for analyzing neuronal populations and the cytoarchitecture of the hDRG. Given these obstacles, cell-to-cell interactions risk being overlooked, marker based functional interpretations become muddied and reproducibility of antibody-based studies remain limited.

Here, we address this gap by establishing a comprehensive resource for immuno-staining and imaging-based spatial analysis of the hDRG. We systematically evaluate how commonly used tissue processing and fixation strategies affect tissue integrity and immuno-staining interpretability. We perform large-scale screening and validation of antibodies targeting neuronal and non-neuronal cell types, providing practical guidance on marker reliability and protocol sensitivity. To enable quantitative and scalable analysis, we developed deep-learning image-analysis workflows that integrate automated segmentation and morphological/spatial analyses that are robust to donor and technical variability. Together, this work provides a robust and accessible foundation for reproducible studies of hDRG biology and enables deeper integration of molecular atlases with spatial and functional investigations relevant to pain and sensory disorders.

Results

Tissue quality and immunohistochemistry optimization of the hDRG:

The lack of standardized tissue-processing guidelines and antibodies validated on post-mortem hDRG tissue represents a major obstacle for reproducible immunohistochemistry (IHC). To aid the community, we first compiled a list of published antibodies targeting 72 proteins said to work on hDRG tissue (Supplementary Table 1). Leveraging cell-type specific expression patterns from single-nucleus and single-cell RNAseq datasets expanded the list to 114 candidate antibodies (Supplementary Table 2-4).

Effects of tissue processing on neuronal morphology

We evaluated the impact of tissue processing methods on hDRG morphology and antigen preservation. Post-mortem hDRGs were either immediately fixed in 4% PFA (iFix; donors 1-11), immediately frozen and subsequently fixed in 4% PFA (iFr-F; donors 1-6, and 12-16) or cryosectioned directly from immediately frozen and fixed on the slide (iFr-Fos; donors 12-17) (Fig. 1a, Supplementary Table 5). Both iFix and iFr-F protocols were cryoprotected in 30% sucrose prior to embedding, while iFr-Fos were not. Across samples, neuronal soma frequently appeared distorted relative to surrounding tissue, consistent with differential contraction or expansion during processing, resulting in apparent "shrunken" neuronal somata surrounded by tissue voids. To objectively evaluate preservation of neuronal morphology, we defined the Tissue Quality Index (TQI) as the fraction of observed neuronal soma area relative to the expected, where expected was the soma plus adjacent voids. Neuronal somata were identified via NF200 staining together with DAPI to visualize surrounding nuclei and tissue architecture (Fig. 1b-c). iFr-Fos samples showed a markedly reduced TQI (0.73±0.13), indicating substantial loss of tissue integrity. In contrast, both iFix and iFr-F protocols preserved neuronal morphology more effectively, with iFix samples exhibiting the highest TQI (0.97±0.02) and significantly higher precision than iFr-F TQI (0.93±0.04, Fig. 1b-c). These data indicate that cryoprotection is essential for preserving hDRG neuronal architecture, and that immediate fixation provides the most consistent tissue integrity.

Fixation duration differentially affects epitope preservation

While immediate fixation is commonly recommended to preserve ultrastructure and minimize protein diffusion[33,36], prolonged fixation can compromise epitope accessibility and limit downstream applications[32,35,37,38]. We assessed the impact of fixation duration on sensitive epitopes (FASN, CD31, PLVAP, CX3CR1) by staining quartered iF-Fr hDRGs from a single donor fixed for 2 or 8 hours (donor 14). CX3CR1 and FASN staining were largely unaffected by fixation duration, whereas CD31 signal intensity was reduced by longer fixation even though signal-to-noise ratio remained similar. In contrast, PLVAP staining showed a clear reduction in signal-to-noise ratio after prolonged fixation (Extended Data Fig. 1a-b). Based on these observations, we adopted a fixation of 3 hours for quartered iFr-F samples and 8–12 hours for iFix to account for larger tissue volumes and ensure adequate penetration. This window also accommodated variation in post-mortem collection timing, which contributed to potential inter-sample variability.

Fixation-dependent antibody performance

To directly compare IHC performance between fixation strategies, paired iFix and iFr-F hDRGs from the same donors were processed on the same slides and stained in parallel (Fig. 1d-f). Among the 114 antibodies screened, 12 exhibited fixation-dependent differences (Supplementary Table 2). While pan-macrophage marker IBA1 showed minor differences in perinuclear staining, cell specificity was preserved across protocols (Extended Data Fig. 1c). PGP 9.5, PVALB, and FABP7 antibodies all exhibited markedly lower signal -to-noise ratios in iFr-F tissue (Fig. 1d), to the point where FABP7 completely lost any recognizable SGC specificity, which was confirmed using a second validated FABP7 antibody (Extended Data Fig. 1d). Antibodies against nuclear and membrane-associated markers

(ATF3, PLVAP, CD31, FOLR2, CX3CR1, PIRT, and KCNA2) showed consistently superior performance in iFr-F samples, whereas staining in iFix samples remained cell specific but exhibited lower signal-to-noise ratios (Fig. 1e and Extended Data Fig. 1e). Of note, fixation-sensitive CD31 staining was restricted to a single antibody clone (AF806).

Five fixation-sensitive markers (ATF3, PLVAP, CLDN5, FOLR2, and CX3CR1) were further evaluated by three blinded investigators using a 0-100 scoring scale in paired samples from six donors. Following our initial observations, all antibodies consistently scored higher in iFr-F samples (Fig. 1f).

Limited utility of signal amplification for low-affinity targets

We next assessed whether tyramide signal amplification (TSA) could rescue staining for antibodies with low signal to noise ratio independent of fixation, including TRPM8 (NBP1-97311SS) and CHRNA3 (15183), or high variability including PGP9.5 (RBK064-05) and FASN (ab128870). TSA substantially increased signal to noise ratio and staining quality for FASN but did not improve specificity for PGP9.5 or enhance staining quality for low-signal antibodies (Supplementary Fig. 1). These results indicate that, for the antibodies tested here, TSA cannot compensate for freezing-induced epitope loss or intrinsically weak antibody performance.

Quenching neuronal autofluorescence

Lipofuscin, an age-associated aggregate of lipids and protein, frequently exhibits a punctate autofluorescent pattern within neuronal somata[39]. Lipofuscin's broad emission spectrum can obscure or confound detection of neuronal and perineuronal markers[40,41]. Reducing lipofuscin autofluorescence is therefore advantageous. We compared an ethanol-based Sudan Black B (SBB) pretreatment with a water-soluble TrueBlack Plus post-treatment. Both approaches effectively attenuated lipofuscin autofluorescence while preserving the signal to noise ratios (Fig. 1g). However, SBB frequently formed insoluble aggregates that persisted after washing and produced artifactual voids (Fig. 1g), additionally its ethanol-based formulation was incompatible with TSA protocols. TrueBlack Plus provided superior performance and was therefore used for all subsequent analyses when required.

Neuronal protein expression in the hDRG extend beyond transcriptomic predictions

Using the optimized IHC workflow described above, we examined how neuronal protein expression compares to published scRNAseq expression (Fig 2). Neuronal subpopulations, clustered via integration of publicly available hDRG RNAseq datasets[8,10], were classified via shared gene expression profiles across datasets, and annotated to match the hDRG atlas[9]. Among 47 antibodies predicted to label neurons, 29 (24 markers) produced neuron-specific staining patterns (Supplementary Table 2). Protein signal for 20 neuronal markers was quantified using one full section each. All neurons were manually classified as negative, detectable, or bright and compared with RNA expression.

Proteins reported as broadly expressed across sensory neurons, PGP9.5 and NF200, had proportions of positive neurons consistent with detectable RNA (Fig. 2b). In contrast, β3-tubulin (TUBB3) displayed a higher proportion of detectable neurons than was reported via RNA expression, nonetheless neurons expressing these pan-neuronal marker associated genes were present in all RNAseq subpopulations (Fig. 2b and Extended Data Fig. 2). Genes encoding proteins highly enriched in human nociceptors[16,42–45], such as TrkA, Substance P, CGRP and Nav1.8, exhibited RNA expression profiles more similar to detectable protein than high expressors. Most additional evaluated subset markers had a broader neuronal protein distribution than suggested by RNAseq data, where transcriptomic prevalence matched the percentage of neurons exhibiting high expression rather than detectable levels (Fig. 2c). These results indicate broad protein expression in human neurons, and that RNA-defined populations correspond preferentially to high-level protein expressors.

hDRG organized into laminar neuron rich islands

During qualitative inspection of hDRGs we observed a striking laminar structural organization of alternating neuron-rich and fiber-rich regions, which extended radially inward from the capsule. This organization was particularly

evident following optical clearing of a quartered hDRG and light-sheet imaging, which revealed repeated neuronal strata separated by thick axonal bundles (Fig. 3a-b). While some studies have described neuronal/fiber density[46] in the hDRG to our knowledge, this, laminar, radial stratification has not been previously described in hDRG.

hDRG neurons exhibit sex dependent differences in size

We developed ensemble deep learning models trained to identify neuronal soma (Methods and Extended Data Fig. 3a-d). Using this, we analyzed the morphology and spatial organization of 35,721 neurons in 4 multi-marker antibody panels across 15 donors (Fig. 3c). Showcasing this high density in neuron-rich islands, the average nearest-neighbor distance was 33.7 µm (Extended Data Fig. 4a), less than the average neuronal diameter of 51.2 µm inferred from maximum Ferret diameter, a measure invariant to shrinkage artifacts. Neuronal soma size varied significantly between donors. Surprisingly, sex explained 50.4% of the between-donor variance, with females having significantly larger neurons. (Fig. 3d). This sex difference scaled exponentially with neuron size percentiles, with no significant difference among small neurons but significant differences in both mid-sized and large neurons (Fig. 3e-f). This remained significant even when accounting for donor age, weight and height, as well as fixation protocol, indicating that sex dependent differences were not driven by confounders. While examining the size of neurons, we noticed that similar sized neurons seemingly clustered together. Quantitative analysis confirmed significant clustering of donor-normalized small, medium, and large neurons across all donors (Fig. 3g-h).

Consistent with our initial analyses, pan-neuronal markers TUBB3, NF200 and peripherin were detectable in most neurons, while NeuN labeled a small subset (Extended Data Fig. 4b). Additionally, we observed that neuronal subset defining proteins CGRP, TrkC, TRPA1, TRPV1, and CHRNA3 were detectable broadly across neurons (Fig. 4). For each marker/panel, the proportion of neurons is shown as detectable and high expressors (++). For additional quantifications, neurons were classified as high expressors (++) or low expressors (low) defined as not a high expressor. For each panel, combinations of high vs low expressors were displayed in Venn diagrams, bar plots displaying donor-normalized neuron diameter, and relative distance plots.

Relationship between neuronal subtypes and soma size

TrkC and CGRP (Fig. 4a-c), enriched in A-fibers and peptidergic nociceptors, revealed TrkC^{++} neurons were larger than CGRP^{++} neurons and TrkC^{++} CGRP^{Low} neurons were significantly larger than CGRP^{++} neurons. TrkC^{++} CGRP^{++}, putative A-fiber nociceptors, had a soma size close to the population mean for each donor.

TUBB3 and TRPA1 were co-expressed in ~70% of high-expressing neurons (Fig. 4d-f). TUBB3^{low} and TRPA1^{low} neurons were smaller, consistent with reduced *TUBB3* expression reported in C-LTMR neurons[47]. In our integrated sequencing data, TUBB3 displayed low expression in C-LTMR as well as other small-soma populations such as C-NP populations (Extended Data Fig. 2). However, in contrast to sequencing data, TRPA1 very high expressors (+++) were significantly larger, highlighting the importance of protein expression characterization in neuronal subsets (Extended Data Fig. 4c).

While ATF3^{++} neurons were more prevalent than previously reported[8–10,48], NF200^{++} neurons were significantly larger than NF200^{low}neurons, as previously reported[10,44,49], which was independent of ATF3 expression (Fig. 4g-i).

Nociceptor-enriched markers showed co-expression in peripherin and TRPV1, and between TRPV1 and CHRNA3, the nicotinic acetylcholine receptor subunit associated with "silent" nociceptors [50] (Fig. 4j). Triple high expressors PRPH^{++}TRPV1^{++}CHRNA3^{++} accounted for 32.3% of quantified neurons. Donor-normalized analyses revealed systematic soma size biases. Peripherin^{++} neurons were significantly smaller than both TRPV1^{++} and CHRNA3^{++} neurons. Across single-marker comparisons, peripherin^{++} neurons were smaller than peripherin^{low} neurons, whereas CHRNA3^{++} neurons were substantially larger than CHRNA3^{low} neurons (Fig. 4j-l). Further classification of peripherin into very high expressors strengthened the relationship between peripherin^{+++} and smaller soma (Extended Data Fig. 4d). While the association of peripherin and TRPV1 with smaller neurons is consistent with prior human and rodent studies[14,44,49,51–54], the enrichment of CHRNA3 protein in larger neurons contrasts with previous publications[9,50].

Noteworthy, differences in neuronal size populations were only apparent after donor normalization and there was not a clear cut for neuronal size for the neuronal populations analyzed (Extended Data Fig. 4e-i). Together, these data demonstrate that neuronal populations exhibit most of the generalized size associations typically observed in animal work, but only when normalizing size to each hDRG.In addition, individual neuronal subtypes also exhibited significant sex-dependent differences in size and abundance (Extended Data Fig. 5).

Molecularly defined neuronal subpopulations exhibit robust spatial clustering

Further clustering evaluation of molecularly defined populations revealed a significant clustering in every subpopulation examined across the four marker panels. Whether defined by low, high, or very high expression levels; whether comprising abundant or sparse populations; and regardless of combinatorial complexity (Fig. 4l). This universal clustering, observed across all classifications tested, demonstrates that spatial organization is a fundamental architectural principle of the hDRG. This is to our knowledge, the first donor level proof of widespread, organized self-clustering of neuron subtypes within the neuron rich islands in the hDRG.

Cell populations form a complex niche in the neuronal islands of the human DRG

The neuron-islands of the hDRG contain a diverse population of non-neuronal cells. While previous studies have shown the presence of glial, immune, vascular, and stromal cells, their spatial organization and proximity to neuronal somata have not been systematically mapped. To address this, we performed a marker-based analysis of major non-neuronal cell populations in the hDRG. Antibody specificity was validated based on expected staining patterns and concordance with published scRNAseq datasets (Fig. 5a, Extended Data Fig. 6). Out of the 68 antibodies tested, 46 displayed their expected specific patterns (Supplementary Table 3).

The hDRG is extensively vascularized as shown with the pan endothelial marker CD31(Fig. 5b). CLDN5^{+} arterioles were primarily observed in the inter-neuron-island regions that transitioned into permeable PLVAP^{+} capillaries and venules in the neuron-island regions[18,55]. PLVAP^{+} vessels were frequently positioned close to neuronal somata, coinciding with absence of CLDN5 expression, indicating spatial organization of vascular permeability. CD34 is present in both endothelial cells and fibroblasts but showed stronger endothelial staining in the hDRG. Mural vascular smooth muscle cells were identified around larger venous and arterial vessels with ACTA2.

Fibroblast markers showed variable specificity across cell types (Fig. 5c). GLUT-1 showed high fibroblasts specificity, while NGFR was found as well in a subpopulation of neurons. Vimentin also detected glial cells (Extended Data Fig. 7a), and EGFR was broadly expressed across fibroblast populations, but with occasional low-level neuronal signal.

We validated 11 antibodies, labelling the following 8 glial cell markers (Fig. 5d). SGCs: FASN, FABP7, Connexin 43, and Kir4.1; myelinating Schwann cells: myelin basic protein (MBP); Schwann cells and SGCs: S100beta and SOX10. Additionally, GFAP labeled a subset of SGCs, but also stained SOX10^{-} fibroblast-like cells (Extended Data Fig. 7a).

Macrophages were the most abundant immune cell type in the hDRG, identified by broad-macrophage markers, IBA1, CD68, FCGR2A, and HvLA-DR (Fig. 5f, Extended Data Fig. 6f). Subset specific markers showed CX3CR1^{+} macrophages intertwined with SGCs and closely associated with neuronal somata, while CD163^{+} macrophages distributed more broadly (Fig. 5f). CD163^{High} macrophages further subdivided into CD163^{high}MRC1^{-} and CD163^{high}MRC1^{+} populations with the latter further containing a subset of FOLR2^{+} macrophages. Finally, an additional population of hDRG macrophages expressing KI67 were observed, indicating recent division, with elevated CX3CR1 expression (Extended Data Fig. 6e-f).

CD3^{+} T-cells were the 2nd largest immune cell population and were dispersed throughout the hDRG, with occasional perineuronal clusters (Fig. 5g). Neutrophils identified by neutrophil elastase (NE) and CD15 antibodies were primarily localized to vascular compartments but were abundant in the DRG parenchyma in some samples (Extended Data Fig. 7b). Additional, less abundant, immune cell populations were identified with markers: CD19 (B cells), S100A4 (enriched in hDRG monocytes), and FcER1/KIT (mast cells). Noteworthy, clusters of immune cells

were occasionally observed near the ganglion capsule (Extended Data Fig. 7c). Together, these data provide a protein-level map of non-neuronal cell populations in the hDRG.

Rich vascular architecture in neuron-rich regions

To characterize the cellular microenvironment of the hDRG, we first focused on the vasculature. The density of vascularization in hDRG was drastically increased in the neuron-island regions, to the point where it appeared as every neuron has its own associated blood vessel. In iFr-F samples we used CD31 to identify all blood vessels and PLVAP to identify fenestrated blood vessels (Fig. 6a). The volume of PLVAP$^+$ vessels in the neuron-island rich regions was 7 times greater than PLVAP$^-$ vessels (Fig. 6b). Identifying all neurons and quantifying each neuron's distance to the nearest PLVAP+ or PLVAP- vessel revealed the average distance from any neuron to a PLVAP$^+$ vessel was only 2.23 µm, which was significantly less than the average distance to PLVAP$^-$ vessels or even the average neuron to nearest neuron distance (Fig. 6c).

The onion layer algorithm, a novel method to classify perineuronal cells

When looking at hDRG neurons and the surrounding cells, it was readily apparent that the size and morphology of nuclei surrounding the neurons appeared concentrically stratified. Thus, we developed the "onion layer" algorithm, which automatically classifies objects in concentric zones radiating outward from neuronal surfaces (see Methods, Fig. 7a, Extended Data Fig. 8). While layer identification is independent of distance, they nonetheless correlate in overlapping distributions (Fig. 7b).

Expanded nuclear volume of supporting cells close to neuronal soma

Nuclear volume showed progressive expansion approaching neurons, with layer 1 nuclei measuring 134.5 µm^3 compared to 86.2 µm^3 in layer 7+ (Fig. 7c). This may reflect increased transcriptional activity in cells directly supporting neurons, as larger nuclei typically correlate with decondensed chromatin and higher gene expression[56–58]. To delve further into the perineuronal niche, we stained hDRGs for SOX10, FASN, IBA1 and DAPI. Interestingly, the size gradient was observed in the nuclei of both IBA1$^+$ and SOX10$^+$ cells and each contained a "large nuclei" subset in layer 1 (Extended Data Fig. 9a). IBA1$^+$ nuclei, located closer to neurons (Extended Data Fig. 9b), were significantly smaller than same layer SOX10$^+$ nuclei and more elongated (Extended Data Fig. 9c). SOX10$^+$ and Iba1$^+$ nuclei were significantly enriched in layers closest to the neuronal soma and displayed a remarkably consistent ratio of 4-fold greater SOX10$^+$ cells per layer. This suggests active regulation of cell type composition in the perineuronal space, rather than stochastic distribution (Fig. 7d).

Macrophages play dynamic role in neuronal soma coverage

Macrophage displayed complex cellular morphologies and were highly entangled with SGCs near the neuronal soma (Fig. 7e-f). To investigate neuronal coverage, we combined models trained to identify and segment the 3D cellular morphology of FASN$^+$ SGCs, and IBA1$^+$ macrophages, with models trained to identify neuronal somata. We quantified coverage of neurons 1, 5 and 10µm from the neuronal soma as it correlated to onion layers 1, 2, and 3-4 respectively. At 1, 5 and 10 µm SGC coverage was 57.2%, 58.6%, and 56.0% respectively, while macrophages covered the remaining 42.8%, 41.3%, and 44.0% (Fig. 7g). Since the ratio of SGCs/macrophage nuclei remained constant, shifts in neuronal-coverage ratios would thus imply morphological remodeling likely driven by macrophages.

When comparing the coverage ratio of 1µm to 10µm for individual neurons, almost all within-donor neurons showed consistent increasing or decreasing coverage directionality (Fig. 7h). Within donor-neurons were sampled across multiple neuron-islands, suggesting that peri-neuronal macrophage organization is either driven by hDRG parenchymal/systemic cues rather than neuron specific signals, or reflects a common intrinsic neuronal state throughout the entire hDRG.

CX3CR1⁺ macrophages form highly interconnected networks surrounding neuronal somata

To further investigate macrophage heterogeneity in the hDRG we stained IBA1, CD163, CX3CR1 and DAPI and observed pronounced inter-donor differences in macrophage quantity and morphology (Fig. 7i). On average, 66% of hDRG macrophages were CD163⁺, which closely resembled data we previously published in mouse[18], and an average of 30% of macrophages were CX3CR1⁺ (Fig. 7j-k). The average distance of CX3CR1⁺ macrophages to neuronal somata was significantly lower than CD163⁺ macrophages, indicating they are the subset intertwined with SGCs surrounding neurons (Fig. 7l). Finally, we noticed that the macrophages on the surface of neurons often formed a net-like structure and connected with one another. To quantify this, we created a connectivity index, where all Iba1 positive signal was segmented by connected components and the number of nuclei for each object became the connectivity number. Individual macrophages were then awarded the connectivity number of the object cluster they came from. CX3CR1⁺ macrophages showed significantly higher connectivity than CD163⁺ macrophages (Fig. 7m).

Proliferating cells in the hDRG are predominantly immediately adjacent to neurons.

Ki67 was stained to identify dividing cells along with SOX10, Iba1 and DAPI to indicate cell type. Ki67⁺ cells showed strong spatial clustering near neurons (Fig. 7n-o), with proliferation significantly enriched in the first layer. Although this is partially explained by higher cell abundance in inner layers, the ratio of dividing cells is significantly higher in layer 1 compared to layer 2 and 7+ respectively (Extended Data Fig. 9d). The majority of Ki67⁺ cells were predominantly IBA1⁺ and layer 1 macrophages constitute 84% of classified proliferative activity, which is striking as SOX10⁺ cells are 4-fold more abundant. There were SOX10⁺Ki67⁺ cells as well, which were also significantly enriched in layer 1 (Fig. 7p).

Perineuronal macrophage proliferation increases with age

Ki67⁺ cell abundance was strongly correlated with donor's age in layer 1 macrophages, but not in SGCs. This relationship in layer 1 macrophages was well described by a Gompertz function (R^2=0.71 which models cumulative, saturable processes common in aging biology[59,60] (Fig. 7q). The exponential nature of the response is consistent with age-associated changes in macrophage turnover that may reflect altered functional states[61].

Discussion

Human DRGs exhibited substantial donor-to-donor variability across multiple structural and molecular parameters, reflecting a combination of biological heterogeneity and technical factors related to tissue collection, handling, and processing that are inherent to post-mortem human tissue. By systematically evaluating these variables, we identified cryoprotection as a critical determinant of neuronal ultrastructural preservation. On this basis, we propose the Tissue Quality Index as a practical quality-control metric for future studies, with samples scoring below 0.9 warranting cautious interpretation. In addition, our results highlight the need to consider signal diffusion in snap frozen tissues, potentially driven by protein redistribution[33,36] as well as epitope loss and fixation induced artifacts when designing and interpreting immunohistochemical analyses of hDRG.

After accounting for technical sources of variability through donor-normalized analyses, the observation of larger neuronal somata in women provides a potential explanation for previously reported sex-dependent differences in human pain processing and may contribute to documented differences in nerve conduction velocities[62–64]. While other anatomical factors may contribute to inter-individual variability; our results highlight the importance of donor-normalized analyses when categorizing hDRG neuronal populations.

Neurons within the ganglion displayed robust spatial clustering based on shared protein-expression profiles and soma size, suggesting that hDRG organization is highly structured rather than stochastic. This organization is consistent with developmental patterning principles previously proposed in transcriptomic studies, suggesting that molecular identity and spatial positioning remain linked in the mature hDRG[7,10,65].

At a higher organizational level, hDRGs are arranged into discrete neuronal islands characterized by dense vascularization, reminiscent of the vascular architecture observed across entire rodent DRGs, including enrichment of permeable microvessels near neurons. This arrangement likely reflects the high metabolic demands of the neuron-SGC-macrophage niche may also create a permissive interface for circulating factors, with potential implications for therapeutic access to the DRG.

Previous studies have identified distinct transcriptional profiles of glial cell and macrophage subpopulations in the hDRG, based on their proximity to neuronal somata[21,23]. Cells in the innermost layer exhibited enlarged nuclei, consistent with increased transcriptional activity associated with direct neuronal support. Macrophages occupying this layer were enriched for CX3CR1, formed interconnected structures and exhibited DRG-wide, coordinated, remodeling/occupancy of the perineuronal space. This suggests the presence of dynamic perineuronal macrophage networks that collectively respond to systemic or tissue-level cues. Such intimate neuron-macrophage interactions have been implicated in pain regulation through mechanisms such as mitochondrial transfer[28,66]. Finally, we observed a strong age-associated increase in proliferation of layer 1 macrophages, indicating increased cellular turnover rather than numerical expansion. This finding may suggest increased metabolic demands and/or decreased perineuronal macrophage function with age. Additionally, macrophage turnover may serve as a quantitative indicator of relative hDRG biological age. Whether chronic pain states or disease-associated conditions further modulate the dynamics of CX3CR1+ perineuronal macrophages remains an important question for future studies.

While derived from a limited number of donors, the organizational principles described here, neuronal clustering, layered perineuronal niches, and vascular specialization, were consistently observed across all samples, supporting their robustness despite inter-individual variability.

By integrating optimized tissue-processing workflows, large-scale antibody benchmarking, quantitative spatial metrics, and deep learning–assisted image analysis, this study establishes a robust and scalable framework for protein-level and spatial interrogation of human DRGs. All analytical pipelines are marker-agnostic and readily adaptable to additional datasets, facilitating reuse across laboratories and future hDRG studies. This resource complements existing transcriptomic atlases by providing spatially resolved protein context and uncovering organizational principles such as neuronal clustering, layered perineuronal niches, and vascular specialization that are not readily accessible through RNA-based approaches alone and provide a scalable reference for future human DRG studies.

Methods

Tissue processing of human dorsal root ganglia.

Human lumbar DRGs (L3-L5) were collected from 16 different organ donors in Canada following consent from the next of kin (Supplementary Table 5, McGill University Health Centre REB2019-4896). At the time of collection whole DRGs were either immediately frozen on dry ice (iFr) or immediately fixed (iFix) in 4% paraformaldehyde (PFA). iFr DRGs were shipped on dry ice and stored at -80°C. When ready for processing, iFr DRGs were quartered, using a 3D printed blade guide (see supplemental material) on dry ice, taking care to not let the samples thaw. Quartered frozen DRGs were either incubated for 3 hours in 4% PFA (iFr-F) or blocked in O.C.T. (Histolab, ref: 45830), cryosectioned and then fixed on the slide for 30 minutes (iFr-Fos). Whole, iFix DRGs were incubated in 4% PFA for 8 hours and shipped in PBS + 0.02% sodium azide at 4°C. Fixation time for iFix hDRGs experienced higher variability due to tissue collection hour. iFix and iFr-F DRGs were cryoprotected in 30% sucrose with 0.02% sodium azide until tissue sunk (3-5 days) at 4°C. Samples were blocked in O.C.T or NEG50 (Epredia, ref: 6502) and stored at -80°C until cryosectioned. We note that NEG50 resulted in superior section quality and consistency. DRGs were sectioned using a CryoStar NX70 cryostat (20-50 μm). Thinner slides (20 μm) were used for initial protein identification and antibody optimization, while 50 mm sections were utilized during analysis of whole tissue fixed samples across donors 1-15.

For donors with both iFix and iFr-F samples, both samples were cryoprotected at the same time and blocked/sectioned together on the same slides.

Immunohistochemistry of hDRG.

We modified IHC treatment for the hDRG using solutions from the iDISCO [64] protocol to improve antibody penetration for 50µm thick sections. Additionally, we add a high salt prewash using 0.1M PBS, which decreases tissue autofluorescence. [64]Tissue sections were thawed at room temperature for 1 hour, then washed twice with 0.1M phosphate-buffered saline (PBS; pH 7.35–7.45 for all PBS solutions (Sigma-Aldrich, ref: P38135) and once with 0.01M PBS for 5 minutes each. Next, sections were incubated at room temperature with a permeabilization solution containing 0.01M PBS, 0.16% Triton X-100 (Sigma-Aldrich cat: X100-100ML), 20% dimethyl sulfoxide (DMSO) (Sigma-Aldrich, cat: D4540-100ML), and 23 g/L glycine (Sigma, cat: G8898-500G) for 30 minutes. Following permeabilization, a blocking solution consisting of 0.01M PBS, 0.2% Triton X-100, 6% normal donkey serum (Millipore, cat: S30-100ML) and 10% DMSO was applied for 1 hour.

Primary antibodies (details provided in Supplementary Table 2) were applied overnight at room temperature in an antibody solution composed of 0.01M PBS, 0.2% Tween-20 (Sigma-Aldrich, cat: P9416-100ML), 10 mg/L heparin (Leo Pharma, ATC-code: B01AB01), 0.02% sodium azide, 5% DMSO, and 3% normal donkey serum. After incubation, slides were washed with a washing solution (0.01M PBS, 0.2% Tween-20, 10 mg/L heparin, and 0.02% sodium azide): a brief 1-minute wash followed by two 5-minute washes.

Tissue sections were then incubated with the appropriate donkey secondary antibodies (Supplementary Table 2). After secondary antibody incubation, sections were washed three times using the washing solution (5 minutes each), followed by incubation with DAPI (Invitrogen, ref: D21490) (1:10,000) for 10 minutes. Additional washes were performed: once with the washing solution for 5 minutes, followed by 0.1M PBS and 0.01M PBS washes. Slides were dried in the dark for 5 minutes and mounted with ProLong Gold Antifade Mountant (Invitrogen, cat: P36934).

Lipofuscin quenching protocols.

Two different lipofuscin quenchers were tested. Sudan Black B (Sigma-Aldrich, ref: 199664-25G) was incubated for 1 hour used at 0.2%, diluted in 70% EtOH, as a pretreatment. True Black Plus (Biotium, ref: 23014) was used as a post-treatment before mounting, applied for 30 min diluted 1:40 in PBS, after which 3 five minutes PBS washes were applied to the samples. All neuronal markers were tested and analyzed with True Black Plus to decrease false positives.

Tyramide signal amplification (TSA).

When the regular protocol did not generate a clear signal, the effect of Tyramide Signal Amplification (TSA) (Akoya Biosciences, Ref: NEL741001KT) was assessed. Slides were allowed to equilibrate at room temperature for 3 hours before being incubated overnight with the primary antibody diluted in 0.01M PBS containing 0.3% Triton X-100. Following primary antibody incubation, slides were washed in TNT buffer (0.05% Tween-20 in 0.1M Tris and 0.15M NaCl, pH 7.4–7.45) for 30 minutes. They were then incubated in TNB buffer (prepared with 0.05 g blocking reagent from the PerkinElmer Life Sciences kit, #NEL741) for 30 minutes, followed by a 30-minute incubation with horseradish peroxidase (HRP)-conjugated secondary antibody (DAKO, HRP Rabbit, 1:200) diluted in TNB buffer. Afterward, slides were washed in TNT buffer for 30 minutes and incubated for 15 minutes with Tyramide-Fluorescein solution (1:100 in Amplification Diluent) that had been centrifuged at 14,000 rpm for 10 minutes at 4°C. This was followed by another 30-minute wash in TNT buffer and three additional 5-minute washes in 0.01M PBS. Slides were

386 then incubated for 1 hour in a blocking solution composed of 0.01M PBS, 0.3% Triton X-100, and 3% normal donkey
387 serum (NDS). For non-amplified targets, primary antibodies were added and incubated overnight in a solution
388 containing 0.1% Triton X-100 and 1% NDS. Primary antibody washes consisted of two 5-minute rinses in 0.01M PBS.
389 Secondary antibodies (1:300 dilution in antibody solution) were applied and incubated for 1.5 hours. Slides were
390 briefly rinsed in PBS, followed by a 10-minute incubation with DAPI (1:10,000). Finally, slides underwent three 5-
391 minute washes in 0.01M PBS before being mounted with ProLong Gold Antifade Mountant.

392 **Data analysis**

393 ***Tissue Quality Index (TQI).***

394 The Tissue Quality Index was defined as the percentage of observed somatic tissue volume relative to the full
395 predicted neuron volume. For iFr-F and iFix samples, full soma volume was estimated using the pan-cytosolic
396 marker NF200 and the DRG-quant pipeline[67]. Due to performance limitations of iFr-Fos predictions, full soma was
397 estimated by manual annotation looking while observing NF200 and DAPI channels. Observed somatic tissue
398 volume was calculated by subtracting shrunken volume from the full volume. A pixel was classified as shrunken if it
399 met two criteria: (1) NF200 signal intensity below 50% of the non-neuron background mean for that sample, and (2)
400 location within a 5-pixel diameter sphere where >50% of pixels met criterion 1.

401 ***Comparison of whole tissue fixation immediately fixed or frozen***

402 To compare fixation protocols, IHC was performed on DRGs from the same donor. One DRG was processed using
403 tissue fixed immediately after DRG collection while the matched DRG was frozen at time of collection. Sections from
404 both samples were mounted on the same slide to ensure comparable conditions. Paired DRGs from 6 donors were
405 used. Representative images of each marker and DAPI were captured with optimized settings for each donor,
406 ensuring identical settings were applied to each pair. The images were exported as TIFF format and blinded for
407 scoring. Three independent researchers evaluated the staining quality based on signal intensity, specificity, and
408 background noise on a 0-100% scale. Representative images shown were selected based on proximity to the average
409 score for each group/ Representative images of paired donor samples were selected to showcase the expected
410 differences for each marker. Statistical significance was assessed with a paired T-test and adjusted for False
411 Discovery Rate using two-stage step-up method of Benjamini, Krieger and Yekutieli.

412 ***Manual quantification of neuronal markers***

413 After confirming antibody human specificity and a visual confirmation of positive staining, we quantify single
414 sections stained for the 20 neuronal proteins. Whole section images of the stained samples were taken with
415 confocal microscopy with an open pinhole (80μm). Neurons were then manually identified with help of the selected
416 markers, background noise, and DAPI signal by an experienced researcher. The neurons were classified in three
417 different categories based on protein expression: Negative neurons had no visual difference with unspecific signal;
418 detectable neurons had enough signal to distinguish them from background staining; and lastly, high expressors
419 were identified after an overview of general neuronal expression, as those with a clear higher expression than the
420 rest of the neurons. For nuclear markers, only neurons with a visible nucleus were quantified, while neuronal
421 selection criteria for non-nuclear proteins included all neurons with clear somata without large coverage of non-
422 neuronal cells.

423 ***RNA sequencing data analysis***

424 Due to the low number of neurons with a single scRNAseq study, and to have a good representation of the different
425 human neuronal subsets, we integrated neuronal scRNAseq studies from all the current hDRG studies on RStudio
426 (R version 4.4.1). Neurons proceeding from single soma RNA sequencing[10] filtered into a Seurat object for genes
427 expressed in at least 3 cells, with a minimum of 200 features per cell. The cells were later filtered for cells with
428 between 4500 and 14000 RNA features, and RNA count of 600000. After normalization, this dataset was then merged

429 with three previously filtered and integrated[8] scRNAseq human studies. To integrate these datasets, previously
430 integrated datasets were re-transformed into human gene symbols using biomaRt in a similar manner as for the
431 original transformation into mouse symbols. All data was normalized based on study, with 2000 variable genes as
432 anchors for integration. The Seurat object was then scaled, and the first 20 PCs were selected (based on elbow Plot)
433 to run the UMAP and find neighbors. The selection of cluster resolution was based on the clustree plugin. The
434 clusters were later compared to the original publications and manually labeled, mapped based on common genes
435 with described populations in the large-scale RNA atlas study of hDRGs[9].

436 To facilitate comparison to protein data, the percentage of neurons expressing more than 0.5 RNA counts was
437 retrieved for the proteins that were manually evaluated for protein expression.

438 For non-neuronal cells, a single dataset was used[20], filtered for RNA features between 600 and 5000, with a count
439 lower than 15000, and mitochondrial percentage under 5%. Data was normalized, integrated between samples,
440 scaled, and the first 24 PCs were used for the UMAP generation. After finding neighbors and identifying cluster
441 resolution, the clusters were identified based on marker genes for each population. Immune cells were then
442 separated, re-normalized, and scaled, with a subplot using the first 15 PCs for UMAP generation and finding
443 neighbors. Cluster resolution was informed with clustree, with marker genes allowing the identification of the main
444 populations of immune cells in the hDRG.

445 For data visualization, the generated UMAPS were plotted using scCustomize package on RStudio.

446 **Image Acquisition**

447 Images were acquired on a Zeiss LSM800 laser-scanning confocal microscope equipped with four lasers (405, 488,
448 561, and 640 nm). Tissue overviews were taken with a 10x air objective. Quantification images were either taken with
449 a 20x air objective, 40x water immersion objective, or 63x oil immersion objective.

450 **iDISCO clearing of hDRG**

451 One hDRG that was glutaraldehyde fixed was quartered as described above. Since the sample was glutaraldehyde
452 fixed it was not stained and followed the strndard iDISCO protocol[68]. In brief, tissue was serially dehydrated with
453 methanol in H2O, 20%, 40%, 60%, 80%,100%,100% for 1 hour each. The sample was then incubated for 3 hours
454 with Dichloromethane (DCM) at room temperature. Followed by two 15-minute washes in 100% DCM. The DRG was
455 then placed in DiBenzyl Ether and imaged with with the LaVision Light Sheet microscope (Biotech, UltraMicroscope
456 II). The extremely high level of autofluorescence from lipofuscin in glutaraldehyde fixed tissue was used to identify
457 neuronal soma and observe the neuron-islands in the hDRG.

458 **Image Analysis**

459 All raw CZI images were processed and run through the DRGquant pipeline[67] to organize, run model prediction, and
460 set up analysis. Any Unet models not described below were trained using yapic, as described in DRGquant. Image
461 analysis was performed on workstations running Ubuntu (linux), with >128GB ram and NVIDIA GPUs (RTX3090 or
462 RTX6000).

463 ***Analysis of neuron-stained panels***

464 Neuron locations were predicted using a two-stage meta-learning ensemble architecture implemented in the
465 MONAI framework (MONAI 1.3.0, PyTorch 2.0.1, Python 3.9.15)[69]. In Stage 1, three channel-specific Attention gated
466 U-Nets were trained independently, with two input channels, each having nuclei stain (DAPI) to ensure nuclei-based
467 information, and one of the 3 IHC based stains to capture cell type specific information. In Stage 2, a meta-learner
468 Attention U-Net received the 4 original channels concatenated with the 3 Stage 1 probability maps (7 channels total)
469 to generate refined predictions by learning optimal integration of the base models.

The Attention U-Net architecture comprised encoder channels (32→64→128 filters) with 2*strided convolution down sampling and 3x3 convolutional kernels, a 256-filter bottleneck, and a symmetric decoder with attention-gated skip connections. Models were trained using the Dice Focal loss function with AdamW optimization (learning rate $2*10^{-4}$, weight decay $1*10^{-5}$) on 352*352-pixel patches with cosine annealing scheduling. Data augmentation included, horizontal/vertical flips, 90° rotations, additive Gaussian noise (σ=0.05), and contrast adjustment ($\gamma \in [0.7, 1.3]$).

Five-fold cross-validation was performed with independent training on each fold. For inference, images were processed with all 5-fold models at 9 spatial offsets (stride/3 grid), generating 45 predictions per pixel. Final masks were created by consensus voting with optimal thresholds determined via cross-validation resulting in a Raw prediction. All Stage 1 models for all panels had a Dice Focal better than 90% while all stage 2 had a Dice Focal better than 95%.

Raw AI predictions were post-processed using ImageJ/Fiji (v1.54p) with CLIJ2 package (v2.5.3.1). Binary predictions underwent morphological refinement and non-disjunct objects separation was done by a size and shape adaptive algorithm based under the assumption of high compactness objects.

Inter-soma hole regions were identified by thresholding each channel at a channel consensus of signal weaker than background-mean/4 (where background was defined as tissue regions outside neurons). Defined hole regions were included in size calculations, while excluded in signal ratio calculations. Neurons with hole ratios ≥0.5 were retained.

Neuron subpopulation classification was done using the same logic as in DRG-quant[67], where expression was related to statistics of the surrounding tissue region. Detectable signal was defined by ~4 times a minimum expected random signal in relation to background (based on neuron size, $>10^{-15}$% chance to happen randomly), high expressors was classified by ~30 times higher and very high expressors ~180 times higher the expected random signal. Data collection from labelled images was done using CLIJ2_statisticsOfLabelledPixels and morphometry metrics was done by 3D ImageJ Suite's 3D Manager.

Inter-neuronal distances were calculated by estimated edge-to-edge measurements. For each neuron pair, edge-to-edge distance was computed as: $d_{edge} = d_{center} - r_1 - r_2$ where d_{center} is the Euclidean distance between centroids, and r_1, r_2 are approximated neuronal radii.

Distance analysis by Cross-type nearest neighbor distance comparison

To assess whether annotated subpopulations exhibit spatial clustering within tissue volumes, we implemented an edge-based cross-type nearest-neighbor comparison approach. For each subpopulation (e.g., A+) within each donor sample, we calculated two metrics: (i) the within-group distance, defined as the mean edge-to-edge Euclidean distance from each A+ object to its three nearest A+ neighbors, averaged across all A+ objects; and (ii) the cross-group distance, defined as the mean edge-to-edge Euclidean distance from each A- object to its three nearest A+ neighbors, averaged across all A- objects. Edge-to-edge distances were calculated by closest Euclidian distance from the estimated object edges. This yielded a single paired measurement per donor: a within-group distance and a cross-group distance for each subpopulation. Spatial clustering is indicated by systematically lower within-group distances compared to cross-group distances, reflecting that objects of the same subpopulation are positioned closer to each other than objects from the complementary population.

Onion layers algorithm for perineuronal nuclear categorization

Nuclei were categorized into concentric layers around individual neurons using the "onion layers algorithm" (Extended Data Fig. 8). For each nucleus, spatial territories were defined via Voronoi tessellation. Layer assignment proceeded iteratively by testing if a nucleus with any Voronoi volume fell within an iteration specific boundary volume. The first boundary was generated by eroding the neuron mask by an estimate of non-neuronal nuclei ($r_{nucleus}$), with subsequent boundaries created by dilating the first boundary volume by $2*r_{nucleus}$ per iteration. Assigned nuclei were excluded from subsequent iterations, and remaining nuclei formed the outermost layer. To reduce unnecessary

computational time, we limited our number of onion layers to 6, where all additional nuclei/cells were classified as 7+.

Onion layers algorithm properties. This approach ensures: mutually exclusive layer assignment (each nucleus assigned to exactly one layer), preservation of spatial relationships through Voronoi territories rather than point distances alone, shape-adaptive boundaries that follow the neuron morphology rather than assuming circular symmetry.

Data availability

The scRNAseq data used in this study are publicly available from previous studies in the Gene Expression Omnibus (GEO), for single soma dataset was available under accession number GSE273557 and previously integrated human dorsal root ganglia datasets can be accessed at https://painseq.shinyapps.io/harmonized_painseq_v1/ . Non-neuronal scRNAseq used can be accessed under accession number GSE169301.

Code availability

Code recourse for the hDRG protein atlas workflow, that is easily adapted with complete documentation is available at: https://github.com/CamillaSvensson/Human-DRG-Protein-Atlas-Workflow. Raw code regarding RNAseq analysis and image analysis for all the panels used is available at https://github.com/CamillaSvensson/Molecular_pain_research.

References

1. Li, C. L. & Bak, A. Excitability characteristics of the A- and C-fibers in a peripheral nerve. *Exp. Neurol.* **50**, 67–79 (1976).
2. Burgess, P. R., Petit, D. & Warren, R. M. Receptor types in cat hairy skin supplied by myelinated fibers. *J. Neurophysiol.* **31**, 833–848 (1968).
3. Adriaensen, H., Gybels, J., Handwerker, H. O. & Van Hees, J. Response properties of thin myelinated (A-δ) fibers in human skin nerves. *J. Neurophysiol.* **49**, (1983).
4. Harper, A. A. & Lawson, S. N. Conduction velocity is related to morphological cell type in rat dorsal root ganglion neurones. *J. Physiol.* **359**, 31–46 (1985).
5. Spencer, P. S., Raine, C. S. & WiśNiewski, H. Axon diameter and myelin thickness—unusual relationships in dorsal root ganglia. *Anat. Rec.* **176**, 225–243 (1973).
6. Tavares-Ferreira, D. *et al.* Spatial transcriptomics of dorsal root ganglia identifies molecular signatures of human nociceptors. *Sci. Transl. Med.* **14**, (2022).
7. Nguyen, M. Q., von Buchholtz, L. J., Reker, A. N., Ryba, N. J. P. & Davidson, S. Single-nucleus transcriptomic analysis of human dorsal root ganglion neurons. *Elife* **10**, (2021).
8. Bhuiyan, S. A. *et al.* Harmonized cross-species cell atlases of trigeminal and dorsal root ganglia. *Sci. Adv.* **10**, (2024).
9. Bhuiyan, S. A. *et al.* A Reference Atlas of the Human Dorsal Root Ganglion. *bioRxiv* 2025.11.05.686654 (2025) doi:10.1101/2025.11.05.686654.
10. Yu, H. *et al.* Leveraging deep single-soma RNA sequencing to explore the neural basis of human somatosensation. *Nature Neuroscience 2024 27:12* **27**, 2326–2340 (2024).
11. Kupari, J. & Ernfors, P. Molecular taxonomy of nociceptors and pruriceptors. *Pain* **164**, 1245 (2023).

12. Jung, M. *et al*. Cross-species transcriptomic atlas of dorsal root ganglia reveals species-specific programs for sensory function. *Nat. Commun.* **14**, (2023).

13. Usoskin, D. *et al*. Unbiased classification of sensory neuron types by large-scale single-cell RNA sequencing. *Nat. Neurosci.* **18**, (2015).

14. Rostock, C., Schrenk-Siemens, K., Pohle, J. & Siemens, J. Human vs. Mouse Nociceptors – Similarities and Differences. *Neuroscience* **387**, (2018).

15. Shiers, S., Klein, R. M. & Price, T. J. Quantitative differences in neuronal subpopulations between mouse and human dorsal root ganglia demonstrated with RNAscope in situ hybridization. *Pain* **161**, (2020).

16. Shiers, S. I. *et al*. Convergence of peptidergic and non-peptidergic protein markers in the human dorsal root ganglion and spinal dorsal horn. *Journal of Comparative Neurology* **529**, (2021).

17. Haberberger, R. V., Barry, C., Dominguez, N. & Matusica, D. Human dorsal root ganglia. *Frontiers in Cellular Neuroscience* vol. 13 Preprint at https://doi.org/10.3389/fncel.2019.00271 (2019).

18. Lund, H. *et al*. CD163+ macrophages monitor enhanced permeability at the blood–dorsal root ganglion barrier. *Journal of Experimental Medicine* **221**, (2024).

19. Jimenez-Andrade, J. M. *et al*. Vascularization of the dorsal root ganglia and peripheral nerve of the mouse: Implications for chemical-induced peripheral sensory neuropathies. *Mol. Pain* **4**, (2008).

20. Avraham, O. *et al*. Profiling the molecular signature of satellite glial cells at the single cell level reveals high similarities between rodents and humans. *Pain* **163**, (2022).

21. Wu, Z. *et al*. Peripheral nervous system microglia-like cells regulate neuronal soma size throughout evolution. *Cell* **188**, 2159-2174.e15 (2025).

22. Boyer, K. *et al*. Single nucleus multiomic atlas of human dorsal root ganglia reveals the contribution of non-neuronal cell types to pain. *bioRxiv* 2025.09.21.677655 (2025) doi:10.1101/2025.09.21.677655.

23. Andreas Ahlgreen, O. *et al*. Mapping Satellite Glial Cell Heterogeneity Reveals Distinct Spatial Organization and Implies Functional Diversity in the Dorsal Root Ganglion. *Advanced Science* **13**, e11569 (2026).

24. Hanani, M. & Spray, D. C. Emerging importance of satellite glia in nervous system function and dysfunction. *Nature Reviews Neuroscience* vol. 21 Preprint at https://doi.org/10.1038/s41583-020-0333-z (2020).

25. Krock, E. *et al*. Fibromyalgia patients with elevated levels of anti-satellite glia cell immunoglobulin G antibodies present with more severe symptoms. *Pain* **164**, (2023).

26. Avraham, O. *et al*. Satellite glial cells promote regenerative growth in sensory neurons. *Nat. Commun.* **11**, (2020).

27. Yu, X. *et al*. Dorsal root ganglion macrophages contribute to both the initiation and persistence of neuropathic pain. *Nature Communications 2020 11:1* **11**, 264- (2020).

28. van der Vlist, M. *et al*. Macrophages transfer mitochondria to sensory neurons to resolve inflammatory pain. *Neuron* **110**, (2022).

29. Feng, R., Saraswathy, V. M., Mokalled, M. H. & Cavalli, V. Self-renewing macrophages in dorsal root ganglia contribute to promote nerve regeneration. *Proc. Natl. Acad. Sci. U. S. A.* **120**, (2023).

30. Oggero, S. *et al*. Dorsal root ganglia CX3CR1 expressing monocytes/macrophages contribute to arthritis pain. *Brain Behav. Immun.* **106**, (2022).

31. Raoof, R. *et al*. Dorsal root ganglia macrophages maintain osteoarthritis pain. *Journal of Neuroscience* **41**, (2021).

32. Lundström, Y., Lundström, P., Popova, S. N., Lindblom, R. P. F. & Alafuzoff, I. Detection of Changes in Immunohistochemical Stains Caused by Postmortem Delay and Fixation Time. *Applied Immunohistochemistry and Molecular Morphology* vol. 27 Preprint at https://doi.org/10.1097/PAI.0000000000000658 (2019).

33. Leduc, A., Xu, Y., Shipkovenska, G., Dou, Z. & Slavov, N. Limiting the impact of protein leakage in single-cell proteomics. *Nature Communications 2025 16:1* **16**, 4169- (2025).

34. Olney, K. C. *et al.* Postmortem Interval Leads to Loss of Disease-Specific Signatures in Brain Tissue. *eNeuro* **12**, (2025).

35. Gallardo-Caballero, M. *et al.* Prolonged fixation and post-mortem delay impede the study of adult neurogenesis in mice. *Communications Biology 2023 6:1* **6**, 978- (2023).

36. Scandella, V., Paolicelli, R. C. & Knobloch, M. A novel protocol to detect green fluorescent protein in unfixed, snap-frozen tissue. *Sci. Rep.* **10**, (2020).

37. Wu, X. *et al.* The effect of prolonged formalin fixation on the expression of proteins in human brain tissues. *Acta Histochem.* **124**, (2022).

38. Pikkarainen, M., Martikainen, P. & Alafuzoff, I. The Effect of Prolonged Fixation Time on Immunohistochemical Staining of Common Neurodegenerative Disease Markers. *J. Neuropathol. Exp. Neurol.* **69**, 40–52 (2010).

39. Moreno-García, A., Kun, A., Calero, O., Medina, M. & Calero, M. An overview of the role of lipofuscin in age-related neurodegeneration. *Frontiers in Neuroscience* vol. 12 Preprint at https://doi.org/10.3389/fnins.2018.00464 (2018).

40. Erben, T., Ossig, R., Naim, H. Y. & Schnekenburger, J. What to do with high autofluorescence background in pancreatic tissues – an efficient Sudan black B quenching method for specific immunofluorescence labelling. *Histopathology* **69**, 406–422 (2016).

41. Sapio, M. R. *et al.* Efficient removal of naturally-occurring lipofuscin autofluorescence in human nervous tissue using high-intensity white light. *J. Pain* **30**, 105359 (2025).

42. Osteen, J. D. *et al.* Pharmacology and Mechanism of Action of Suzetrigine, a Potent and Selective NaV1.8 Pain Signal Inhibitor for the Treatment of Moderate to Severe Pain. *Pain Ther.* **14**, 655–674 (2025).

43. Vega, J. A. *et al.* Immunohistochemical localization of the high-affinity NGF receptor (gp 140-trkA) in the adult human dorsal root and sympathetic ganglia and in the nerves and sensory corpuscles supplying digital skin. *Anat. Rec.* **240**, 579–588 (1994).

44. Holford, L. C., Case, P. & Lawson, S. N. Substance P, neurofilament, peripherin and SSEA4 immunocytochemistry of human dorsal root ganglion neurons obtained from post-mortem tissue: a quantitative morphometric analysis. *J. Neurocytol.* **23**, 577–589 (1994).

45. Landry, M. *et al.* Galanin expression in adult human dorsal root ganglion neurons: Initial observations. *Neuroscience* **117**, 795–809 (2003).

46. Sperry, Z. J., Graham, R. D., Peck-Dimit, N., Lempka, S. F. & Bruns, T. M. Spatial models of cell distribution in human lumbar dorsal root ganglia. *J. Comp. Neurol.* **528**, 1644 (2020).

47. Keeler, A. B. *et al.* A developmental atlas of somatosensory diversification and maturation in the dorsal root ganglia by single-cell mass cytometry. *Nature Neuroscience 2022 25:11* **25**, 1543–1558 (2022).

48. Donovan, L. J. *et al.* Aging and injury drive neuronal senescence in the dorsal root ganglia. *Nature Neuroscience 2025 28:5* **28**, 985–997 (2025).

49. Bae, J. Y., Kim, J. H., Cho, Y. S., Mah, W. & Bae, Y. C. Quantitative analysis of afferents expressing substance P, calcitonin gene-related peptide, isolectin B4, neurofilament 200, and Peripherin in the sensory root of the rat trigeminal ganglion. *J. Comp. Neurol.* **523**, 126–138 (2015).

50. Prato, V. *et al.* Functional and Molecular Characterization of Mechanoinsensitive "Silent" Nociceptors. *Cell Rep.* **21**, 3102–3115 (2017).

51. Kobayashi, K. *et al.* Distinct expression of TRPM8, TRPA1, and TRPV1 mRNAs in rat primary afferent neurons with aδ/c-fibers and colocalization with trk receptors. *Journal of Comparative Neurology* **493**, 596–606 (2005).

52. Kudo, M., Wupuer, S., Kubota, S. & Seki, K. Distribution of Large and Small Dorsal Root Ganglion Neurons in Common Marmosets. *Front. Syst. Neurosci.* **15**, 801492 (2021).

53. Caterina, M. J. *et al.* The capsaicin receptor: a heat-activated ion channel in the pain pathway. *Nature 1997 389:6653* **389**, 816–824 (1997).

54. Tominaga, M. *et al.* The cloned capsaicin receptor integrates multiple pain-producing stimuli. *Neuron* **21**, 531–543 (1998).

55. Pigatto, G. R. *et al.* GM-CSF instructs vertebral emergency myelopoiesis in neuropathic pain. *bioRxiv* 2025.11.23.690022 (2025) doi:10.1101/2025.11.23.690022.

56. Schmidt, E. E. & Schibler, U. Cell size regulation, a mechanism that controls cellular RNA accumulation: consequences on regulation of the ubiquitous transcription factors Oct1 and NF-Y and the liver-enriched transcription factor DBP. *J. Cell Biol.* **128**, 467–483 (1995).

57. Wu, C. Y., Alexander Rolfe, P., Gifford, D. K. & Fink, G. R. Control of Transcription by Cell Size. *PLoS Biol.* **8**, e1000523 (2010).

58. Jorgensen, P. *et al.* The size of the nucleus increases as yeast cells grow. *Mol. Biol. Cell* **18**, 3523–3532 (2007).

59. Nielsen, P. Y., Jensen, M. K., Mitarai, N. & Bhatt, S. The Gompertz Law emerges naturally from the inter-dependencies between sub-components in complex organisms. *Scientific Reports 2024 14:1* **14**, 1196- (2024).

60. Karin, O., Agrawal, A., Porat, Z., Krizhanovsky, V. & Alon, U. Senescent cell turnover slows with age providing an explanation for the Gompertz law. *Nature Communications 2019 10:1* **10**, 5495- (2019).

61. Yamamoto, T. *et al.* Macrophage immunosenescence prolongs intraocular inflammation in aged mice via impaired induction of regulatory T cells. *bioRxiv* 2026.01.15.697975 (2026) doi:10.64898/2026.01.15.697975.

62. Ray, P. R. *et al.* RNA profiling of human dorsal root ganglia reveals sex differences in mechanisms promoting neuropathic pain. *Brain* **146**, (2023).

63. Barry, A. M. *et al.* Multi-omic integration with human DRG proteomics highlights TNFα signalling as a relevant sexually dimorphic pathway. *bioRxiv* 2024.12.06.626968 (2025) doi:10.1101/2024.12.06.626968.

64. Hodzelmans, J. J. A. *et al.* Reference values for nerve conduction studies of the peroneal, tibial, and sural nerve derived from a large population-based cohort: Associations with demographic and anthropometric characteristics—The Maastricht study. *Muscle Nerve* **69**, 588–596 (2024).

65. Krauter, D. *et al.* Spatial organization, chromatin accessibility and gene-regulatory programs defining mouse sensory neurons. *Communications Biology 2025 8:1* **8**, 908- (2025).

66. Xu, J. *et al.* Mitochondrial transfer from glia to neurons protects against peripheral neuropathy. *Nature 2026* 1–10 (2026) doi:10.1038/s41586-025-09896-x.

67. Hunt, M. A. *et al.* DRGquant: A new modular AI-based pipeline for 3D analysis of the DRG. *J. Neurosci. Methods* **371**, (2022).

68. Renier, N. *et al*. IDISCO: A simple, rapid method to immunolabel large tissue samples for volume imaging. *Cell* **159**, (2014).

69. Consortium, M. MONAI: Medical Open Network for AI. Preprint at https://doi.org/10.5281/zenodo.17179097 (2025).

Acknowledgements

We would thank the McGill Scoliosis and Spine team for providing the hDRGs.

Funding

This work was supported by the Swedish Research Council (2023-02139, CIS), the Knut and Alice Wallenberg Foundation (CIS), the European Research Council (ERC) under the European Union's Horizon 2020 research and innovation programme under the grant agreement no. 866075 (CIS), the Swedish Society for Medicine (MAH), the KI Foundation Grants for doctoral studies (SDA, ZZ), the Canada Foundation for Innovation and the Canada Research Chairs program (EK).

Author information

Authors affiliations

Department of Physiology and Pharmacology, Karolinska Institutet, Stockholm, Sweden

Matthew Adam Hunt, Sven David Arvidsson, Gustaf Wängberg, Zhening Zhang, Zerina Kurtovic, Camilla I Svensson

Faculty of Dental Medicine and Oral Health Sciences, Alan Edwards Centre for Research on Pain, McGill University, Montreal, QC, Canada

Emerson Krock

Division of Orthopaedic Surgery, Department of Surgery, McGill University, Montreal, QC, Canada

Lisbet Haglund

Contributions

M.H, S.D.A, and C.I.S. conceived the project and designed the experiments. C.I.S. supervised the work. E.K. and L.H. provided the human dorsal root ganglia and controlled for the initial collection protocol. M.H. processed the samples and prepared tissue slides. S.D.A and Z.Z. compiled antibody information and performed immunofluorescence stainings. S.D.A performed confocal imaging, initial evaluation of antibody performance, and neuronal protein manual quantification. Z.Z., Z.K., and E.K. scored the antibody signal. S.D.A. and Z.K. contributed to RNAseq analysis of publicly available data. G.W. developed the novel algorithms and neural network architecture used in this study, performed image analysis, and generated deep learning models for neuronal panels. M.H. and G.W. jointly developed deep learning models and conducted image analysis for non-neuronal panels. G.W. prepared the online analysis resource. M.H., S.D.A., G.W., and C.I.S. wrote the paper with assistance from all authors.

Corresponding author

Correspondence to Camilla I. Svensson

Ethics declaration

Human lumbar DRGs were obtained from organ donors through a collaboration with Transplant Quebec. All procedures were approved by and performed in accordance with the ethical review board at McGill University (McGill University Health Centre REB 2019-4896) and the Swedish Ethics Review Board (ethics permit number 2025-05433). Familial consent was obtained for each subject.

Competing interests

The authors declare no competing interests.

Figures in order of appearance

Fig. 1

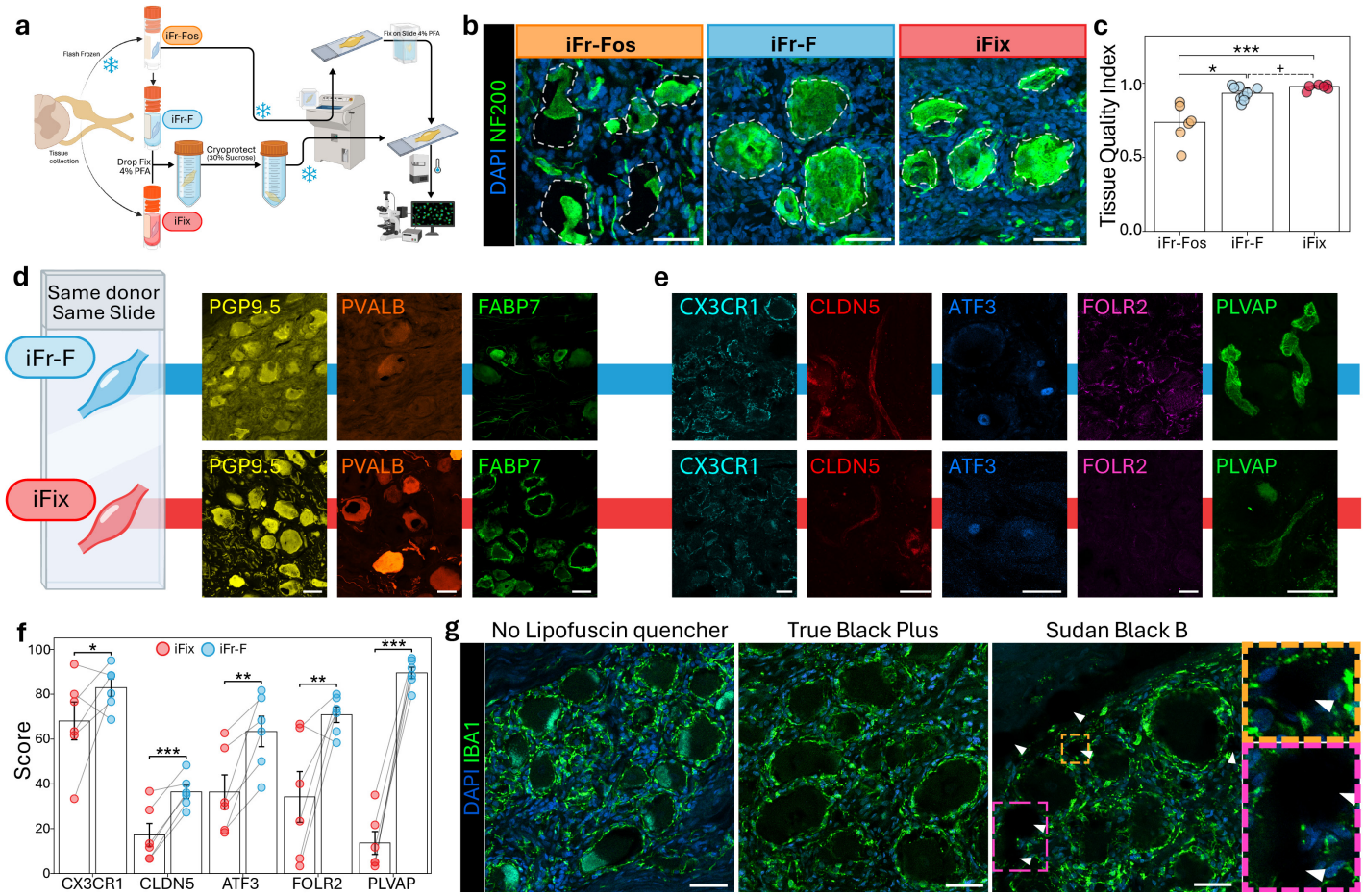

Fig. 1: Optimization of hDRG staining. **a**, Schematic representation of preprocessing protocols used. **b**, Representative images of pan-neuronal staining NF200 (green) and DAPI (Blue) showcasing the effect of different preprocessing protocols or neuronal soma. Dotted line simulates the expected coverage of neuronal tissue. **c**, Quantification of neuronal preservation in iFr-Fos (n=6), iFr-F (n=9), and iFix (n=6) samples. $*P < 0.05$, $***P < 0.001$. + indicates significant ($P < 0.05$) difference in precision by comparing variance in Levene's test **d**, Representative images from paired samples of PGP9.5 (yellow), PVALB (orange), and FABP7 (green) showing a loss of specificity in iFr-F samples while maintaining a clean signal on iFix samples. **e**, Representative images of antibodies with diminished signal in iFix samples while keeping specific signal in iFr-F samples. **f**, Average from 3 different investigators scoring staining quality (0-100) across paired samples from 6 different donors for PLVAP, CLDN5, ATF3, FOLR2, and CX3CR1. Paired T-test with False Discovery Rate (FDR) calculated with two-stage step-up method of Benjamini, Krieger and Yekutieli. $*q < 0.05$, $**q < 0.01$, $***q < 0.001$. **g**, Representative images of same donor stainings for DAPI (Blue) and IBA1 (green) showing regular amount of lipofuscin (No Lipofuscin quencher) and the loss of lipofuscin signal following True Black Plus post-treatment or Sudan Black B 0.02% pre-treatment. Zoom-in regions in the Sudan Black B staining highlight the unspecific accumulation of Sudan Black B. Scale bar = 50 µm.

715 **Supplemental Fig. 1**

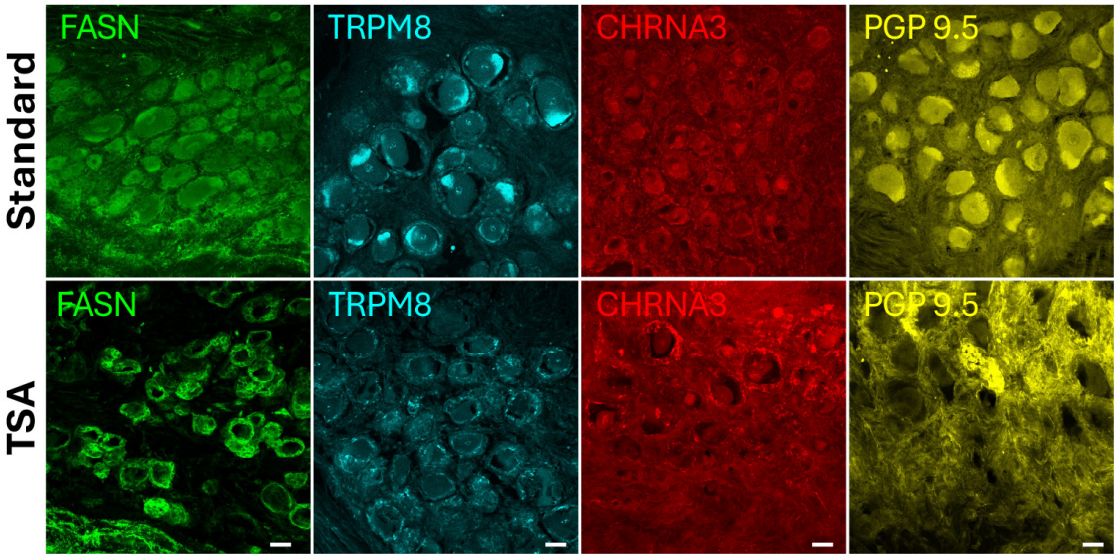

Supplementary Fig. 1 **TSA effect on sensitive antibodies.** Representative images of neuron rich regions with FASN (green), TRPM8 (cyan), CHRNA3 (red) and PGP 9.5 (yellow) using a regular protocol (top row) or TSA (bottom row). Scale bar = 50 μm.

716 **Extended Data Fig. 1**

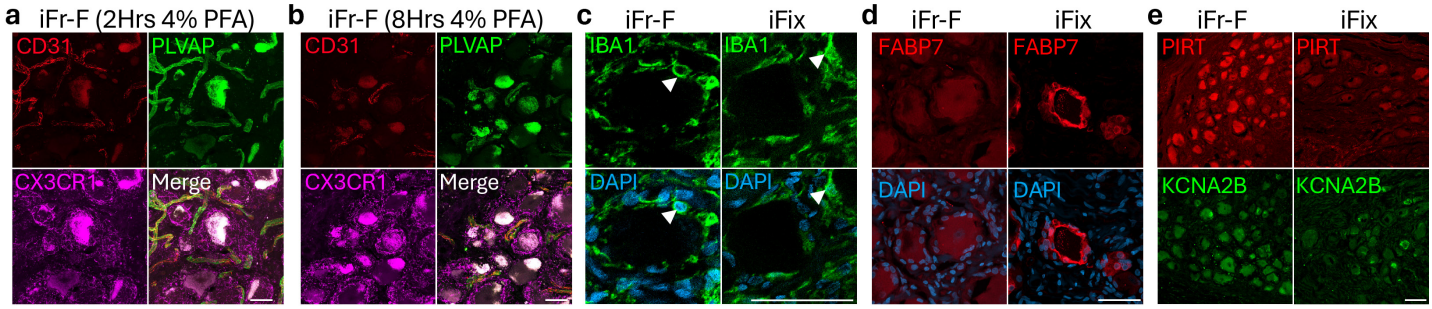

Extended Data Fig. 1 **Fixation time affects antibody specificity. a**, Staining pattern for CD31 (red), PLVAP (green), CX3CR1 (magenta) after 2 hours of whole tissue fixation of iFr tissue. **b**, Paired donor staining for CD31, PLVAP, CX3CR1 after 8 hours of whole tissue fixation. Scale bar = 50 μm. **c**, Staining pattern for IBA1 (green) and DAPI (blue) in iFr-F and iFix samples from the same donor. Arrows highlight the change in macrophage nuclear region. **d**, FABP7 (rabbit, cat: PA5-24949) and DAPI (blue) staining showing perineuronal staining in paired donor iFr-F and iFix samples showing loss of SGC staining in iFr-F samples. **e**, Paired donor images of iFr-F and iFix samples for PIRT (red) and KCNA2B (green) taken with equal laser settings highlighting a weak staining in iFix samples. Scale bars = 50 μm.

717 **Fig. 2**

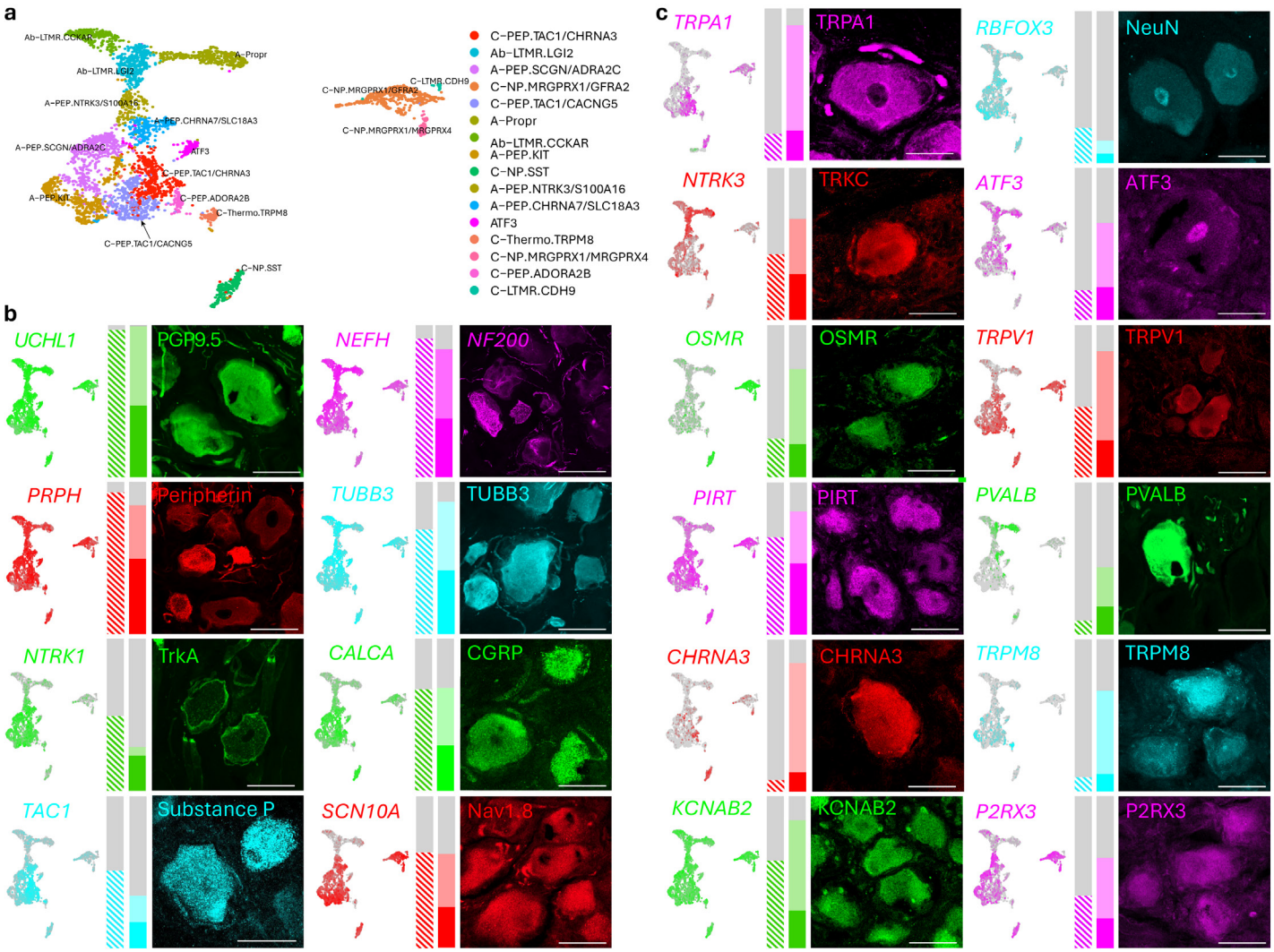

***Fig. 2*:** **Protein and transcriptomics correlation of neuronal markers. a**, UMAP showing identified neuronal subpopulations in an integrated dataset from 4 studies matched to previous single soma populations and newly identified populations from the hDRG transcriptomics atlas. **b-c**, Comparison of RNA and protein. Feature plots representing RNA transcript expression in the previously define neuronal populations followed by the percentage of neurons with $\log_2$Fc>0.5 for each associated marker to the left. To the right, a column showing single slide quantifications (210-966 neurons) showing neurons with negative staining (gray), detectable protein expression (dim colored portion), or bright protein expression (strong colored portion) followed with a representative 40x image highlighting high expressors. Columns in B show genes and proteins with a high similarity between RNA percentage and detectable protein. Column C shows genes and proteins with high similarity between RNA percentage and bright expressors.

718 **Extended Data Fig. 2**

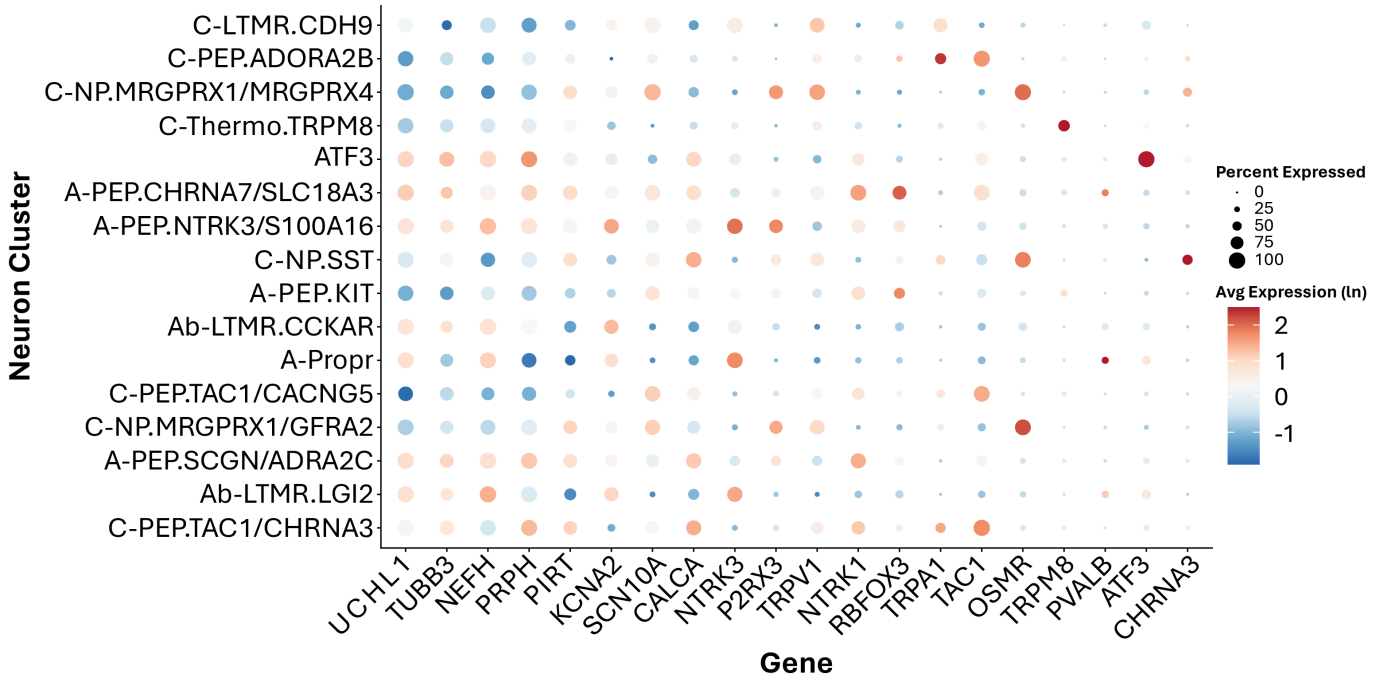

Extended Data Fig. 2 Neuronal RNA differential expression of selected markers. Dotplot showing average log normalized RNA expression for each neuronal subpopulation. The selected genes correspond to RNA transcripts for manually quantified neuronal markers.

719 **Fig. 3**

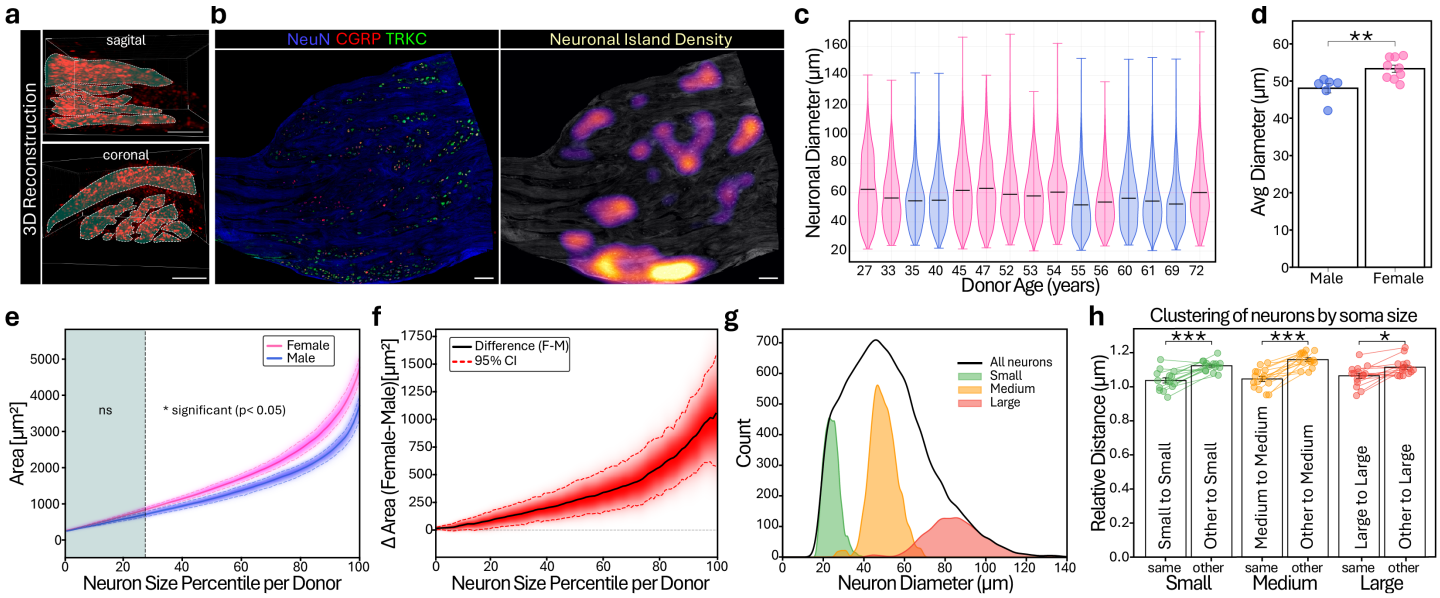

Fig. 3: hDRG neuronal characterization. **a**, Neuron-rich regions separated by thick fiber regions from cleared hDRG with neuronal cell bodies marked by lipofuscin autofluorescence (red), where neuronal islands are highlighted by dotted lines. **b**, Immunostaining of NeuN (blue), CGRP (red), and TrkC (green) in an hDRG section showing neuronal clusters, followed by a heatmap of neuronal density highlighting neuron-islands. Scale bar = 500 µm. **c**, Violin plot of neuronal size (35,721 neurons) across all donors (n = 15), ordered by age and colored by sex (female: pink; male: blue). **d**, Bar plot of donors' means neuronal size (female: pink; male: blue). ** indicates p < 0.01, Mann–Whitney U test. **e**, Average neuron size (cross-sectional area) for in-donor percentile averages for females (magenta) and males (blue). The area to the right of the black dashed line shows a significant difference ($P < 0.05$) between percentile averages (Benjamini–Hochberg FDR-corrected Mann–Whitney U test). Density clouds represent bootstrap distribution probability (white = low; saturated color = high), with colored dashed lines representing the bootstrap-estimated 95% confidence interval. **f**, The female–male difference in average neuron size (cross-sectional area) for in-donor percentile averages (black). Density clouds represent bootstrap distribution probability (white = low; saturated red = high), with red dashed lines representing the bootstrap-estimated 95% confidence interval. **g**, Size distribution of small (green), medium (orange), and large (red) neurons by Feret diameter. Neurons are classified per donor as: small (≤12.5th percentile), medium (37.5th–62.5th percentile), and large (≥87.5th percentile), with 25% padding between classes to ensure distinct populations. **h**, Spatial clustering of neurons by size class. For each size class, two distances are compared: (1) from each neuron of that class to its three nearest same-class neighbors, and (2) from each neuron outside that class to its three nearest neighbors within that class. Distances were averaged per donor and normalized to the median of the between-class distances. Bars show donor means, paired by donor (Wilcoxon signed-rank test: *P < 0.05, **P < 0.01, ***P < 0.001).

Extended Data Fig. 3

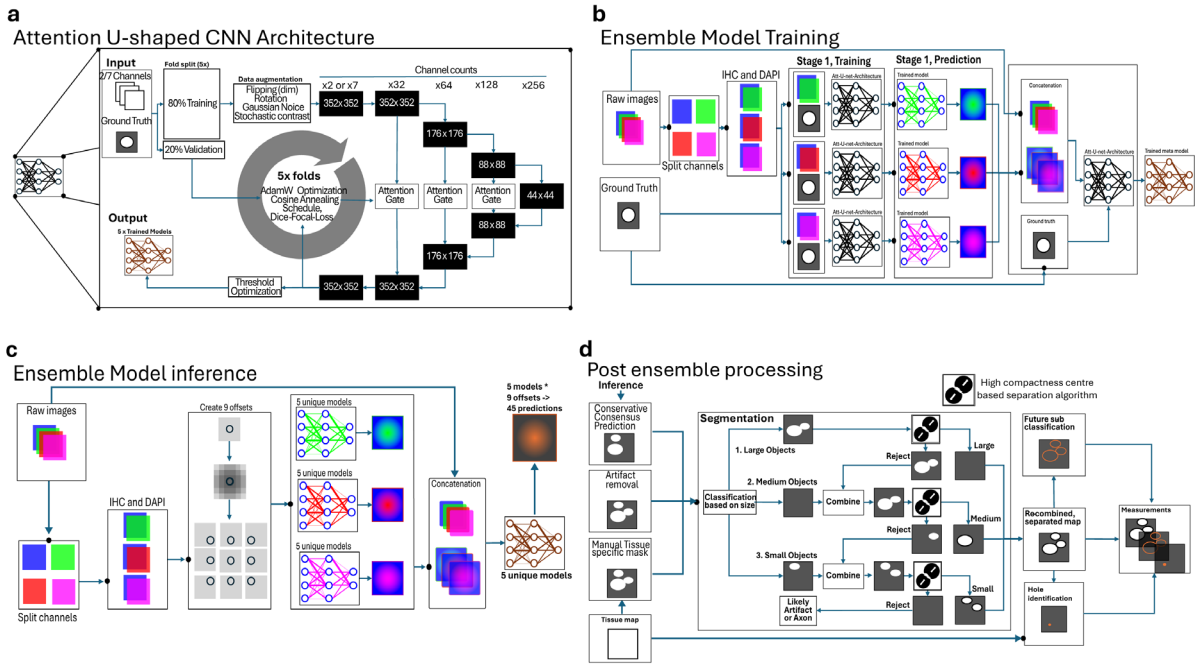

Extended Data Fig. 3 Neural network-based image segmentation pipeline. a, Neural network architecture. Input consists of either 2- or 7-channel images and binary ground truth masks. Data are split 80/20 for 5-fold cross-validation. Each fold is trained independently on augmented data using an attention-gated U-Net architecture with fold-specific threshold optimization. **b**, Two-stage ensemble model training. All images were acquired with DAPI and three different IHC stains. Stage 1: Models were trained on paired combinations of DAPI with each IHC channel using binary ground truth labels, generating 15 models total (3 IHC-DAPI pairs 5 folds). Each model outputs a prediction map. Stage 2: An ensemble network is trained using the three prediction maps from each Stage 1-fold plus the four original image channels (7 channels total). **c**, Ensemble prediction strategy. Each of the five ensemble models predicts independently using a tiled approach with nine different shifted windows, yielding 45 predictions per pixel (5 models * 9 windows) to improve contextual information and robustness. **d**, Post-processing and mask refinement. The 45-layer prediction stack is thresholded to generate a binary mask, then filtered using a manually drawn tissue boundary outlining the dorsal root ganglion (DRG). Sequential filters are applied, including edge-preserving operations. Masks are categorized by size (pixel count). Assuming high object compactness within each size category, objects are eroded to achieve separation, followed by acceptance or rejection based on morphological criteria. Finally, region-specific annotations are applied (e.g., tissue holes, membrane regions).

721 **Extended Data Fig. 4**

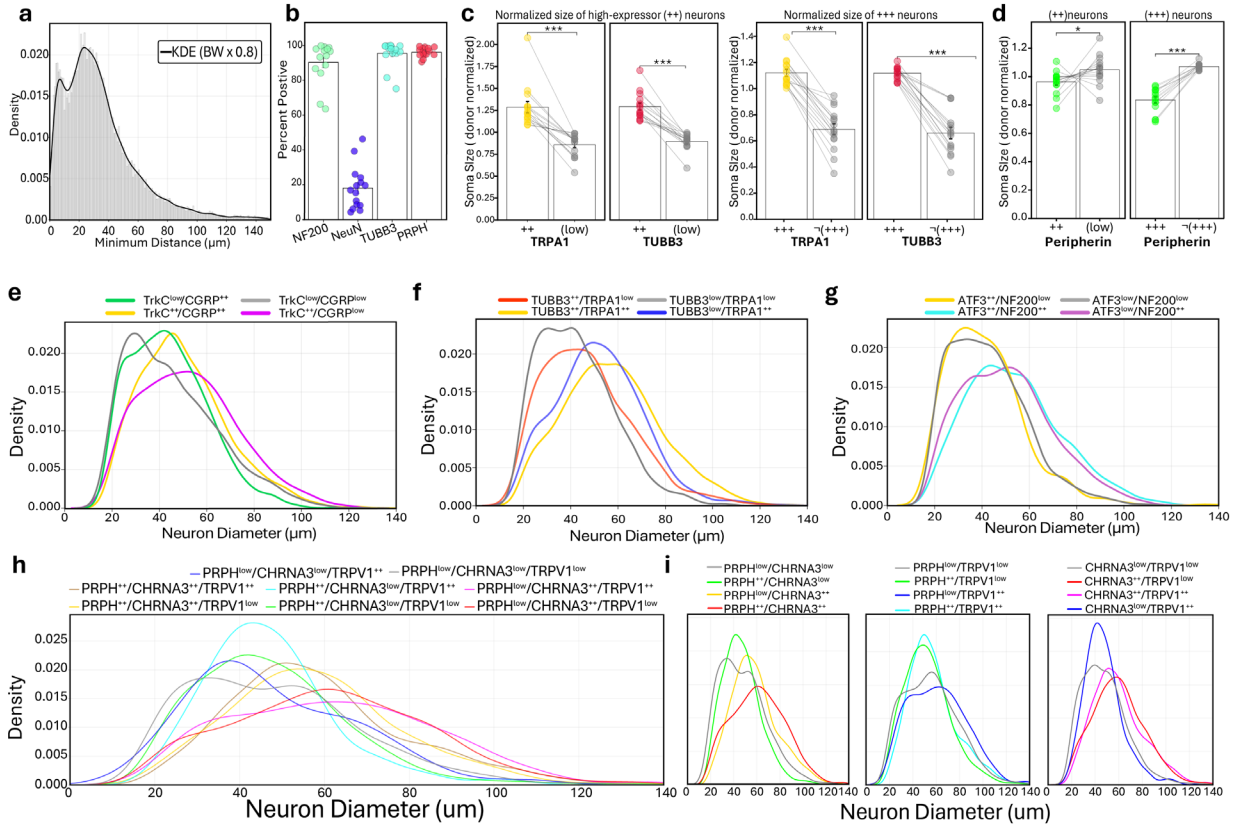

Extended Data Fig. 4 Additional morphometric and spatial analyses of human DRG neurons. a, Histogram (gray) and kernel density estimate (black line) showing the distribution of minimum distances between Neurons in the hDRG. **b,** Percentage of higher than detectable signal at neurons for 4 putative pan-neuronal markers across 15 donors. **c**, Normalized neuron size for TRPA1 and β3-tubulin high expressors (++) and very high expressors (+++) versus the rest low/not very high ¬(+++); Wilcoxon signed-rank test (two-sided); $*P < 0.05$, $**P < 0.01$, $***P < 0.001$. **d**, Normalized neuron size for peripherin high expressors (++) and very high expressors (+++) versus the rest low/ ¬(+++); Wilcoxon signed-rank test (two-sided); $*P < 0.05$, $**P < 0.01$, $***P < 0.001$. **e-h** KDE curves of neuronal soma diameter for high expressor subpopulations, e, TRKC and CGRP n=9223; f, TUBB3 and TRPA1 n=10408; g, ATF3 NF200 n=8298; h, PRPH, CHRNA3 and TRPV1 n=7972.**e-h** KDE curves of neuronal soma diameter for high expressor subpopulations, e, TRKC and CGRP n=9,223; f, TUBB3 and TRPA1 n=10,408; g, ATF3 NF200 n=8,298; h, PRPH, CHRNA3 and TRPV1 n=7,972.

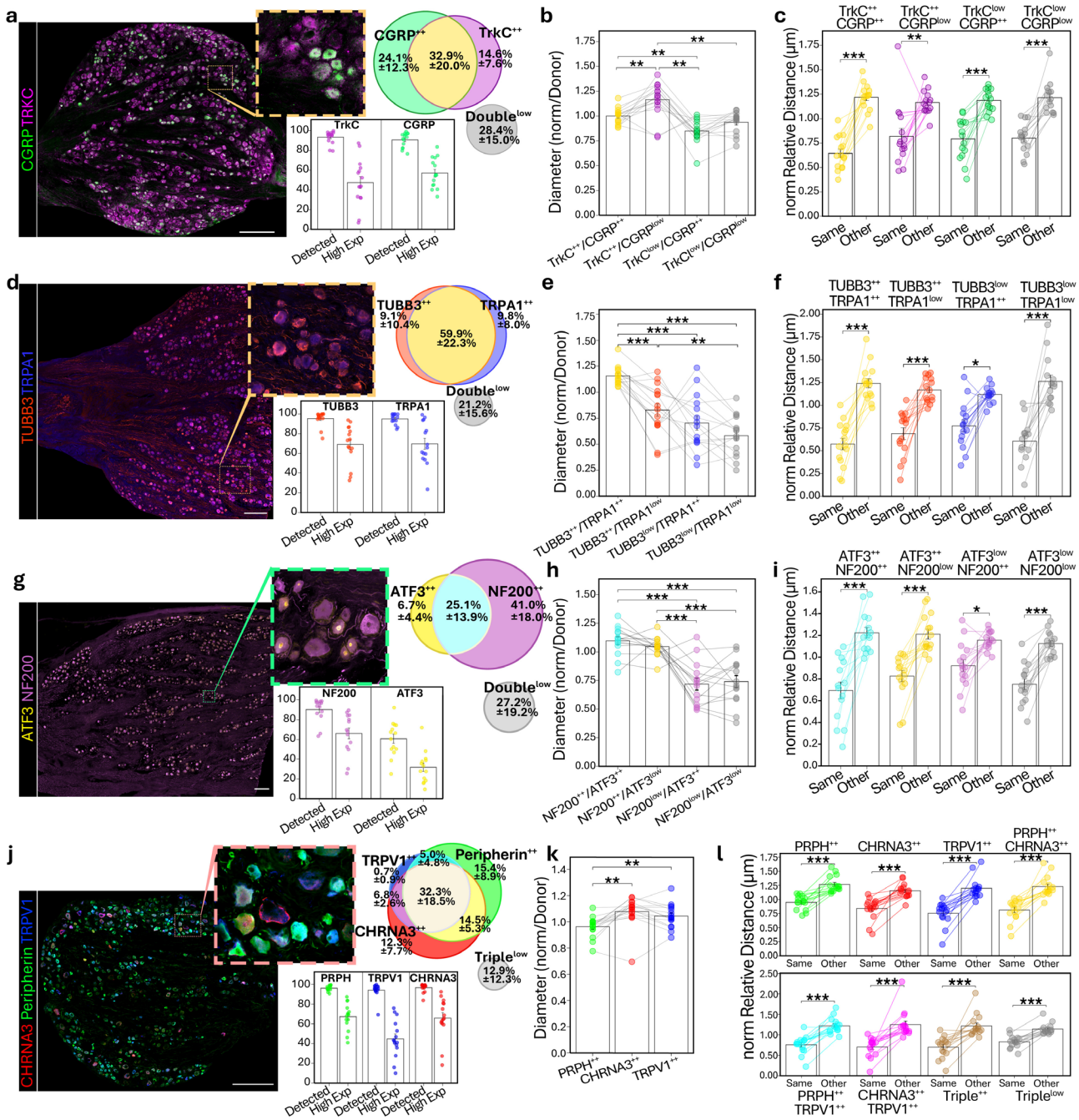

Fig. 4: hDRG neuronal characterization. a-c, Panel 1, CGRP (Green), TrkC (Magenta) 15 donors, 9,223 neurons. **d-f**, Panel 2, TUBB3 (Red), TRPA1 (Blue) 14 donors, 10,408 neurons. **g-i**, Panel 3 ATF3 (yellow), Nf200 (Magenta), 15 donors, 8,298 neurons. **j-l**, Panel 4, Peripherin (Green), TRPV1 (blue), CHRNA3 (red) 15 donors, 7,972 neurons. **a, d, g, j**, Representative whole-section Immunostaining of panel specific markers, Scale bar = 500 um. Bar plot of donors means prevalence of detectable and high expressor. Venn diagram of high expressor (++) with sd. **b, e, h, k** Normalized somata size by donor across combinations in the different panels. (Statistics: *$P < 0.05$, **$P < 0.01$, ***$P < 0.001$, Wilcoxon signed-rank, Benjamini-Hochberg FDR correction). **c, f, i, l,** Spatial clustering of neurons by marker-defined subpopulation. For each subpopulation, two distances are compared: (1) from each neuron of that subpopulation to its three nearest same-subpopulation neighbors, and (2) from each neuron outside that subpopulation to its three nearest neighbors within that subpopulation. Distances were averaged per donor and normalized to the median of the between-subpopulation distances. Bars show donor means, paired by donor (Wilcoxon signed-rank test: *P < 0.05, **P < 0.01, ***P < 0.001).

723 **Extended Data Fig. 5**

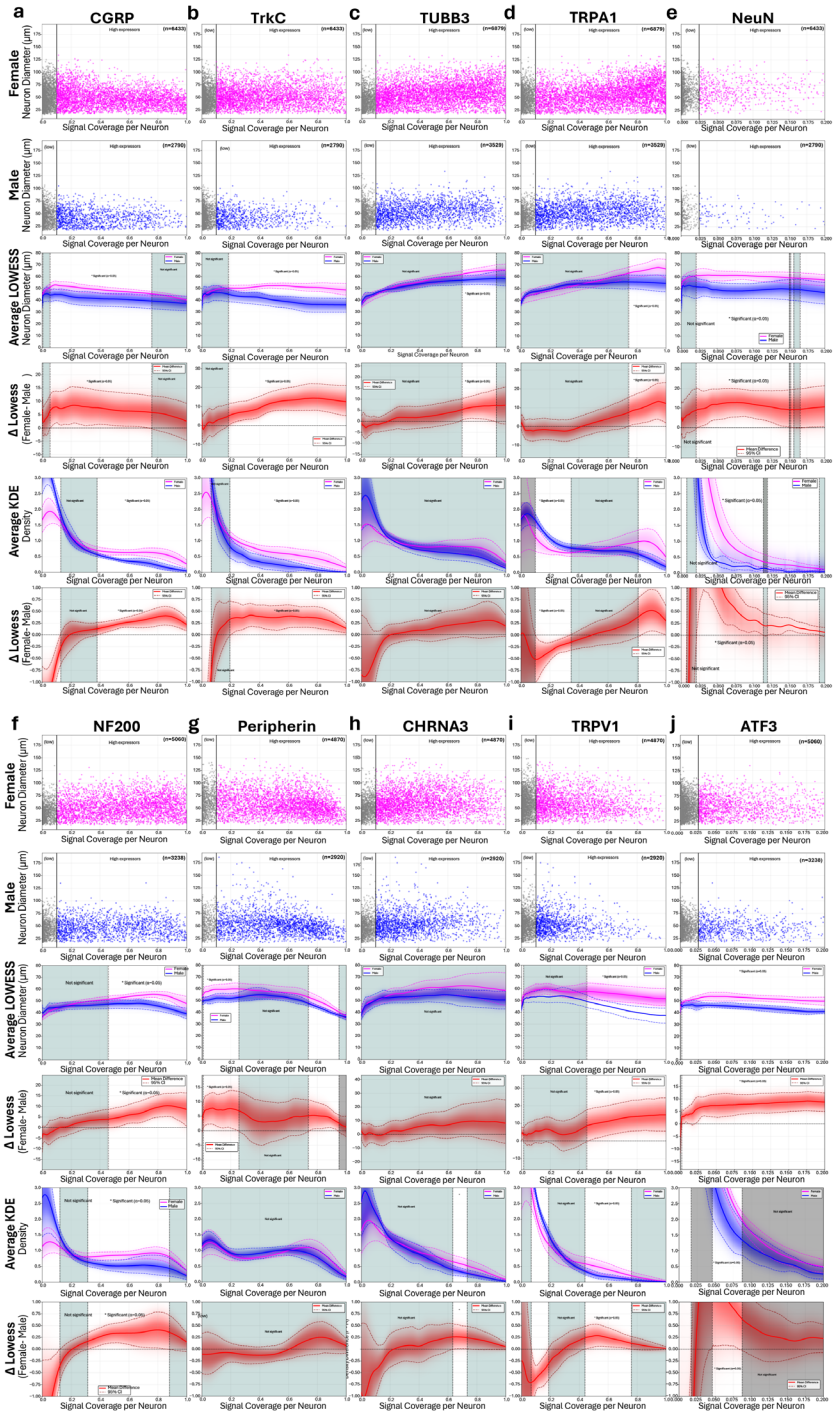

Extended data Fig. 5. Marker specific neuronal sex-dependent differences in the hDRGa, CGRP, **b,** TrkC, **c,** TUBB3, **d,** TRPA1, **e**, NeuN, **f,** NF200, **g,** Peripherin, **h**, CHRNA3, **i**, TRPV1, **j,** ATF3. **Row 1-2**, Raw data distributions showing individual neurons from male (blue) and female (red) donors. **Row 3**, Locally weighted scatterplot smoothing (LOWESS) regression curves (solid lines) with 95% confidence intervals (dashed lines) derived from bootstrap resampling of donor-level LOWESS fits (n=1,000 iterations). Density clouds represent bootstrap density distributions. Gray background shading indicates regions where sex differences are not statistically significant (Percentile Bootstrap Method, 95% CI of the difference includes zero). Vertical dashed lines mark transitions between significant and non-significant regions. **Row 4**, Difference donor-level LOWESS fits (Female-Male) with 95% bootstrap confidence intervals (red=mean difference, dark red dashed=CI bounds). Red density cloud shows bootstrap distribution of the difference Kernel density estimation (KDE) of marker expression distributions with 95% bootstrap confidence intervals. Density clouds and significance annotations as in the left figure. **Row 5**, Kernel density estimation (KDE) of marker expression distributions with 95% bootstrap confidence intervals. Density clouds and significance annotations as in the third row. **Row 6**, Difference in KDE distributions (Female minus Male) with 95% confidence intervals. The red density cloud shows bootstrap distribution. Horizontal dashed line at zero indicates no difference. Significance regions annotated as in previous panels. All statistical comparisons account for donor-level variability through bootstrap resampling at the donor level rather than individual neuron level.

724 Fig. 5

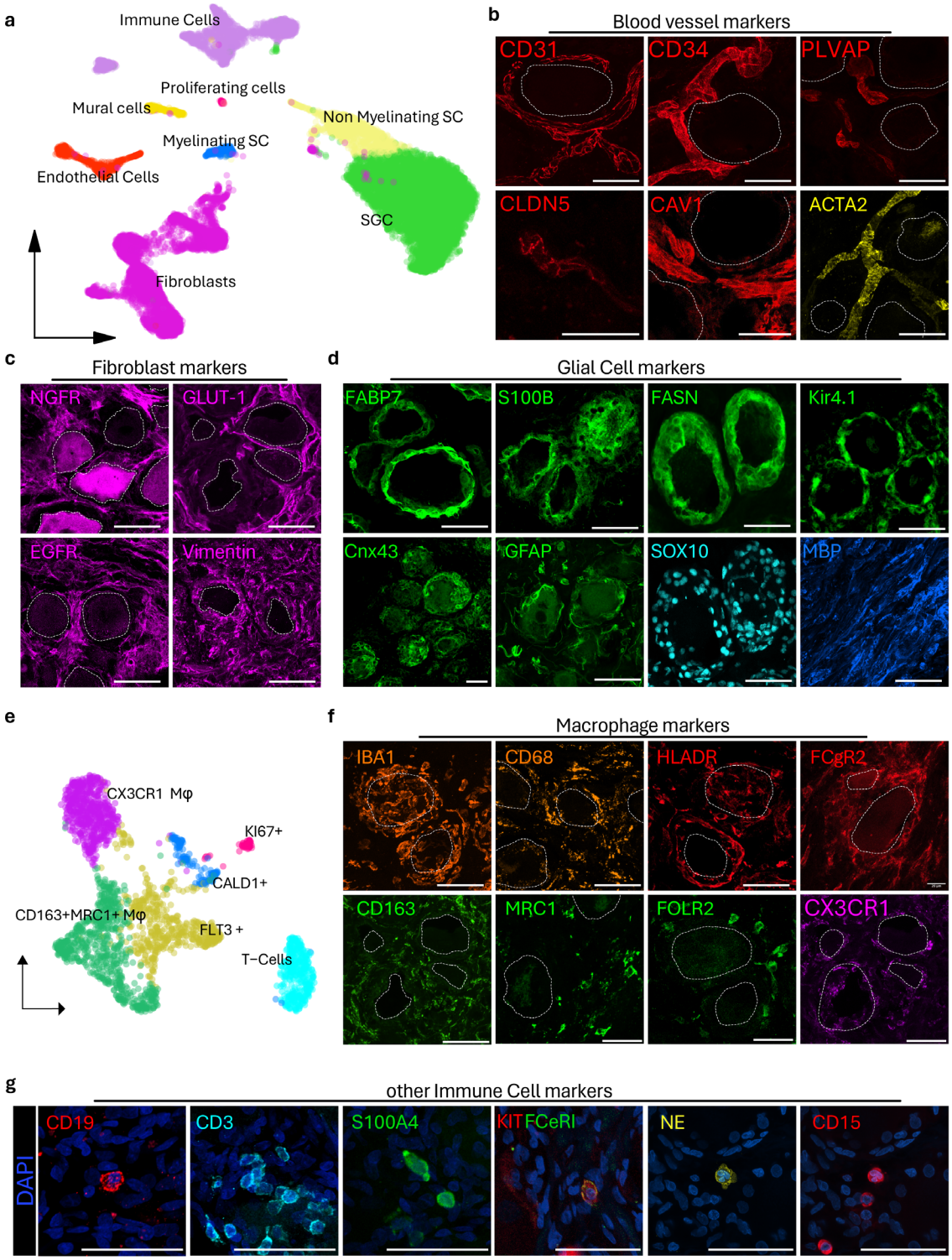

Fig. 5: **Non-neuronal markers in hDRG**. **a**, UMAP showing main populations of non-neuronal cells found in the hDRG. **b**, Markers that stain endothelial and mural cells. **c**, Fibroblasts markers. **d**, Markers expressed SGCs and Schwann cells. **e**, UMAP showing main subpopulations of immune cells found in the hDRG. **f**, Pan macrophage markers (top row) and subset specific macrophage markers (bottom row). **g**, Additional immune cell markers with DAPI (blue). Scale = 50 µm. Dotted line represents neuronal soma coverage.

Extended Data Fig. 6

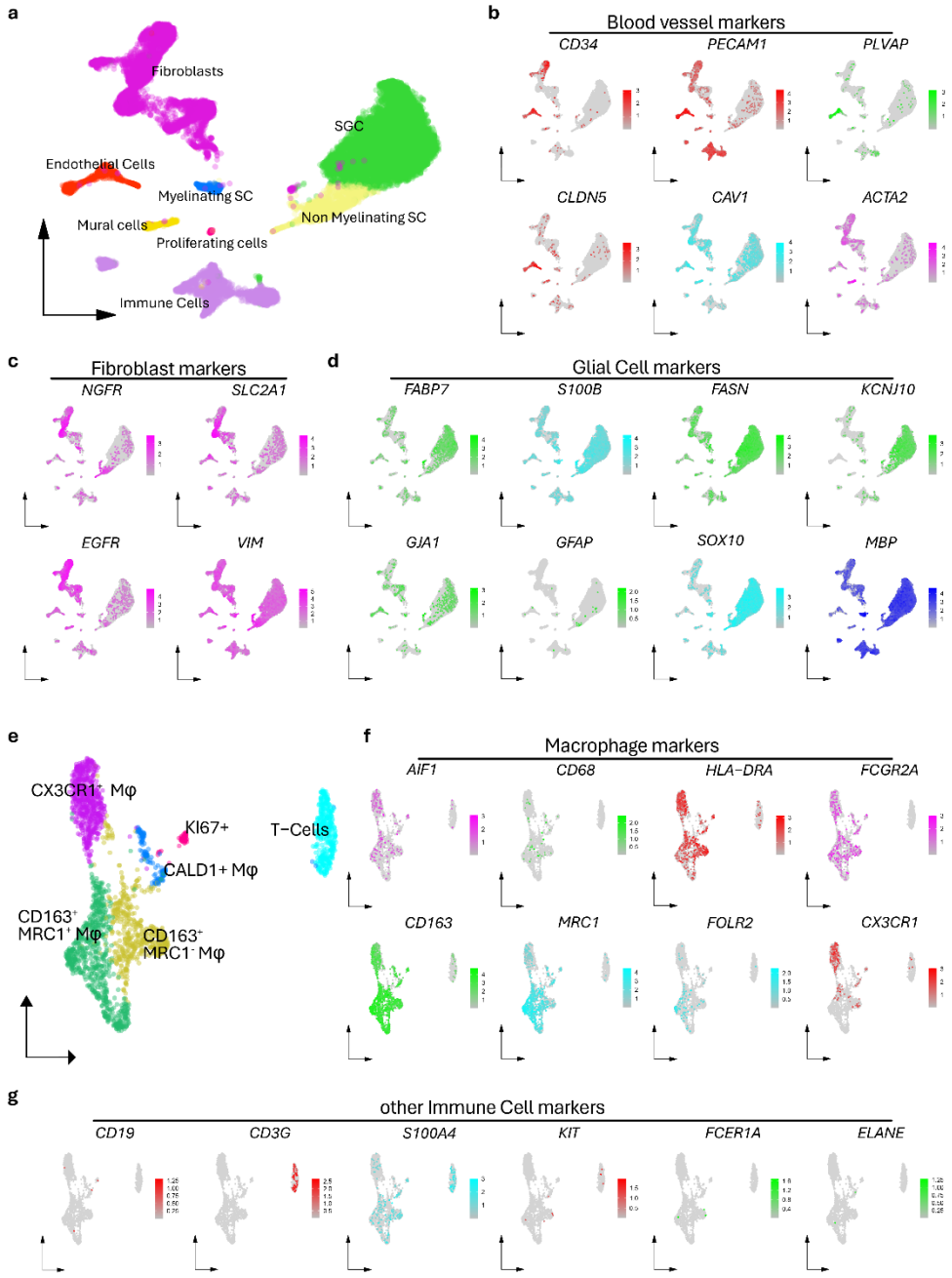

Extended Data Fig. 6 ***Non neuronal cells in the hDRG. a,*** UMAP showing cell type clustering in the hDRG. **b-d**, Feature plots showing RNA expression of markers for blood vessels (**b**), fibroblasts (**c**), and glial cells (**d**). **e**, UMAP subsetting immune cells showing different immune cell clusters. **f-g**, Feature plots of immune cell subset showing RNA expression of markers for macrophages (**f**) and other immune cells (**g**).

727 **Extended Data Fig. 7**

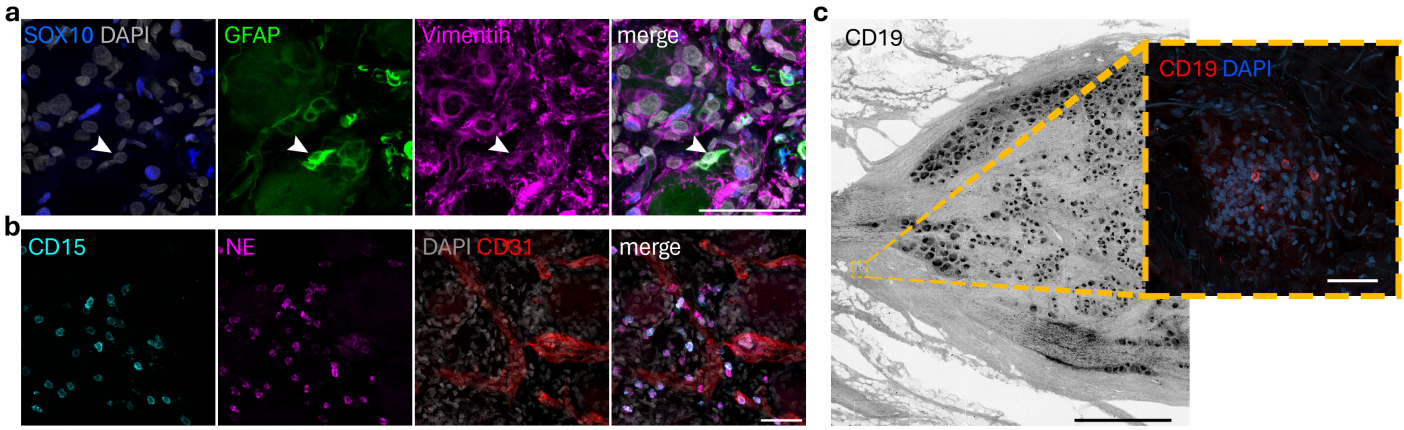

Extended Data Fig. 7 Unexpected marker location. **a,** Costaining of classical glial and fibroblast markers showing events of Sox10- GFAP+ cells (white arrow), and broad expression of vimentin across cell types. **b,** Sample with high neutrophil number in a neuron-island. To the left, overview image of neuron-island for nuclear marker (DAPI, Blue), and neutrophil markers CD15 (cyan), and NE (magenta), along with CD31-based masking of blood vessels (red), showing parenchymal localization of neutrophils as well as vascular **c,** Overview image of a DRG section where lipofuscin highlights neurons, and closeup image of a capsule border region showing clustering of immune cells, including B Cells (CD19, red) among others black scale bar: 500 µm, white scale bars: 50 µm.

728 Fig. 6

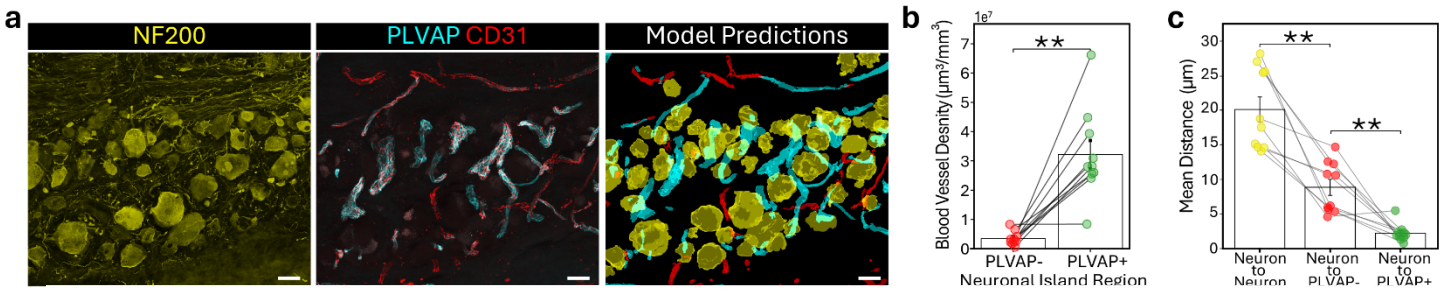

Fig. 6: hDRG non-neuronal cells characterization. a, Representative images of neuron island stained with NF200 (yellow), followed by the colocalization of general blood vessel marker CD31 (red), and fenestrated vessels PLVAP (cyan) followed by the prediction output from the prediction model. **b**, Bar plot donor means showing blood predicted vessels volume in neuron-island regions. **c**, Bar plot from showing donor mean distance from neurons to each of other neurons, blood vessels, and fenestrated blood vessels respectively (Statistics: (iFr-F samples, n=10, $^{**}p < 0.01$, Wilcoxon signed-rank, Benjamini-Hochberg FDR correction).**c**, Bar plot from showing donor mean distance from neurons to each of other neurons, blood vessels, and fenestrated blood vessels respectively (Statistics: (iFr-F samples, n=10, $^{**}P < 0.01$, Wilcoxon signed-rank, Benjamini-Hochberg FDR correction).

729 **Fig. 7**

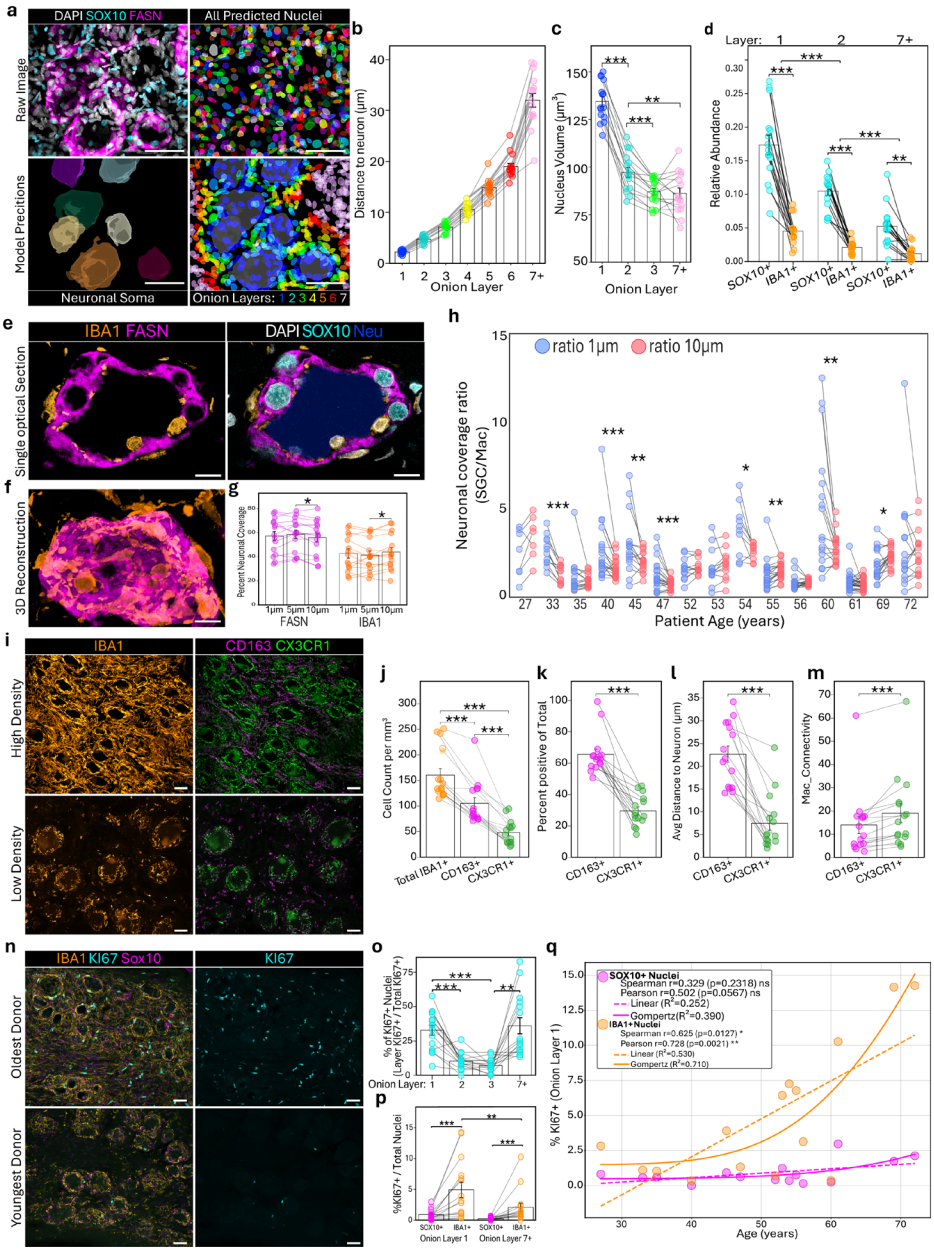

Fig. 7: 7hDRG non-neuronal cells characterization. a, Cellular layers around neurons in the hDRG. Glial marker staining in neuronal rich region (top left) and prediction models output for nuclei identification (top right), predicted neuronal location (bottom left), and onion layer classification (bottom right). **b**, Distance of layers. Bar plot showing the distance to closest neuron for cells on each category. **c**, Bar plot showing average nuclear volume for cells in layers 1,2,3, and 7+. **d**, Relative abundance of cell types with glial marker Sox10, and macrophage marker IBA1 on layers 1, 2, and 7+. **e-f**, Representative close-up image of neuronal surrounding region with SGC marker FASN, macrophage marker Iba1, glial marker SOX10, and model output for neuronal soma. **g**, Percentage of FASN and Iba1 coverage in the first 1, 5, and 10 mm. **h**, Ratio of SGC and macrophage coverage in the first 1, and 10 mm for the different donors analyzed. **i**, Macrophage analysis Representative image of general macrophage marker IBA1 (orange, left column) and marker for close neuronal contact macrophages, CX3CR1 (green), and other macrophages (CD163, magenta) in the hDRG for a sample with high (top) and low macrophage density (bottom). **j**, Macrophage density bar plot of number of macrophages per mm^3. **k**, Macrophage CD163 and CX3CR1 relative class abundance within macrophages. **l**, CD163 and CX3CR1 distance to neuron bar plot. **m**, Quantification of macrophage connectivity. **n**, Representative images showing macrophage marker Iba1 (yellow), glial marker Sox10 (magenta), and dividing cell marker KI67 (cyan) for the oldest (top), and youngest (bottom) donor analyzed. **o**, Percentage of dividing cells on each nuclear layer. **p**, Percentage of Sox10 and Iba1 dividing cells for the first layer, and layer 7+. **q**, Scatter plot showing positive nuclei percentage in cell layer 1 for SOX10+ and Iba1+ nuclei and their respective linear and Gompertz R-squared adjusted values. N= 15 donors. $P < 0.05$, $^{**}P < 0.01$, $^{***}P < 0.001$.

Extended Data Fig. 8

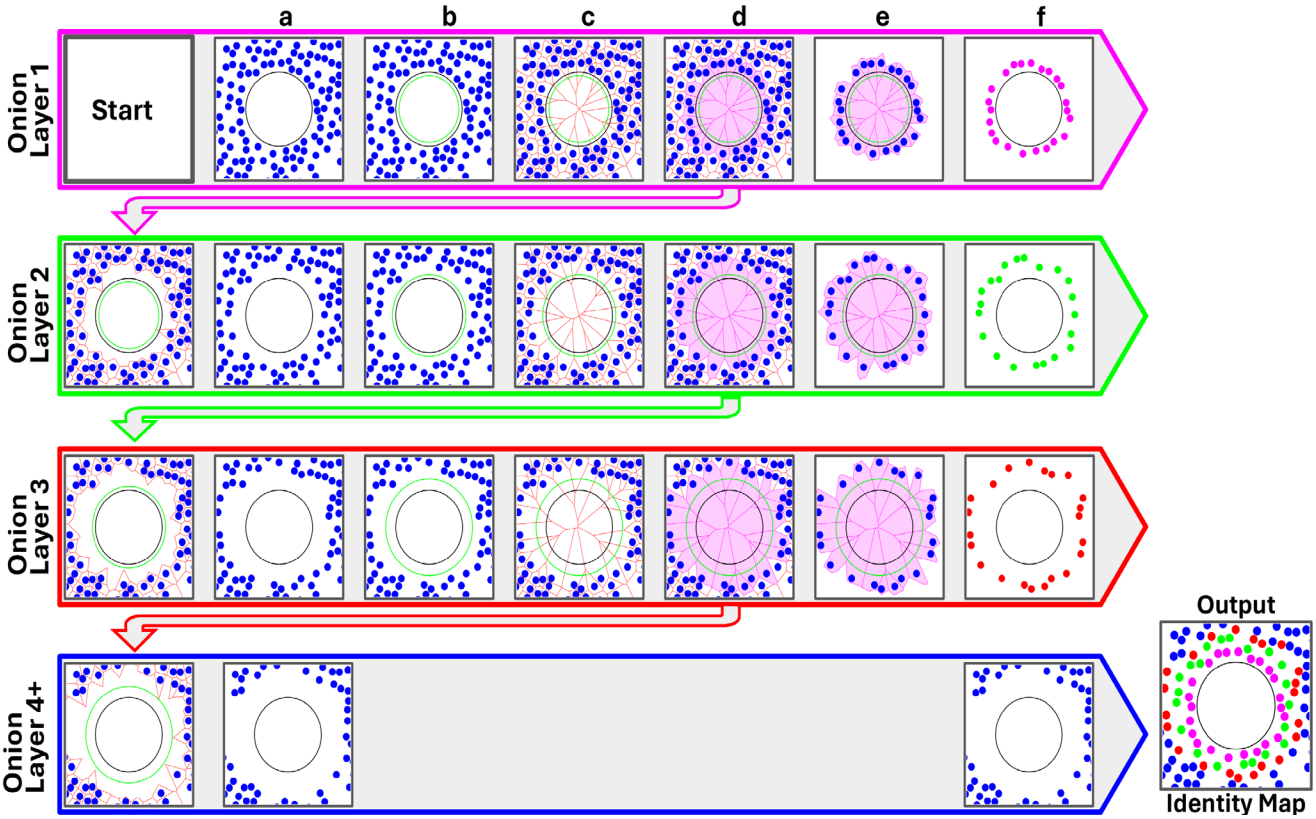

Extended Data Fig. 8 **Cyclical onion-layer algorithm for spatial nuclei classification**. The onion-layer algorithm classifies nuclei surrounding individual neurons into concentric n-spheres. Algorithm inputs are a nuclei label mask and a neuron label mask. The algorithm iterates for a specified number of layers (4 in this example). **a,** Input maps: nuclei label mask (blue dots) and neuron label mask (black circle) are defined for the current layer. **b**, The competitive zone for the current layer (green circle) is defined by dilating the neuron label mask by (LC − 1.5) * Dn, where LC is the layer count and Dn is the estimated average nucleus diameter. **c,** Current nuclei map used for Voronoi tessellation (red borders). **d**, The map is partitioned into two subsets: nuclei with Voronoi regions overlapping the competitive zone, and nuclei outside this zone. The latter serves as input for the subsequent layer. **e**, Overlapping nuclei are reset to their original unlabeled state. **f,** The classified nuclei for the current layer are saved as an independent label map.

Extended Data Fig. 9

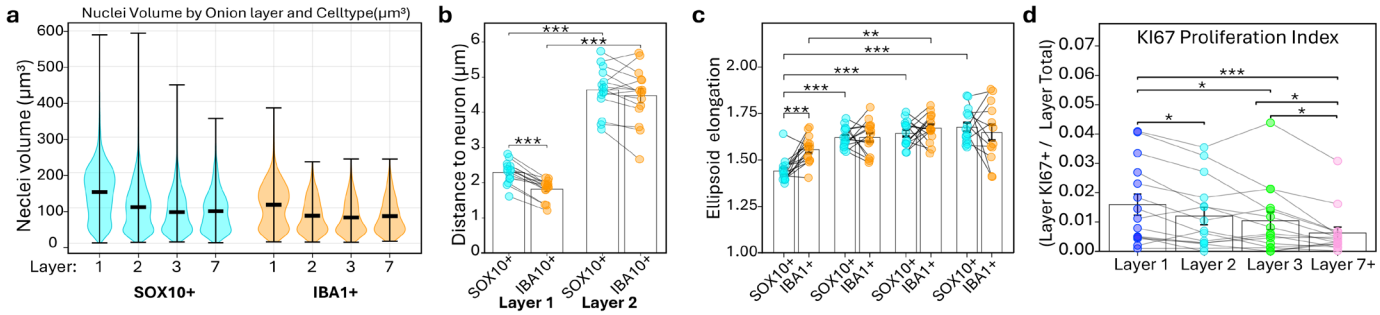

Extended Data Fig. 9 SOX10+ and IBA1+ cell morphology, distance, and proliferation across perineuronal layers. a, Nuclei volume distribution of SOX10+ and IBA1+ cells by onion layer. Violins show full distribution; lines indicate means. **b,** Distance from SOX10+ and IBA1+ nuclei to nearest neuron surface by perineuronal layer; donor means paired. Wilcoxon signed-rank test with FDR correction; **P* < 0.05, ***P* < 0.01, ****P* < 0.001. **c,** Nuclei elongation and compactness of SOX10+ and IBA1+ cells across onion layers. Points represent donor means; bars show mean ± standard error mean; lines connect paired samples. Wilcoxon signed-rank test (two-sided) with FDR correction; **P* < 0.05, ***P* < 0.01, ****P* < 0.001. **d,** Proportion of proliferating (KI67+) cells by onion ring, normalized to total KI67+ cells per donor; all cell types pooled. Points show individual donors; bars show mean ± standard error mean. Wilcoxon signed-rank test; **P* < 0.05, ***P* < 0.01, ****P* < 0.001.

hDRG IHC in prior publications

Cells marked	Marker	Species	Brand	Cat number	Dilution/Conc.	Notes on tissue	Notes on IHC	First author	Publication year	DOI
Neuronal Markers										
Neurons - Pan-Neuronal	brain-specific homeobox/POU domain protein 3A	Rabbit	Merck		1:200	3-8 h postmortem, non-diseased donors	20 µm cuts; Blocking 10% goat; 1ºAb ONight 4ºC; 2º 3hs room temp.	Rostock, C.	2018	https://doi.org/10.1016/j.neuroscience.2017.11.047
Neurons - Pan-Neuronal	NEFL	Rabbit	Cell Signaling Technology	10768		Obtained from organ donors	Embedded, cut at 7µm, and fixed on slide with 4%PFA for 30min at 4°C. Blocked with 3%BSA for 45 min. Primary antibodies overnight at room temperature.	Boyer, K.	2026	https://doi.org/10.1101/2025.09.21.677655
Neurons - Pan-Neuronal	NF200	Rabbit			1:200	3 Post-mortem DRG (24-36 hrs Post Mortem Interval)	Slice longitudinally, fixed in Zamboni's fixative at 4°C for 4 hrs.30% Sucrose and cut at 10 µm.48 hr Primary incubation at 4°C	Holford, L.C.	1994	10.1007/BF01262058
Neurons - Pan-Neuronal	NF200					Avulsed DRG and post mortem sections	Snap frozen in liquid nitrogen, Fixed on Slide in 4%PFA. Treated with 0.3% hydrogen peroxide.8 µm. ON primary incubation. Nickel enhanced for antibody reveal.	Anand, U.	2006	https://doi.org/10.1016/j.neulet.2006.01.046
Neurons - Pan-Neuronal	NF200	Chicken	Millipore		1:25000	3-8 h postmortem, non-diseased donors	20 µm cuts; Blocking 10% goat; 1ºAb ONight 4ºC; 2º 3hs room temp.	Rostock, C.	2018	https://doi.org/10.1016/j.neuroscience.2017.11.047
Neurons - Pan-Neuronal	NF200	Mouse	Sigma		1:600	3-8 h postmortem, non-diseased donors	20 µm cuts; Blocking 10% goat; 1ºAb ONight 4ºC; 2º 3hs room temp.	Rostock, C.	2018	https://doi.org/10.1016/j.neuroscience.2017.11.047
Neurons - Pan-Neuronal	NF200	Mouse	Sigma		1:1000	15 donors, 24-72h postmortem, healthy donors	12 µm cuts; 1 Ab overnight 4°C; secondary	Chang, W.	2018	https://doi.org/10.1007/s12264-017-0132-3
Neurons - Pan-Neuronal	NF200	Chicken	Neuromics	CH22104	1:500	1 hDRG from a 53 year-old female without chronic pain;	frozen at the time of collection and stored at -80°C . 14 µm thick cuts; fixed 30 min in PFA 4%; blocked with 3%Goat serum, hIgG overnight, other primaries for 2 h	Goebel, A.	2021	https://doi.org/10.1172/jci144201
Neurons - Pan-Neuronal	NF200	Chicken	Millipore	AB5539	1:200/0.5mg/mL	13 patients with brachial plexus injury 3-8months after injury; 7 controls post-mortem during routine autopsy with potential CNS injury	Transfered to ice-cold 4%PFA/PBS fixed ON 4°C, washed 30min PBSand ON 30%Sucrose 4°C. Longitudinally cut in 2, OCT embedded & stored at -80°C. 20 µm cuts. Slides incubated in quenching solution 15 min	Schulte, A.	2023	https://doi.org/10.1101/2023.02.06.526934
Neurons - Pan-Neuronal	NF200	Chicken	BioTechne	NB300-217		Obtained from organ donors	Embedded, cut at 7µm, and fixed on slide with 4%PFA for 30min at 4°C. Blocked with 3%BSA for 45 min. Primary antibodies overnight at room temperature.	Boyer, K.	2026	https://doi.org/10.1101/2025.09.21.677655
Neurons - Pan-Neuronal	Nissl		Thermo	N21483	1:100	Healthy and diabetic donors. Fresh human DRG L2-L5	Fixed upon delivery with 4%PFA and immersed in 30% sucrose for at least 3 night at 4°C. Blocking with 5%BSA for 1h. Nissl incubated with secondary antibodies for 1 hour.	Xu, J.	2026	https://doi.org/10.1038/s41586-025-09896-x
Neurons - Pan-Neuronal	PGP9.5	Mouse	Abcam	AB86808	1:100	3xT11+3xT12 DRGs;	35 µm cuts; 1 Ab overnight 4ºC;	Desormeaux, C.	2018	https://doi.org/10.1097/j.pain.0000000000001208
Neurons - Pan-Neuronal	Tubulin β3	Mouse	Covance		1:750	3-8 h postmortem, non-diseased donors	20 µm cuts; Blocking 10% goat; 1ºAb ONight 4ºC; 2º 3hs room temp.	Rostock, C.	2018	https://doi.org/10.1016/j.neuroscience.2017.11.047
Neurons - Pan-Neuronal	Tubulin β3		Proteintech		1:500	5 donors	20 µm cuts;	Nguyen, M. Q.	2021	https://doi.org/10.7554/eLife.71752
Neurons - Pan-Neuronal	Tubulin β3		BioLegend	#802001		4 donors for IHC studies	40 µm cuts, Blocking 10%, primary antibodies overnight; secondary antibodies	Avraham, O.	2022	https://doi.org/10.1371/journal.pone.0128951
Neurons - Pan-Neuronal	Tubulin β3	Mouse	Sigma	T8578	1:1000	Surgically extracted from organ donors within 4 hours of cross-clamp and frozen in dry ice, stored in -80°C.	12µm cuts. Rehydrated in PBST after thawing and fixed on slide with 10% formaldehyde RT for 15min. Blocked in 4%NDS in PBST for 1 hour, primary antibodies incubated overnight at 4°C.	Ahlgreen, O.A.	2025	https://doi.org/10.1002/advs.202511569
Neurons - Pan-Neuronal	Tubulin β3	Mouse	Thermo	MA1-19187		Adult human tissues from organ transplant donors. Thoracic DRG washed with cold PBS and immediately fixed with 4% PFA.	Two protocols: Paraffin-embedded cut at 4 µm, followed TSA Kit protocol with horse radish peroxidase secondary antibodies, after counterstaining repairing with antigen repair solution at 100°C for 10 min ;Cryoprotected in 30% sucrose for 24 hours, OCT embedded and cut at 50µm. Free floating sections blocked with 1%BSA, primary antibodies incubated overnight at 4°C.	Wu, Z.	2025	https://doi.org/10.1016/j.cell.2025.02.007
Neurons - Pan-Neuronal (Bright in small)	Peripherin	Rabbit			1:200	3 Post-mortem DRG (24-36 hrs Post Mortem Interval)	Slice longitudinally, fixed in Zamboni's fixative at 4°C for 4 hrs.30% Sucrose and cut at 10 µm.48 hr Primary incubation at 4°C	Holford, L.C.	1994	10.1007/BF01262058
Neurons - Pan-Neuronal (Bright in small)	Peripherin					Avulsed DRG	Snap frozen in liquid nitrogen, Fixed on Slide in 4%PFA. Treated with 0.3% hydrogen peroxide.8 µm. ON primary incubation. Nickel enhanced for antibody reveal.	Anand, U.	2006	https://doi.org/10.1016/j.neulet.2006.01.046
Neurons - Pan-Neuronal (Bright in small)	Peripherin	Rabbit	Sigma		1:500	15 donors, 24-72h postmortem, healthy donors	12 µm cuts; 1 Ab overnight 4°C; secondary antibodies 2h rt	Chang, W.	2018	https://doi.org/10.1007/s12264-017-0132-3
Neurons - Pan-Neuronal (Bright in small)	Peripherin	Chicken	Encor	CPCA-Peri	1:1000	Tissues collected within 4 hours of cross-clamp	Frozen at the time of collection and stored at 80ºC. 10%Formalin fixation; 10%Goat Serum 1hr; antibody incubation ON 4ºC; Sudan Black as post-treatment	Shiers, S.I.	2020	https://doi.org/10.1002/cne.25122
Neurons - Pan-Neuronal (Bright in small)	Peripherin	Chicken	Encorbio	CPCA-Peri	1:500	Surgically extracted from organ donors within 4 hours of cross-clamp and frozen in dry ice, stored in -80°C.	12µm cuts. Rehydrated in PBST after thawing and fixed on slide with 10% formaldehyde RT for 15min. Blocked in 4%NDS in PBST for 1 hour, primary antibodies incubated overnight at 4°C.	Ahlgreen, O.A.	2025	https://doi.org/10.1002/advs.202511569
Neurons - Pan-Neuronal (Bright in small)	Peripherin	Chicken	Encor Biotechnologies	CPCA-Peri	1:1000	Broad donor screening (90 donors)- Four groups of donors based on diabetes and pain conditions.	Frozen in dry ice, kept at -80°C. Gradually embedded in OCT. 20 cuts and fixed on slide with 10% formalin. Dehydrated. Blocked with 10%NDS with Triton-X 100, and incubated with primary antibodies overnight at 4°C	Shiers, S.I.	2025	https://doi.org/10.1038/s41467-025-59538-z
Neurons - Pan-Neuronal (Bright in small)	Peripherin	Rabbit	Abcam	ab269861		Obtained from organ donors	Embedded, cut at 7µm, and fixed on slide with 4%PFA for 30min at 4°C. Blocked with 3%BSA for 45 min. Primary antibodies overnight at room temperature.	Boyer, K.	2026	https://doi.org/10.1101/2025.09.21.677655
Neurons - Nociceptive	NaV1.8					Avulsed DRG	Snap frozen in liquid nitrogen, Fixed on Slide in 4%PFA. Treated with 0.3% hydrogen peroxide.8 µm. ON primary incubation. Nickel enhanced for antibody reveal.	Anand, U.	2006	https://doi.org/10.1016/j.neulet.2006.01.046
Neurons - Non peptidergic	IB4	Griffonia Simplicifolia	Vector Laboratories		2.5µg/mL	children with obstetric brachial plexus lesions	12um cuts, TSA, horse radish peroxidase secondary antibodies	Shi, T.J.	2008	https://doi.org/10.1073/pnas.0810899105
Neurons - Non peptidergic	P2X3R	Mouse	Santa Cruz	B-5	5 µg/mL	Tissues collected within 4 hours of cross-clamp	Frozen at the time of collection and stored at 80ºC. 10%Formalin fixation; 10%Goat Serum 1hr; antibody incubation ON 4ºC; Sudan Black as post-treatment	Shiers, S.I.	2020	https://doi.org/10.1002/cne.25122
Neurons - Peptidergic	CGRP				-	children with obstetric brachial plexus lesions	12um cuts, TSA, horse radish peroxidase secondary antibodies	Shi, T.J.	2008	https://doi.org/10.1073/pnas.0810899105
Neurons - Peptidergic	CGRP	Chicken	GenTex		1:500	adult human individuals autopsies	30 µm cuts, incubated free floating for 36 h at 4 °C primary antibodies; 90 min secondary antibodies	Patil, J.	2010	https://doi.org/10.1016/j.regpep.2010.03.004
Neurons - Peptidergic	CGRP	Mouse	Abcam		1:1000	6 DRGs from 3 patients; each went through surgery where the spinal nerve root was to be sacrificed	Immediately stored 4ºC and then processed. 8 µm longitudinal cuts, overnight 4ºC both 1 & 2 Ab	Li, Y.	2018	https://doi.org/10.1523/JNEUROSCI.0899-17.2017
Neurons - Peptidergic	CGRP	Rabbit	Immunostar	24112	1:1000	Tissues collected within 4 hours of cross-clamp	Frozen at the time of collection and stored at -80ºC. 10%Formalin fixation; 10%Goat Serum 1hr; antibody incubation ON 4ºC; Sudan Black as post-treatment	Shiers, S.I.	2020	https://doi.org/10.1002/cne.25122
Neurons - Peptidergic subset	Substance P	Rat	Seralab		1:50	3 Post-mortem DRG (24-36 hrs Post Mortem Interval)	Slice longitudinally, fixed in Zamboni's fixative at 4°C for 4 hrs.30% Sucrose and cut at 10 µm.48 hr Primary incubation at 4°C	Holford, L.C.	1994	10.1007/BF01262058
Neurons - Peptidergic subset	Substance P	Mouse	Novus Biologicals	SP-DE4- 21	0.5 µg/mL	adult human individuals autopsies	30 µm cuts, incubated free floating for 36 h at 4 °C primary antibodies; 90 min secondary antibodies	Patil, J.	2010	https://doi.org/10.1016/j.regpep.2010.03.004
Neurons - Synaptic vesicles	Synaptophysin	Rabbit	Epitomics		1:1200	adult human individuals autopsies	30 µm cuts, incubated free floating for 36 h at 4 °C primary antibodies; 90 min secondary antibodies	Patil, J.	2010	https://doi.org/10.1016/j.regpep.2010.03.004
Neurons - Thermal sensing	TRPA1	Goat	Santa Cruz	C19 sc-32353		Avulsion injured DRG (7male, 7 female), and uninjured DRG (8 male)	Snap frozen in liquid nitrogen, Fixed on Slide in 4%PFA. Treated with 0.3% hydrogen peroxide in methanol.10 µm. ON primary incubation. Nickel enhanced ABC for antibody reveal.	Anand, U.	2008	https://doi.org/10.1016/j.neulet.2008.04.007
Neurons - Thermal sensing	TRPA1	Rabbit	GSK	1962		Avulsion injured DRG (7male, 7 female), and uninjured DRG (8 male)	Snap frozen in liquid nitrogen, Fixed on Slide in 4%PFA. Treated with 0.3% hydrogen peroxide in methanol.10 µm. ON primary incubation. Nickel enhanced ABC for antibody reveal.	Anand, U.	2008	https://doi.org/10.1016/j.neulet.2008.04.007
Neurons - Thermal sensing	TRPV1	Rabbit		C-22		Cervical avulsed DRGs collected during surgical repair (n=10) and post mortem (<12h Post Mortem Interval) donors (n=6)	Snap frozen in liquid nitrogen, Fixed on Slide in 4%PFA. Treated with 0.3% hydrogen peroxide.8 µm. ON primary incubation. Nickel enhanced for antibody reveal.	Smith, G.D.	2002	https://doi.org/10.1038/nature00894
Neurons - Thermal sensing	TRPV1					Avulsed DRG	Snap frozen in liquid nitrogen, Fixed on Slide in 4%PFA. Treated with 0.3% hydrogen peroxide.8 µm. ON primary incubation. Nickel enhanced for antibody reveal.	Anand, U.	2006	https://doi.org/10.1016/j.neulet.2006.01.046
Neurons - Thermal sensing	TRPV1	-	GSK	C-22		Avulsion injured DRG (7male, 7 female), and uninjured DRG (8 male)	Snap frozen in liquid nitrogen, Fixed on Slide in 4%PFA. Treated with 0.3% hydrogen peroxide in methanol.10 µm. ON primary incubation. Nickel enhanced ABC for antibody reveal.	Anand, U.	2008	https://doi.org/10.1016/j.neulet.2008.04.007
Neurons - Thermal sensing	TRPV1	Rabbit	GSK	CC2	1:10,000	control hDRG (n = 5), avulsion injured hDRG (n = 8).	Tissue stored at −70°C until use or immersed in Zamboni's fixative for 2 h and stored in PBS . 15um cuts, post-fixed in 4% PFA 30 min, peroxidase blocked with methanol containing 0.3% w/v hydrogen peroxide for 30 min,primary antibodies overnight, avidin–biotin peroxidase	Anand, U.	2015	https://doi.org/10.1186/s12990-015-0038-x
Neurons - Thermal sensing	TRPV1	Rabbit	Neuromics, Edina, MN		1:400	15 donors, 24-72h postmortem, healthy donors	12 µm cuts; 1 Ab overnight 4ºC; secondary antibodies 2h rt	Chang, W.	2018	https://doi.org/10.1007/s12264-017-0132-3
Neurons - Thermal sensing	TRPV1	Guinea pig	Abcam		1:250	6 DRGs from 3 patients; each went through surgery where the spinal nerve root was to be sacrificed	Immediately stored 4ºC and then processed. 8 µm longitudinal cuts, overnight 4ºC both 1 & 2 Ab	Li, Y.	2018	https://doi.org/10.1523/JNEUROSCI.0899-17.2017
Neurons - Thermal sensing	TRPV1	Rabbit	Thermo Fisher Scientific	PA1-748	1:500	Tissues collected within 4 hours of cross-clamp	Frozen at the time of collection and stored at 80ºC. 10%Formalin fixation; 10%Goat Serum 1hr; antibody incubation ON 4ºC; Sudan Black as post-treatment	Shiers, S.I.	2020	https://doi.org/10.1002/cne.25122
Neurons - Thermal sensing	TRPV1	Rabbit	Thermo Fisher Scientific	PA1-748	2µg/mL	Broad donor screening (90 donors)- Four groups of donors based on diabetes and pain conditions.	Frozen in dry ice, kept at -80°C. Gradually embedded in OCT. 20 cuts and fixed on slide with 10% formalin. Dehydrated. Blocked with 10%NDS with Triton-X 100, and incubated with primary antibodies overnight at 4°C	Shiers, S.I.	2025	https://doi.org/10.1038/s41467-025-59538-z
Neurons - Thermal sensing	TRPV3	Rabbit		N-63		Cervical avulsed DRGs collected during surgical repair (n=10) and post mortem (<12h Post Mortem Interval) donors (n=6)	Snap frozen in liquid nitrogen, Fixed on Slide in 4%PFA. Treated with 0.3% hydrogen peroxide.8 µm. ON primary incubation. Nickel enhanced for antibody reveal.	Smith, G.D.	2002	https://doi.org/10.1038/nature00894
Neurons - Thermal sensing	TRPV3					Avulsed DRG	Snap frozen in liquid nitrogen, Fixed on Slide in 4%PFA. Treated with 0.3% hydrogen peroxide.8 µm. ON primary incubation. Nickel enhanced for antibody reveal.	Anand, U.	2006	https://doi.org/10.1016/j.neulet.2006.01.046

Neurons - small	ROBO2	Goat	BioTechne	AF3147		Obtained from organ donors	Embedded, cut at 7µm, and fixed on slide with 4%PFA for 30min at 4°C. Blocked with 3%BSA for 45 min. Primary antibodies overnight at room temperature.	Boyer, K.	2026	https://doi.org/10.1101/2025.09.21.677655
Neuron	Nav 1.7	rabbit	Alomone Labs		1:250	6 DRGs from 3 patients; each went through surgery where the spinal nerve root was to be sacrificed	Immediately stored 4ºC and then processed. 8 µm longitudinal cuts, overnight 4ºC both 1 & 2 Ab	Li, Y.	2018	https://doi.org/10.1523/JNEUROSCI.0899-17.2017
Neurons	NaV 1.7	Mouse	NeuroMab	N68/6	2µmL	Tissues collected within 4 hours of cross-clamp	Frozen at the time of collection and stored at 80ºC. 10%Formalin fixation; 10%Goat Serum 1hr; antibody incubation ON 4ºC; Sudan Black as post-treatment	Shiers, S.I.	2020	https://doi.org/10.1002/cne.25122
Neurons	Nav 1.7	Mouse	NeuroMab	N68/6	2µg/mL	Broad donor screening (90 donors)- Four groups of donors based on diabetes and pain conditions.	Frozen in dry ice, kept at -80°C. Gradually embedded in OCT. 20 cuts and fixed on slide with 10% formalin. Dehydrated. Blocked with 10%NDS with Triton-X 100, and incubated with primary antibodies overnight at 4°C	Shiers, S.I.	2025	https://doi.org/10.1038/s41467-025-59538-z
Neurons	AngII (Angiotensin II)	Murine		Purified using MabTrap G II column, Amersham Sciences	0.3 µg/mL	adult human individuals autopsies	30 µm cuts; incubated free floating for 36 h at 4 °C primary antibodies; 90 min secondary antibodiess	Patil, J.	2010	https://doi.org/10.1016/j.regpep.2010.03.004
Neurons	AngII (Angiotensin II)	Rabbit	BIOSS-USA	bs-0587R	1:5-1:1,000	control hDRG (n = 5), avulsion injured hDRG (n = 8)	Tissue stored at –70°C until use or immersed in Zamboni's fixative for 2 h and stored in PBS. 15um cuts, post-fixed in 4% PFA 30 min, peroxidase blocked with methanol containing 0.3% w/v hydrogen peroxide for 30 min,primary antibodies overnight, avidin–biotin peroxidase	Anand, U.	2015	https://doi.org/10.1186/s12990-015-0038-x
Neurons	AT2R (Angiotensin II receptor)	Goat	Santa Cruz	sc-48452	1:50-1:100	control hDRG (n = 5), avulsion injured hDRG (n = 8)	Tissue stored at –70°C until use or immersed in Zamboni's fixative for 2 h and stored in PBS. 15um cuts, post-fixed in 4% PFA 30 min, peroxidase blocked with methanol containing 0.3% w/v hydrogen peroxide for 30 min,primary antibodies overnight, avidin–biotin peroxidase	Anand, U.	2015	https://doi.org/10.1186/s12990-015-0038-x
Neurons	Cathepsin D	Rabbit	Epitomics		1:500	adult human individuals autopsies	30 µm cuts; incubated free floating for 36 h at 4 °C primary antibodies; 90 min secondary antibodiess	Patil, J.	2010	https://doi.org/10.1016/j.regpep.2010.03.004
Neurons	CXCR2	Rabbit	Genetex	GTX14935		Post-mortem	4%PFA fixation, 30% sucrose for 3 days	Yin, C.	2024	https://doi.org/10.1038/s41467-024-47640-7
Neurons	FcγRIII / CD16	Mouse	BioLegend		1:100	n=4 ;Brain dead subjects after asystole	14 µm cuts; postfixed with acetone; primary antibodies overnight rt;	Bersellini Farinotti, A.	2019	http://doi.org/10.1084/jem.20181657
Neurons	hIK1					Avulsed DRG	Snap frozen in liquid nitrogen, Fixed on Slide in 4%PFA. Treated with 0.3% hydrogen peroxidel.8 µm. ON primary incubation. Nickel enhanced for antibody reveal.	Anand, U.	2006	https://doi.org/10.1016/j.neulet.2006.01.046
Neurons	MAP2 (Microtubule-associated protein 2)	Mouse	Sigma	M1406	1:500/ 0.5mg/mL	13 patients with brachial plexus injury 3-8months after injury; 7 controls post-mortem during routine autopsy with potential CNS injury	Transfered to ice-cold 4%PFA/PBS fixed ON 4°C, washed 30min PBSand ON 30%Sucrose 4°C. Longitudinally cut in 2, OCT embedded & stored at -80°C. 20 µm cuts. Slides incubated in quenching solution 15 min	Schulte, A.	2023	https://doi.org/10.1101/2023.02.06.526934
Neurons	NaN/SNS2		Rabbit	K186	0.6 µg/mL	Avulsion injured DRG (12male), and post-mortem DRG (2 male, 2 days Post Mortem Interval)	Snap frozen in liquid nitrogen, Fixed on Slide in 4%PFA. Treated with 0.3% hydrogen peroxidel.8 µm. ON primary incubation. Nickel enhanced for antibody reveal.	Coward, K.	2000	10.1016/S0304-3959(99)00251-1
Neurons	NeuN	Rabbit	Millipore	ABN78A4	1:100	n=4 ;Brain dead subjects after asystole	14 µm cuts; postfixed with acetone; primary antibodies overnight rt;	Bersellini Farinotti, A.	2019	http://doi.org/10.1084/jem.20181657
Neurons	NeuN		Millipore		1:1000	5 donors	20 µm cuts;	Nguyen, M. Q.	2021	https://doi.org/10.7554/eLife.71752
Neurons	NeuN	Mouse	Sigma Aldrich	MAB377X	1:100	Non diabetic and without chronic pain controls and DPN donors (n not specified for IHC); L4, L5 and S1 DRGs were collected under cold ischemic conditions, within 3 h of aorta cross-clamp	Formalin fixed parafin embedded DRG tissue sections, deparafnized and subject to citrate bufered antigen retrieval.	Doty, M.	2022	https://doi.org/10.1038/s41598-022-21394-y
Neurons	NeuN					Post-mortem	4%PFA fixation, 30% sucrose for 3 days	Yin, C.	2024	https://doi.org/10.1038/s41467-024-47640-7
Neurons	NeuN	Rabbit	Huabio	#ET1602-12		Adult human tissues from organ transplant donors. Thoracic DRG washed with cold PBS and immediately fixed with 4% PFA.	Paraffin-embedded cut at 4 µm, followed TSA Kit protocol with horse radish peroxidase secondary antibodies, after counterstaining repairing with antigen repair solution at 100°C for 10 min.	Wu, Z.	2025	https://doi.org/10.1016/j.cell.2025.02.007
Neurons	PLC β3 (Phospholipase C β3)				-	children with obstetric brachial plexus lesions	12um cuts, TSA, horse radish peroxidase secondary antibodies	Shi, T. J.	2008	https://doi.org/10.1073/pnas.0810899105
Neurons	SNS/PN3	Rabbit		K104		Avulsion injured DRG (12male), and post-mortem DRG (2 male, 2 days Post Mortem Interval)	Snap frozen in liquid nitrogen, Fixed on Slide in 4%PFA. Treated with 0.3% hydrogen peroxidel.8 µm. ON primary incubation. Nickel enhanced for antibody reveal.	Coward, K.	2000	10.1016/S0304-3959(99)00251-1
Neurons	SNS/PN3	Rabbit		K107	1 µg/mL	Avulsion injured DRG (12male), and post-mortem DRG (2 male, 2 days Post Mortem Interval)	Snap frozen in liquid nitrogen, Fixed on Slide in 4%PFA. Treated with 0.3% hydrogen peroxidel.8 µm. ON primary incubation. Nickel enhanced for antibody reveal.	Coward, K.	2000	10.1016/S0304-3959(99)00251-1
Neurons	SSE4	Mouse			1:150	3 Post-mortem DRG (24-36 hrs Post Mortem Interval)	Slice longitudinally, fixed in Zamboni's fixative at 4°C for 4 hrs.30% Sucrose and cut at 10 µm.48 hr Primary incubation at 4°C	Holford, L.C.	1994	10.1007/BF01262058
Neurons	ATF3	Rabbit	Novus Biologicals	NBP1-855816	1:200	L4 DRG from two youg and two aged donors	Flash frozen on dry ice and stored at -80°C. 20 µm cuts. Fixed on slide in 10% formalin. IHC after fluorescent in situ hybridization. Primary overnight at 4°C.	Donovan, L.J.	2025	https://doi.org/10.1038/s41593-025-01954-x
Neurons and other cells	CD44	Rabbit	Abclonal	A19020	2µg/mL	Broad donor screening (90 donors)- Four groups of donors based on diabetes and pain conditions.	Frozen in dry ice, kept at -80°C. Gradually embedded in OCT. 20 cuts and fixed on slide with 10% formalin. Dehydrated. Blocked with 10%NDS with Triton-X 100, and incubated with primary antibodies overnight at 4°C	Shiers, S.I.	2025	https://doi.org/10.1038/s41467-025-59538-z
Neurons and other cells	PAR1 (Protese-Activated Receptor 1)	Goat	Abcam	AB111976	1:100	3xT11+3xT12 DRGs	35 µm cuts; 1 Ab overnight 4ºC;	Desormeaux, C.	2018	https://doi.org/10.1097/j.pain.0000000000001208
Neurons and other cells	PAR2 (Protese-Activated Receptor 2)	Mouse	LifeSpan	LSB2321	1:100	3xT11+3xT12 DRGs	35 µm cuts; 1 Ab overnight 4ºC;	Desormeaux, C.	2018	https://doi.org/10.1097/j.pain.0000000000001208
Neurons and other cells	PAR4 (Protese-Activated Receptor 4)	-	Abcam	AB70400	1:100	3xT11+3xT12 DRGs	35 µm cuts; 1 Ab overnight 4ºC;	Desormeaux, C.	2018	https://doi.org/10.1097/j.pain.0000000000001208
Sympathetic fibers	TH	Rabbit	Sigma	AB152	2µg/mL	Broad donor screening (90 donors)- Four groups of donors based on diabetes and pain conditions.	Frozen in dry ice, kept at -80°C. Gradually embedded in OCT. 20 cuts and fixed on slide with 10% formalin. Dehydrated. Blocked with 10%NDS with Triton-X 100, and incubated with primary antibodies overnight at 4°C	Shiers, S.I.	2025	https://doi.org/10.1038/s41467-025-59538-z
Non-neuronal markers										
Endothelial cells	CD31	Rabbit	Abcam	Ab28364	1:50	6 donors	25 µm cuts; primary antibodies overnight	Lund, H.	2023	https://doi.org/10.1084/jem.20230675
Endothelial cells	CD31	Sheep	R&D Systems	AF806	1:50	6 donors	25 µm cuts; primary antibodies overnight	Lund, H.	2023	https://doi.org/10.1084/jem.20230675
Endothelial cells	CD31	Mouse	Invitrogen	14-0319-82	2µg/mL	Broad donor screening (90 donors)- Four groups of donors based on diabetes and pain conditions.	Frozen in dry ice, kept at -80°C. Gradually embedded in OCT. 20 cuts and fixed on slide with 10% formalin. Dehydrated. Blocked with 10%NDS with Triton-X 100, and incubated with primary antibodies overnight at 4°C	Shiers, S.I.	2025	https://doi.org/10.1038/s41467-025-59538-z
Endothelial cells - Arteries & Capillaries	CLDN5	Rabbit	Thermo	34-1600	1:200	6 donors	25 µm cuts; primary antibodies overnight	Lund, H.	2023	https://doi.org/10.1084/jem.20230675
Endothelial cells - Veins & Capillaries	PLVAP	Mouse	Abcam	Ab81719	1:200	6 donors	25 µm cuts; primary antibodies overnight	Lund, H.	2023	https://doi.org/10.1084/jem.20230675
Basal lamina	Laminin	Mouse	Sigma	L8271	1:1000	15 patients with Friedreich ataxia and 12 "normal" controls obtain during autopsy	6 µm cuts in paraffin, blocking 10% horse/donkey; overnight 4ºC, horse-radish peroxidase-labeled for secondaries or AF-488 or Cy3	Koeppen, A.H.	2016	https://doi.org/10.1186/s40478-016-0288-5
Extra Cellular Matrix	TNR (Tenascin R)	Goat	R&D Systems	AF3865	1:50	Non diabetic and without chronic pain controls and DPN donors (n not specified for IHC); L4, L5 and S1 DRGs were collected under cold ischemic conditions, within 3 h of aorta cross-clamp	Formalin fixed parafin embedded DRG tissue sections, deparafnized and subject to citrate bufered antigen retrieval.	Doty, M.	2022	https://doi.org/10.1038/s41598-022-21394-y
Connective tissue	COL IV	Rabbit	Abcam	ab6586		Obtained from organ donors	Embedded, cut at 7µm, and fixed on slide with 4%PFA for 30min at 4°C. Blocked with 3%BSA for 45 min. Primary antibodies overnight at room temperature.	Boyer, K.	2026	https://doi.org/10.1101/2025.09.21.677655
Satellite Glial Cells & Neurons - Study target	FMS IgG (Fibromyalgia Syndrome Immunoglobulin)	Human	Extracted from patients	-	100µg/mL	1 hDRG from a 53 year-old female without chronic pain	Frozen at the time of collection and stored at -80°C . 14 µm thick cuts; fixed 30 min in PFA 4%; blocked with 3%Goat serum, hIgG overnight, other primaries for 2 h	Goebel, A.	2021	https://doi.org/10.1172/jci144201
Satellite Glial Cells & Schwann Cells	S100	Mouse	Santa Cruz	sc-53438	0.4 µg/mL	15 patients with Friedreich ataxia and 12 "normal" controls obtain during autopsy	6 µm cuts in paraffin, blocking 10% horse/donkey; overnight 4ºC, horse-radish peroxidase-labeled for secondaries or AF-488 or Cy3	Koeppen, A.H.	2016	https://doi.org/10.1186/s40478-016-0288-5
Satellite Glial Cells & Schwann Cells	S100	Mouse	Fisher Scientific	MA126621	2 µg/mL	Broad donor screening (90 donors)- Four groups of donors based on diabetes and pain conditions.	Frozen in dry ice, kept at -80°C. Gradually embedded in OCT. 20 cuts and fixed on slide with 10% formalin. Dehydrated. Blocked with 10%NDS with Triton-X 100, and incubated with primary antibodies overnight at 4°C	Shiers, S.I.	2025	https://doi.org/10.1038/s41467-025-59538-z
Satellite Glial Cells & Schwann Cells	SOX10	Mouse	Abcam	ab216020	2 µg/mL	Broad donor screening (90 donors)- Four groups of donors based on diabetes and pain conditions.	Frozen in dry ice, kept at -80°C. Gradually embedded in OCT. 20 cuts and fixed on slide with 10% formalin. Dehydrated. Blocked with 10%NDS with Triton-X 100, and incubated with primary antibodies overnight at 4°C	Shiers, S.I.	2025	https://doi.org/10.1038/s41467-025-59538-z
Satellite Glial Cells & Schwann Cells	SOX10	Goat	BioTechne	AF2864		Obtained from organ donors	Embedded, cut at 7µm, and fixed on slide with 4%PFA for 30min at 4°C. Blocked with 3%BSA for 45 min. Primary antibodies overnight at room temperature.	Boyer, K.	2026	https://doi.org/10.1101/2025.09.21.677655
Satellite Glial Cells	Apolipoprotein J / clusterin	Goat	Abcam	ab39991	1:50/0.5mg/mL	13 patients with brachial plexus injury 3-8months after injury; 7 controls post-mortem during routine autopsy with potential CNS injury	Transfered to ice-cold 4%PFA/PBS fixed ON 4°C, washed 30min PBSand ON 30%Sucrose 4°C. Longitudinally cut in 2, OCT embedded & stored at -80°C. 20 µm cuts. Slides incubated in quenching solution 15 min	Schulte, A.	2023	https://doi.org/10.1101/2023.02.06.526934
Satellite Glial Cells	Connexin 43	Rabbit	Abcam	ab113470	0.75 µg/mL	15 patients with Friedreich ataxia and 12 "normal" controls obtain during autopsy	6 µm cuts in paraffin, blocking 10% horse/donkey; overnight 4ºC, horse-radish peroxidase-labeled for secondaries or AF-488 or Cy3	Koeppen, A.H.	2016	https://doi.org/10.1186/s40478-016-0288-5
Satellite Glial Cells	Connexin 43	Rabbit	Cell Signaling Technology	#3512	1:200	Surgically extracted from organ donors within 4 hours of cross-clamp and frozen in dry ice, stored in -80°C.	12µm cuts. Rehydrated in PBST after thawing and fixed on slide with 10% formaldehyde RT for 15min. Blocked in 4%NDS in PBST for 1 hour, primary antibodies incubated overnight at 4°C.	Ahlgreen, O.A.	2025	https://doi.org/10.1002/advs.202511569
Satellite Glial Cells	FABP7	Rabbit	Thermo Fisher Scientific	#PA5-24949		4 donors for IHC studies	40 µm cuts; Blocking 10%; primary antibodies overnight; secondary antibodies 1h	Avraham, O.	2022	https://doi.org/10.1097/j.pain.0000000000002628

Satellite Glial Cells	FABP7	Rabbit	Invitrogen	#PA5-24949	1:100/0.29mg/mL	13 patients with brachial plexus injury 3-8months after injury; 7 controls post-mortem during routine autopsy with potential CNS injury	Transfered to ice-cold 4%PFA/PBS fixed ON 4°C, washed 30min PBSand ON 30%Sucrose 4°C. Longitudinally cut in 2, OCT embedded & stored at -80°C. 20 µm cuts. Slides incubated in quenching solution 15 min	Schulte, A.	2023	https://doi.org/10.1101/2023.02.06.526934
Satellite Glial Cells	FABP7	Goat	R&D Systems	AF3166	1:30	Surgically extracted from organ donors within 4 hours of cross-clamp and frozen in dry ice, stored in -80°C.	12µm cuts. Rehydrated in PBST after thawing and fixed on slide with 10% formaldehyde RT for 15min. Blocked in 4%NDS in PBST for 1 hour, primary antibodies incubated overnight at 4°C.	Ahlgreen, O.A.	2025	https://doi.org/10.1002/advs.202511569
Satellite Glial Cells	FABP7	Rabbit	Thermo	PA5-24949	1:100	Healthy and diabetic donors. Fresh human DRG L2-L5	Fixed upon delivery with 4%PFA and immersed in 30% sucrose for at least 3 night at 4°C. Blocking with 5%BSA for 1h. Primary incubated overnight at 4°C	Xu, J.	2026	https://doi.org/10.1038/s41586-025-09896-x
Satellite Glial Cells	FASN	Rabbit	Abcam	#ab128870		4 donors for IHC studies	40 µm cuts; blocking 10%, primary antibodies overnight; secondary antibodies	Avraham, O.	2022	https://doi.org/10.1097/j.pain.0000000000002628
Satellite Glial Cells	FASN	Rabbit	Abcam	Ab128870		6 donors	25-40 µm cuts; primary antibodies overnight 4°C, secondary antibodies 2h rt	Lund, H.	2023	https://doi.org/10.1084/jem.20230675
Satellite Glial Cells	GLAST1 / EAAT1	Goat	Santa Cruz	sc-77557	0.5 µg/mL	15 patients with Friedreich ataxia and 12 "normal" controls obtain during autopsy	6 µm cuts in paraffin, blocking 10% horse/donkey; overnight 4ºC, horse-radish peroxidase-labeled for secondaries or AF-488 or Cy3	Koeppen, A.H.	2016	https://doi.org/10.1186/s40478-016-0288-5
Satellite Glial Cells	GS	mouse	Santa Cruz	sc-74430	1 µg/mL	15 patients with Friedreich ataxia and 12 "normal" controls obtain during autopsy	6 µm cuts in paraffin, blocking 10% horse/donkey; overnight 4ºC, horse-radish peroxidase-labeled for secondaries or AF-488 or Cy3	Koeppen, A.H.	2016	https://doi.org/10.1186/s40478-016-0288-5
Satellite Glial Cells	GS		-	-	-	4 donors for IHC studies	40 µm cuts; blocking 10%, primary antibodies overnight; secondary antibodies	Avraham, O.	2022	https://doi.org/10.1097/j.pain.0000000000002628
Satellite Glial Cells	GS	Mouse	BD Transduction	610517	1:200/0.25mg/mL	13 patients with brachial plexus injury 3-8months after injury; 7 controls post-mortem during routine autopsy with potential CNS injury	Transfered to ice-cold 4%PFA/PBS fixed ON 4°C, washed 30min PBSand ON 30%Sucrose 4°C. Longitudinally cut in 2, OCT embedded & stored at -80°C. 20 µm cuts. Slides incubated in quenching solution 15 min	Schulte, A.	2023	https://doi.org/10.1101/2023.02.06.526934
Satellite Glial Cells	GS	Mouse	Genetex	GTX630654	1:500	Surgically extracted from organ donors within 4 hours of cross-clamp and frozen in dry ice, stored in -80°C.	12µm cuts. Rehydrated in PBST after thawing and fixed on slide with 10% formaldehyde RT for 15min. Blocked in 4%NDS in PBST for 1 hour, primary antibodies incubated overnight at 4°C.	Ahlgreen, O.A.	2025	https://doi.org/10.1002/advs.202511569
Satellite Glial Cells	GS	Rabbit	Thermo	11037-2-AP	1:200	Surgically extracted from organ donors within 4 hours of cross-clamp and frozen in dry ice, stored in -80°C.	12µm cuts. Rehydrated in PBST after thawing and fixed on slide with 10% formaldehyde RT for 15min. Blocked in 4%NDS in PBST for 1 hour, primary antibodies incubated overnight at 4°C.	Ahlgreen, O.A.	2025	https://doi.org/10.1002/advs.202511569
Satellite Glial Cells	GS	Rabbit	Abcam	ab73593		Adult human tissues from organ transplant donors. Thoracic DRG washed with cold PBS and immediately fixed with 4% PFA.	Paraffin-embedded cut at 4 µm, followed TSA Kit protocol with horse radish peroxidase secondary antibodies, after counterstaining repairing with antigen repair solution at 100°C for 10 min.	Wu, Z.	2025	https://doi.org/10.1016/j.cell.2025.02.007
Satellite Glial Cells	Kir 3.1					4 donors for IHC studies	40 µm cuts; blocking 10%, primary antibodies overnight; secondary antibodies	Avraham, O.	2022	https://doi.org/10.1097/j.pain.0000000000002628
Satellite Glial Cells	Kir 4.1	Rabbit	Alomone	APC-035	4 µg/mL	15 patients with Friedreich ataxia and 12 "normal" controls obtain during autopsy	6 µm cuts in paraffin, blocking 10% horse/donkey; overnight 4ºC, horse-radish peroxidase-labeled for secondaries or AF-488 or Cy3	Koeppen, A.H.	2016	https://doi.org/10.1186/s40478-016-0288-5
Satellite Glial Cells	Kir 4.1	Rabbit	Alomone	APC-035	1:500	Surgically extracted from organ donors within 4 hours of cross-clamp and frozen in dry ice, stored in -80°C.	12µm cuts. Rehydrated in PBST after thawing and fixed on slide with 10% formaldehyde RT for 15min. Blocked in 4%NDS in PBST for 1 hour, primary antibodies incubated overnight at 4°C.	Ahlgreen, O.A.	2025	https://doi.org/10.1002/advs.202511569
Satellite Glial Cells	mGluR2/3 (Metabotropic glutamate receptor 2/3)	Rabbit	Novus	NBPI-00924	1 µg/mL	15 patients with Friedreich ataxia and 12 "normal" controls obtain during autopsy	6 µm cuts in paraffin, blocking 10% horse/donkey; overnight 4ºC, horse-radish peroxidase-labeled for secondaries or AF-488 or Cy3	Koeppen, A.H.	2016	https://doi.org/10.1186/s40478-016-0288-5
Satellite Glial Cells	OR6B2 (Olfatory Receptor 6B2)	Rabbit	Novus Biologicals	NBP1-71360	1:30	Commercially available human DRG	Paraffin tissue sections with a thickness of 5 µm (Zyagen, San Diego, CA, USA) were deparaffinized . Primaries overnight 4ºC, Secondaries 45 min	Flegel, C.	2015	https://doi.org/10.1371/journal.pone.0128951
Satellite Glial Cells	S100α	Rabbit	Santa Cruz	SC-7489-R	0.4 µg/mL	15 patients with Friedreich ataxia and 12 "normal" controls obtain during autopsy	6 µm cuts in paraffin, blocking 10% horse/donkey; overnight 4ºC, horse-radish peroxidase-labeled for secondaries or AF-488 or Cy3	Koeppen, A.H.	2016	https://doi.org/10.1186/s40478-016-0288-5
Satellite Glial Cells	Tissue Inhibitor of Metalloprotease 3 (TIMP3)	Mouse	R&D Systems	MAB973	1:500	Deidentified biospecimens	Fixed with 4% PFA 2h, cryoprotected 30% Sucrose. 12 µm thick cuts, primaries incubated Overnight 4C, 2aries 1h RT	Tonello, R.	2023	https://doi.org/10.1016/j.bbi.2023.08.005
Satellite Glial Cells - Subset	GFAP	Mouse	Cell Signaling Technology		1:1000	6 DRGs from 3 patients; each went through surgery where the spinal nerve root was to be sacrificed	Immediately stored 4ºC and then processed. 8 µm longitudinal cuts, overnight 4ºC both 1 & 2 Ab	Li, Y.	2018	https://doi.org/10.1523/JNEUROSCI.0899-17.2017
Satellite Glial Cells - Subset	GFAP	Mouse	Millipore	Mab360	1:500	1 hDRG from a 53 year-old female without chronic pain	Frozen at the time of collection and stored at -80°C . 14 µm thick cuts; fixed 30 min in PFA 4%; blocked with 3%Goat serum, hIgG overnight, other primaries for 2 h	Goebel, A.	2021	https://doi.org/10.1172/jci144201
Satellite Glial Cells - Subset	GFAP					4 donors for IHC studies	40 µm cuts; blocking 10%, primary antibodies overnight; secondary antibodies	Avraham, O.	2022	https://doi.org/10.1097/j.pain.0000000000002628
Satellite Glial Cells - Subset	GFAP		Addgene	1934450		Obtained from organ donors	Embedded, cut at 7µm, and fixed on slide with 4%PFA for 30min at 4°C. Blocked with 3%BSA for 45 min. Primary antibodies overnight at room temperature.	Boyer, K.	2026	https://doi.org/10.1101/2025.09.21.677655
Satellite Glial Cells - Subset	GFAP	Rabbit	Origene	DP-014	1:100	13 patients with brachial plexus injury 3-8months after injury; 7 controls post-mortem during routine autopsy with potential CNS injury	Transfered to ice-cold 4%PFA/PBS fixed ON 4°C, washed 30min PBSand ON 30%Sucrose 4°C. Longitudinally cut in 2, OCT embedded & stored at -80°C. 20 µm cuts. Slides incubated in quenching solution 15 min	Schulte, A.	2023	https://doi.org/10.1101/2023.02.06.526934
Satellite Glial Cells - Subset	GFAP	Mouse	NeuroMab	N206A/8	2µg/mL	Broad donor screening (90 donors)- Four groups of donors based on diabetes and pain conditions.	Frozen in dry ice, kept at -80°C. Gradually embedded in OCT. 20 cuts and fixed on slide with 10% formalin. Dehydrated. Blocked with 10%NDS with Triton-X 100, and incubated with primary antibodies overnight at 4°C	Shiers, S.I.	2025	https://doi.org/10.1038/s41467-025-59538-z
Satellite Glial Cells - Subset	SCN7A/NaV2.1	Rabbit	Novus Biologicals	NB100-81029	1:200	Surgically extracted from organ donors within 4 hours of cross-clamp and frozen in dry ice, stored in -80°C.	12µm cuts. Rehydrated in PBST after thawing and fixed on slide with 10% formaldehyde RT for 15min. Blocked in 4%NDS in PBST for 1 hour, primary antibodies incubated overnight at 4°C.	Ahlgreen, O.A.	2025	https://doi.org/10.1002/advs.202511569
Satellite Glial Cells - Subset	SCN7A/NaV2.1	Rabbit	BioTechne	NBP1-87075		Obtained from organ donors	Embedded, cut at 7µm, and fixed on slide with 4%PFA for 30min at 4°C. Blocked with 3%BSA for 45 min. Primary antibodies overnight at room temperature.	Boyer, K.	2026	https://doi.org/10.1101/2025.09.21.677655
Schwann Cells - Myelinating	MBP		Millipore Sigma	AB9348		Obtained from organ donors	Embedded, cut at 7µm, and fixed on slide with 4%PFA for 30min at 4°C. Blocked with 3%BSA for 45 min. Primary antibodies overnight at room temperature.	Boyer, K.	2026	https://doi.org/10.1101/2025.09.21.677655
Macrophages	CD68	Mouse	Santa Cruz	sc-20060	4 µg/mL	15 patients with Friedreich ataxia and 12 "normal" controls obtain during autopsy	6 µm cuts in paraffin, blocking 10% horse/donkey; overnight 4ºC, horse-radish peroxidase-labeled for secondaries or AF-488 or Cy3	Koeppen, A.H.	2016	https://doi.org/10.1186/s40478-016-0288-5
Macrophages	CD68	Mouse	Abcam	AB783	1:500	L4 DRGs from 5 control and 5 DPN donors	DRGs held at -20C for cutting, sliced in half, and placed in 10% bufered formalin. 6um cuts; r citrate-based (CD20), or tris/EDTA-based (CD3 and CD68) antigen retrieval; immunodetection with a polymer-based reagent	Hall, B.E.	2022	https://doi.org/10.1038/s41598-022-08100-8
Macrophages	FcγRI (Fc-gamma receptor 1) / CD64	Mouse	Serotec	MCA756g	1:100	n=4 ;Brain dead subjects after asystole	14 µm cuts; postfixed with acetone; primary antibodies overnight rt;	Bersellini Farinotti, A.	2019	http://doi.org/10.1084/jem.20181657
Macrophages	IBA1	Rabbit	Sigma	HPA049234	1 µg/mL	15 patients with Friedreich ataxia and 12 "normal" controls obtain during autopsy	6 µm cuts in paraffin, blocking 10% horse/donkey; overnight 4ºC, horse-radish peroxidase-labeled for secondaries or AF-488 or Cy3	Koeppen, A.H.	2016	https://doi.org/10.1186/s40478-016-0288-5
Macrophages	IBA1	Chicken	Synaptic Systems	234 006	1:50	6 donors	25-40 µm cuts; primary antibodies overnight 4ºC, secondary antibodies 2h rt	Lund, H.	2023	https://doi.org/10.1084/jem.20230675
Macrophages	IBA1	Rabbit	FujiFilm Wako	019-19741	1:100/0.5mg/mL	13 patients with brachial plexus injury 3-8months after injury; 7 controls post-mortem during routine autopsy with potential CNS injury	Transfered to ice-cold 4%PFA/PBS fixed ON 4°C, washed 30min PBSand ON 30%Sucrose 4°C. Longitudinally cut in 2, OCT embedded & stored at -80°C. 20 µm cuts. Slides incubated in quenching solution 15 min	Schulte, A.	2023	https://doi.org/10.1101/2023.02.06.526934
Macrophages	IBA1	Rabbit	Novus Biologicals	NBP2-19019		Adult human tissues from organ transplant donors. Thoracic DRG washed with cold PBS and immediately fixed with 4% PFA.	Paraffin-embedded cut at 4 µm, followed TSA Kit protocol with horse radish peroxidase secondary antibodies, after counterstaining repairing with antigen repair solution at 100°C for 10 min.	Wu, Z.	2025	https://doi.org/10.1016/j.cell.2025.02.007
Macrophage subset	CD163	Mouse	Novus Biologicals	NB110-40686	1:500	6 donors	25-40 µm cuts; primary antibodies overnight 4ºC, secondary antibodies 2h rt	Lund, H.	2023	https://doi.org/10.1084/jem.20230675
Macrophage subset	MRC1	Mouse	Thermo	MA5-44147	1:50	6 donors	25-40 µm cuts; primary antibodies overnight 4ºC, secondary antibodies 2h rt	Lund, H.	2023	https://doi.org/10.1084/jem.20230675
Macrophage subset	MRC1	Rabbit	Cell Signaling Technology	# 24595		Adult human tissues from organ transplant donors. Thoracic DRG washed with cold PBS and immediately fixed with 4% PFA.	Paraffin-embedded cut at 4 µm, followed TSA Kit protocol with horse radish peroxidase secondary antibodies, after counterstaining repairing with antigen repair solution at 100°C for 10 min.	Wu, Z.	2025	https://doi.org/10.1016/j.cell.2025.02.007
Macrophage subset	CX3CR1	Rat	BioSite	D070-3	1:50	6 donors	25-40 µm cuts; primary antibodies overnight 4ºC, secondary antibodies 2h rt	Lund, H.	2023	https://doi.org/10.1084/jem.20230675
Macrophage subset	P2RY12	Rabbit	Abcam	ab300140		Adult human tissues from organ transplant donors. Thoracic DRG washed with cold PBS and immediately fixed with 4% PFA.	Two protocols: Paraffin-embedded cut at 4 µm, followed TSA Kit protocol with horse radish peroxidase secondary antibodies, after counterstaining repairing with antigen repair solution at 100°C for 10 min ;Cryoprotected in 30% sucrose for 24 hours, OCT embedded and cut at 50µm. Free floating sections blocked with 1%BSA, primary antibodies incubated overnight at 4°C.	Wu, Z.	2025	https://doi.org/10.1016/j.cell.2025.02.007
B-Cells	CD20	Mouse	Abcam	AB9475	1:100	L4 DRGs from 5 control and 5 DPN donors	DRGs held at -20C for cutting, sliced in half, and placed in 10% bufered formalin. 6um cuts; r citrate-based (CD20), or tris/EDTA-based (CD3 and CD68) antigen retrieval; immunodetection with a polymer-based reagent	Hall, B.E.	2022	https://doi.org/10.1038/s41598-022-08100-8
T-Cells	CD3	Mouse	Abcam	AB17143	1:100	L4 DRGs from 5 control and 5 DPN donors	DRGs held at -20C for cutting, sliced in half, and placed in 10% bufered formalin. 6um cuts; r citrate-based (CD20), or tris/EDTA-based (CD3 and CD68) antigen retrieval; immunodetection with a polymer-based reagent	Hall, B.E.	2022	https://doi.org/10.1038/s41598-022-08100-8

Mithocondrial	Frataxin	Mouse	Abcam	ab110328	10 µg/mL	15 patients with Friedreich ataxia and 12 "normal" controls obtain during autopsy	6 µm cuts in paraffin, blocking 10% horse/donkey; overnight 4ºC, horse-radish peroxidase-labeled for secondaries or AF-488 or Cy3	Koeppen, A.H.	2016	https://doi.org/10.1186/s40478-016-0288-5
Initiation of translation	phospho-eIF4E	Rabbit	Abcam	ab76256	2µg/mL	Broad donor screening (90 donors)- Four groups of donors based on diabetes and pain conditions.	Frozen in dry ice, kept at -80°C. Gradually embedded in OCT. 20 cuts and fixed on slide with 10% formalin. Dehydrated. Blocked with 10%NDS with Triton-X 100, and incubated with primary antibodies overnight at 4°C	Shiers, S.I.	2025	https://doi.org/10.1038/s41467-025-59538-z

Cell population targeted	Marker	Comments	Host	Vendor	Catalog	Dilution	Verified methods
Neuronal markers							
Pan-neuronal	Beta tubulin 3		Mouse	Promega	G7121(A)	1:100 ; 1:500	iFix & iFr-F
Pan-neuronal	NF200 /NFH		Chicken	Neuromics	CH22104	1:500, 1:1000	iFix & iFr-F
Pan-neuronal	Peripherin	Brighter in small neurons	Chicken	Neuromics	CH22111	1:100, 1:500	iFix & iFr-F
Pan-neuronal	PGP 9.5	**Fixation variability:** Weak staining in iFr-F samples	Chicken	Novus Biological	NB110-58872S	1:200	iFix
Pan-neuronal	PGP 9.5	**Fixation variability:** Weak staining in iFr-F samples	Mouse	Biorad	7863-2004	1:200	iFix
Pan-neuronal	PGP 9.5	**Fixation variability:** Weak staining in iFr-F samples	Rabbit	Nordic Biosite (Zytomed)	RBK064-05	1:200,1:2000 (TSA)	iFix
Pan-neuronal	NeuN	High percentage of neurons with dim or absent staining. Appears to also mark lipofuscin	Mouse	Merck/ Millipore	MAB377	1:100	iFix & iFr-F
Pan-neuronal	NeuN	High percentage of neurons with dim or absent staining. Appears to also mark lipofuscin	Mouse	Merck/ Millipore	MAB377 X	1:100	iFix & iFr-F
Pan-neuronal - Membrane	PIRT	**Fixation variability:** Weaker staining in iFix samples	Rabbit	Proteintech	20990-1-AP	1:100	iFix & iFr-F
Pan-neuronal - Membrane	KCNA2B	**Fixation variability:** Weaker staining in iFix samples	Rabbit	Invitrogen	PA5-115447	1:100	iFr-F
Neuron subpopulation - Peptidergic neurons	CGRP		Rabbit	Sigma-Aldrich	C8198	1:500	iFix & iFr-F
Neuron subpopulation - Peptidergic neurons	CGRPalpha	**Batch variability:** May mark neurons dimmly, with high immune cells signal in iFix samples	Guinea Pig	Peninsula Laboratories	T-5027	1:500	iFr-F

Neuron subpopulation - classical non peptidergic	P2X3	Dim staining	Guinea Pig	Neuromics	GP10108	1:500	iFix & iFr-F
Neuron subpopulation - Nociceptors	SCN10A / NaV 1.8		Rabbit	Alomone	ASC016	1:500	iFix & iFr-F
Neuron subpopulation - Nociceptors	SCN10A / NaV 1.8	Dim staining	Rabbit	Abcam	ab66743	1:200	iFix & iFr-F
Neuron subpopulation - Putative small peptidergic nociceptors	TRKA / NTRK1		Goat	R&D Systems	AF175	1:50	iFix & iFr-F
Neurons and fibroblasts	P75NTR /NGFR	Not tested in iFr-F; also stains fibroblasts	Rabbit	Abcam	ab52987	1:200	iFix
Neuron subpopulation - Putative nociceptor population	Substance P / TAC1		Rabbit	Immunostar	20064	1:500	iFix & iFr-F
Neuron subpopulation - Themal sensing	TRPV1	Batch & sample variability: Staining might present high background and dim signal	Guinea Pig	Neuromics	GP14100	1:500, 1:100	iFix & iFr-F
Neuron subpopulation - Themal sensing	TRPA1		rabbit	Abnova	PAB11992	1:100	iFix & iFr-F
Neuron subpopulation - Themal sensing	TRPA1	Not tested in iFr-F	Rabbit	Novus Biological	NB110-40763SS	1:200	iFix
Neuron subpopulation - Silent nociceptor	CHRNA3		Rabbit	Alomone	ANC-003	1:50	iFix & iFr-F
Neuron subpopulation - Propioceptors	Parvalbumin	**Fixation variability:** Weak staining in iFr-F samples	Sheep	R&D Systems	AF5058	1:50	iFix
Neuron subpopulation - A fiber subpopulation	TrkC/ NTRK3	**Sample variability:** May present high signal from surrounding cells	Sheep	Osenses	OST00119W	1:200, 1:500	iFix & iFr-F

Neuron subpopulation - Cold sensing	TRPM8	**Sample variability**: May stain different ammount of neurons and nuclear staining in some samples	Rabbit	Origene	TA336867	1:200	iFix & iFr-F
Neuron subpopulation - Itch sensation sensory neurons	OSMR		Rabbit	Abcam	ab232684	1:50	iFix & iFr-F
Neurodegeneration	ATF3	**Fixation variability:** Additionally to neuronal signal, may present a dim staining of non-neuronal nuclei in iFr-F tissue	Rabbit	Santa Cruz	sc-188	1:200	iFix & iFr-F
Synaptic vesicles	Synapsin 1/2		Chicken	Synaptic Systems	1006006	1:200	iFix & iFr-F
Neuronal membrane	Neurexin-2	Dim signal	Rabbit	ThermoFisher	BS-11104R	1:50	iFix & iFr-F
Non-neuronal markers							
Blood Vessels - Pan-endothelial	CD31	Clean blood vessel signal.	Rabbit	Abcam	Ab28364	1:50	iFix & iFr-F
Blood Vessels - Pan-endothelial	CD31	**Fixation variability:** Weak staining in iFix samples. **Sample variability**: May stain macrophages.	Sheep	R&D Systems	AF806	1:50, 1:500, 1: 1000	iFix & iFr-F
Blood Vessels - Pan-endothelial	CD31	Some non-specific staining appearing in neurons .	Goat	R&D Systems	AF3628	1:100, 1:200	iFix & iFr-F
Blood Vessels - Veins & capillaries	Aquaporin 1	Not tested in iFix samples.	Mouse	Santa Cruz	sc-25287	1:50	iFr-F
Blood Vessels - Veins & capillaries	Caveolin 1 (D46G3)	Not tested in iFix samples.	Rabbit	Cell Signaling	3267	1:500, 1:800	iFr-F
Blood Vessels - Veins & capillaries	CD34	Predominant Blood vessel staining, dim fibroblast signal.	Mouse	DAKO	M7165	1:50	iFr-F
Blood Vessels - Veins & capillaries	PLVAP	**Fixation variability:** Weak staining in iFix samples.	Mouse	Abcam	ab81719	1:200	iFr-F
Blood Vessels - Arteries & capillaries	CLDN5	High non-specific staining in neurons. **Fixation variability:** Weak staining in iFix samples.	Rabbit	Invitrogen	34-1600	1:50	iFix & iFr-F
Smooth Muscle Cells	ACTA2 (alpha SMA)		Mouse	Santa Cruz	c-32251 AF64	1:500	iFix & iFr-F
Pericytes	NG2	Also highly present in SGCs and other cells	Rabbit-Biotin Conjugated	Abcam	AB5320B	1:100	iFix & iFr-F

Fibroblasts	EGFR	Some neuronal staining, specially high in neuronal nuclei.	Rabbit	Invitrogen	PA1-1100	1:100	iFix & iFr-F
Fibroblasts	Glut-1 (SLC2A1)		Rabbit	EMD Milipore	07-1401	1:500	iFix & iFr-F
Fibroblasts, neurons	P75NTR / NGFR	Not tested in iFr-F samples; it is also a neuronal marker.	Rabbit	Abcam	ab52987	1:200	iFix
Fibroblasts & glial cells	Vimentin	Express at variable degree in most non-neuronal cells.	Goat	R&D Systems	AF2105	1:100	iFix & iFr-F
Neural crest-Schwann cells & Satellite Glial Cells	S100beta	Also present in some neurons.	Rabbit	Abcam	ab52642	1:500	iFix
Neural crest-Schwann cells & Satellite Glial Cells	SOX10		Goat	R&D Systems	AF2864-SP	1:200	iFix & iFr-F
Neural crest-Schwann cells & Satellite Glial Cells	SOX10		Mouse	Santa Cruz	Sc-365692	1:200	iFix & iFr-F
Myelinating Schwann cells	MBP		Rat	Abcam	AB7349	1:200	iFix & iFr-F
Satellite Glial Cells	Connexin 43	Not tested in iFix samples.	Rabbit	Sigma	C6219-25UL	1:200	iFr-F
Satellite Glial Cells	FABP7	**Fixation variability:** Loss of specific SGC signal and high neuronal background in iFr-F samples.	Rabbit	Invitrogen	PA5-24949	1:100	iFix
Satellite Glial Cells	FABP7	Unspecific fiber and small neuron labeling. **Fixation variability:** Loss of specific SGC signal in iFr-F samples.	Goat	R&D Systems	AF3166	1:200	iFix
Satellite Glial Cells	FASN	**Sample variability:**May present high signal/noise ratio (solvable with TSA).	Rabbit	Abcam	ab128870	1:100, 1:500, 1:5000(TSA)	iFix & iFr-F
Satellite Glial Cells	Kir 4.1	Not tested in iFix samples.	Rabbit	Milipore	AB5818	1:500, 1:1000	iFr-F
Satellite Glial Cells	Kir 4.1	Not tested in iFix samples.	Rabbit	Alomone	APC-035	1:200	iFr-F
Satellite Glial Cells - Subset	GFAP	Present in a subset of glia cells and other non-neuronal cells.	Rabbit	DAKO	Z0334	1:1000	iFix & iFr-F
Macrophages - pan-marker	IBA1	**Fixation variability:** May not stain nuclear region in iFr-F samples.	Chicken	Synaptic Systems	234009	1:500	iFix & iFr-F
Macrophages - pan-marker	IBA1	**Fixation variability:** May not stain nuclear region in iFr-F samples.	Rabbit	Wako	019-19741	1:200	iFix & iFr-F
Macrophages	CD32		Goat	R&D Systems	AF1330	1:50	iFix & iFr-F

Macrophages and antigen presenting cells	HLA-Dr		Rabbit	Abcam	ab103998	1:50	iFix & iFr-F
Macrophage - Perivascular macrophages	CD163		Mouse	Novus Biologicals	NB110-40686	1:500	iFix & iFr-F
Macrophage subset	FOLR2	**Fixation variability**: May stain dim in iFix samples	Mouse	Abcam	327002	1:500	iFix & iFr-F
Macrophage subset	MRC1	Not tested in iFix samples.	Mouse	Thermo	MA5-44147	1:50	iFr-F
Macrophage subset	VSIG4	Appears to stain all macrophages.	Mouse	BioTechne	MAB46463-SP	1:50	iFix & iFr-F
Macrophages - Perineuronal macrophages	CX3CR1	**Fixation variability**: Weaker in iFix samples.	Rat	Nordic Biosite	341602	1:50	iFix & iFr-F
B-Cells	CD19	Not tested in iFr-F samples.	Rabbit	Abcam	ab134114	1:50, 1:500	iFix
T-Cells	CD3		Rabbit	DAKO	A0452	1:200	iFix & iFr-F
Monocytes & other immune cells	S100A4	Bright staining of monocytes and dimmer staining in some T-cells.	Mouse	Atlas Antibodies	AMAb90599	1:3000	iFix & iFr-F
Mast Cells	FCeR1alpha	Dim staining, difficult to distinguish from background.	mouse	Invitrogen	12-5899-42	1:50	iFix & iFr-F
Mast Cells	KIT / C-KIT / CD177	Also in FCER1A- cells.	Mouse	BD	333233	1:100	iFix & iFr-F
Neutrophils	CD15	**Sample variability**: May present different cell numbers.	Mouse	DAKO	GA062	1:1 (Sold as solution ready to stain)	iFix & iFr-F
Neutrophils	Neutrophil Elastase	Also present in cells with no trilobular nuclei. Sample variability: May present different cell numbers.	Rabbit	Abcam	B131260-100	1:50	iFix & iFr-F
Melanocytes	MelanA		Sheep	R&D Systems	AF8008	1:200	iFix & iFr-F
Cell structure - F-Actin	Phalloidin		Amanita phalloides	Abcam	AB176753	1:2000	iFix & iFr-F
Mitochondrial activity	TSPO		Rabbit	Abcam	ab109497	1:500	iFix & iFr-F
Cell Proliferation	KI67	**Sample variability:** May present different staining levels.	Rat	Invitrogen	14-5698-82	1:100	iFix & iFr-F
Cell senescence	P16	**Sample variability:** May present different staining levels, mostly glial cells.	Mouse	Invitrogen	MA5-17054	1:500	iFix & iFr-F
Not Working							
Neuronal markers							

Neuron subpopulation - Silent nociceptor	CHRNA3	Suboptimal staining: High signal from surrounding cells	Rabbit	BiCell Scientific	15183	1:100, 1:1000 (TSA)	iFix & iFr-F
Neuron subpopulation - Cold sensing	TRPM8	Only neuronal nuclei and scarce fibers might be stained. High unspecific backround from surrounding cells	Rabbit	Novus Biological	NBP1-97311S	1:100, 1:1000 (TSA)	iFix & iFr-F
Pan-neuronal - membrane	GNAL	Nuclear staining, present in most cells but stronger in neurons.	Rabbit	Invitrogen	PA5-27964	1:500	iFix & iFr-F
Neuron subpopulation - Themal sensing	TRPV1	Despite neuronal signal, human cross-reactivity was not expected and staining pattern doesn't match completely to the human specific TRPV1 (Guinea Pig).	Goat	Neuromics	GT15129	1:200	iFix & iFr-F
Neuron subpopulation - Themal sensing	TRPV1	Neuronal signal, but the antibody was not checked for cross-reactivity in human.	Rabbit	Santa Cruz	SC-28759	1:500	iFix & iFr-F
Neuron subpopulation - Putative nociceptors	SCN10A / NaV 1.8	No signal.	Mouse	LifeSpan	LS-C109037	1:100	iFix & iFr-F
Putative A-fiber nociceptor	CHRNA7	Signal mostly in glia (SGC and Schwann Cells)	Rabbit	Invitrogen	PA5-115651	1:200	iFix & iFr-F
Neuron subpopulation - Putative non peptidergic	IB4	No neuronal signal.	*Griffonia simplicifolia*	121411	Thermo Fisher Scientific	1:200	iFix & iFr-F
Neuron subpopulation - Putative cold sensing population	STUM	Scarce signal from small cells, not present in neurons.	Rabbit	Atlas Antibodies	HPA074381	1:50; 1:500 (TSA)	iFix & iFr-F
Neuron subpopulation - Themal sensing	TRPV1	No signal.	Guinea Pig	Novus Biologicals	NB300-122	1:500, 1:200	iFr-F
Peptidergic neurons	CGRP	Very low signal/noise ratio, high nuclear signal in neurons.	Goat	Abcam	ab36001	1:500	iFix & iFr-F
Neuron subpopulation - A fiber subpopulation	TRKB / NTRK2	No signal.	Rabbit	Cell Signaling	4603; lot 3	1:100	iFix & iFr-F
Neuron subpopulation - Inflammation and itch	SST	No signal.	Rat	Millipore	MAB354	1:50	iFix & iFr-F
Neurons	GABBR2	Unexpected nuclear signal.	Rabbit			1:250	

Neuron subpopulation - Degenaration	ATF3	No signal.	Mouse	Santa Cruz	sc-81189	1:1000	iFix & iFr-F
Synaptic vesicles	Synaptophysin	No specific signal.	Mouse	Millipore	S5768	1:500	iFix & iFr-F
Neuron subpopulation - Putative nociceptor modulation	NMDA / GRIN1	Dim signal, difficult to distinguish from background.	Goat	Santa Cruz	sc-1467	1:50	iFix & iFr-F
Neuron subpopulation - peptidergic	TRKA	Unspecific SGC binding.	Mouse	R&D Systems	MAB175	1:200	iFix & iFr-F
Non neuronal markers							
Fibroblasts	DCN	No signal.	Goat	R&D Systems	AF1060	1:200	iFix & iFr-F
Pericytes/Fibroblasts	PDGFRb	No signal.	Rabbit	Invitrogen	14-1402-81	1:50	iFr-F
Satellite Glial Cells	Aquaporin 4	Dim staining, unexpected Macrophages signal instead of SGCs.	Mouse	Novus Biologicals	NB600-716	1:50	iFix & iFr-F
Schwann cells / Glial Cells	S100	No signal.	Mouse	Abcam	ab4066	1:200	iFr-F
Schwann cells / Glial Cells	S100beta	Dim signal, difficult to distinguish from background.	Goat	R&D Systems	AF1820	1:50	iFr-F
Schwann cells	Myelin PLP	No signal.	Mouse	Abcam	AB9311	1:500	iFix & iFr-F
Satellite Glial Cells	GLAST	Low signal.	Mouse	Militenyi Biotec	130-118-483 ;clone ACSA-1	1:50	iFix & iFr-F
Satellite Glial Cells	GLAST	Not specific to SGCs, high neuronal signal.	Rabbit	Novus Biologicals	NB100-1869	1:250	iFix
Satellite Glial Cells	GFAP	Dim staining with high background.	mouse	Milipore	MAB360	1:100	iFix & iFr-F
Glial progenitor	Sox 2	No signal.	mouse	R&D Systems	MAB2018	1:200	iFix & iFr-F
Macrophages	CSF1R	No signal.	mouse	Thermo / Invitrogen	MA5-38504	1:500	iFix & iFr-F
Macrophages / Lymphatic vessels	LYVE1	No signal.	Rat	Invitrogen	50-0443-82	1:50	iFr-F
Said to be expressed in neurons in DRG by Yin C. et al., 2024	CXCR2	No signal.	Rabbit	GeneTex	GTX14935	1:50	iFr-F
Macrophages and T-Cells	CCR2	No immune signal. Unexpected neuronal signal.	Rabbit	LSBio	LS-A1899/6085	1:100	iFr-F
T-Cells	CD3	No signal.	Rat	BioRad	MCA1477	1:50	iFix
T-Cells	CD3	No signal.	rat	Biolegend	100201	1:50	iFix

T-Cells	CD3	No signal.	mouse	DAKO	M7193	1:250, 1:100. 1:50	iFix
T-Cells (Helper T cell)	CD4	No signal.	Rat	Biolegend	100401	1:50	iFix
T-Cells (Cytotoxic T cell)	CD8a	No signal.	Rat	Biolegend	100701	1:500	iFix & iFr-F
Dendritic Cells	CD1a	No signal.	mouse	BioRad	MCA80	1:500	iFr-F
Melanocytes	MlanA	No signal.	Rabbit	Abcam	ab210546	1:1000	iFix & iFr-F
Cell structure: Beta-actin	Beta-actin	Mostly noise, dispersed and scarce signal.	Mouse	Cell Signaling	3700	1:400	iFix & iFr-F

Secondary antibodies

	Vendor	Host	Anti-	Fluorophore	Catalog	Dilution	
Secondary antibodies	Jackson Immuno Research	Donkey	Rabbit	Cy2	711-225-152	1:200	
		Donkey	Rabbit	Cy3	711-165-152	1:600	
		Donkey	Rabbit	Cy5	711-175-152	1:500	
		Donkey	Mouse	Cy2	715-225-151	1:200	
		Donkey	Mouse	Cy3	715-165-151	1:600	
		Donkey	Mouse	Cy5	715-175-151	1:500	
		Donkey	Rat	Cy2	712-225-150	1:200	
		Donkey	Rat	Cy3	712-165-150	1:600	
		Donkey	Rat	Cy5	712-175-153	1:500	
		Donkey	Chicken	Cy2	703-225-155	1:200	
		Donkey	Chicken	Cy3	703-165-155	1:600	
		Donkey	Chicken	Cy5	703-175-155	1:500	
		Donkey	Goat	Cy2	705-225-147	1:200	
		Donkey	Goat	Cy3	705-165-147	1:600	
		Donkey	Goat	Cy5	705-175-147	1:500	
		Donkey	Guinea Pig	Cy2	706-225-148	1:200	
		Donkey	Guinea Pig	Cy3	706-165-148	1:600	
		Donkey	Guinea Pig	Cy5	706-175-148	1:500	
	Invitrogen	Donkey	Sheep	AF488	A-11015	1:500	
		Donkey	Sheep	AF555	A-21436	1:500	
		Donkey	Mouse	AF488	A11015	1:500	
		Streptavidin antibody	Biotin	AF647	S32357	1:500	Used for NG2

Neuronal markers							
Cell population targeted	**Marker**	**Host**	**Vendor**	**Catalog**	**Dilution**	**Verified methods**	**Comments**
Pan-neuronal	Beta tubulin 3*	Mouse	Promega	G7121(A)	1:100 ; 1:500	iFix & iFr-F	
Pan-neuronal	NF200 /NFH*	Chicken	Neuromics	CH22104	1:500, 1:1000	iFix & iFr-F	
Pan-neuronal	Peripherin*	Chicken	Neuromics	CH22111	1:100, 1:500	iFix & iFr-F	Brighter in small neurons
Pan-neuronal	PGP 9.5*	Chicken	Novus Biological	NB110-58872S	1:200	iFix	**Fixation variability:** Weak staining in iFr-F samples
Pan-neuronal	PGP 9.5	Mouse	Biorad	7863-2004	1:200	iFix	**Fixation variability:** Weak staining in iFr-F samples
Pan-neuronal	PGP 9.5	Rabbit	Nordic Biosite (Zytomed)	RBK064-05	1:200,1:2000 (TSA)	iFix	**Fixation variability:** Weak staining in iFr-F samples
Pan-neuronal	NeuN	Mouse	Merck/ Millipore	MAB377	1:100	iFix & iFr-F	High percentage of neurons with dim or absent staining. Appears to also mark lipofuscin
Pan-neuronal	NeuN*	Mouse	Merck/ Millipore	MAB377 X	1:100	iFix & iFr-F	High percentage of neurons with dim or absent staining. Appears to also mark lipofuscin
Pan-neuronal - Membrane	PIRT*	Rabbit	Proteintech	20990-1-AP	1:100	iFix & iFr-F	**Fixation variability:** Weaker staining in iFix samples
Pan-neuronal - Membrane	KCNA2B*	Rabbit	Invitrogen	PA5-115447	1:100	iFr-F	**Fixation variability:** Weaker staining in iFix samples
Neuron subpopulation - Peptidergic neurons	CGRP*	Rabbit	Sigma-Aldrich	C8198	1:500	iFix & iFr-F	
Neuron subpopulation - Peptidergic neurons	CGRPalpha	Guinea Pig	Peninsula Laboratories	T-5027	1:500	iFr-F	**Batch variability:** May mark neurons dimmly, with high immune cells signal in iFix samples
Neuron subpopulation - classical non peptidergic	P2X3*	Guinea Pig	Neuromics	GP10108	1:500	iFix & iFr-F	Dim staining
Neuron subpopulation - Nociceptors	SCN10A / NaV 1.8*	Rabbit	Alomone	ASC016	1:500	iFix & iFr-F	
Neuron subpopulation - Nociceptors	SCN10A / NaV 1.8	Rabbit	Abcam	ab66743	1:200	iFix & iFr-F	Dim staining
Neuron subpopulation - Putative small peptidergic nociceptors	TRKA / NTRK1*	Goat	R&D Systems	AF175	1:50	iFix & iFr-F	
Neurons and fibroblasts	P75NTR /NGFR	Rabbit	Abcam	ab52987	1:200	iFix	Not tested in iFr-F; also stains fibroblasts
Neuron subpopulation - Putative nociceptor population	Substance P / TAC1*	Rabbit	Immunostar	20064	1:500	iFix & iFr-F	
Neuron subpopulation - Themal sensing	TRPV1*	Guinea Pig	Neuromics	GP14100	1:500, 1:100	iFix & iFr-F	Batch & sample variability: Staining might present high background and dim signal
Neuron subpopulation - Themal sensing	TRPA1*	rabbit	Abnova	PAB11992	1:100	iFix & iFr-F	
Neuron subpopulation - Themal sensing	TRPA1	Rabbit	Novus Biological	NB110-40763SS	1:200	iFix	Not tested in iFr-F
Neuron subpopulation - Silent nociceptor	CHRNA3*	Rabbit	Alomone	ANC-003	1:50	iFix & iFr-F	
Neuron subpopulation - Propioceptors	Parvalbumin*	Sheep	R&D Systems	AF5058	1:50	iFix	**Fixation variability:** Weak staining in iFr-F samples
Neuron subpopulation - A fiber subpopulation	TrkC/ NTRK3*	Sheep	Osenses	OST00119W	1:200, 1:500	iFix & iFr-F	**Sample variability:** May present high signal from surrounding cells
Neuron subpopulation - Cold sensing	TRPM8*	Rabbit	Origene	TA336867	1:200	iFix & iFr-F	**Sample variability**: May stain different ammount of neurons and nuclear staining in some samples
Neuron subpopulation - Itch sensation sensory neurons	OSMR*	Rabbit	Abcam	ab232684	1:50	iFix & iFr-F	
Neurodegeneration	ATF3*	Rabbit	Santa Cruz	sc-188	1:200	iFix & iFr-F	**Fixation variability:** Additionally to neuronal signal, may present a dim staining of non-neuronal nuclei in iFr-F tissue
Synaptic vesicles	Synapsin 1/2	Chicken	Synaptic Systems	1006006	1:200	iFix & iFr-F	
Neuronal membrane	Neurexin-2	Rabbit	ThermoFisher	BS-11104R	1:50	iFix & iFr-F	Dim signal

*: Used in manual quantification

Non-neuronal markers							
Cell population targeted	**Marker**	**Host**	**Vendor**	**Catalog**	**Dilution**	**Verified method**	**Comments**
Blood Vessels - Pan-endothelial	CD31	Rabbit	Abcam	Ab28364	1:50	iFix & iFr-F	Clean blood vessel signal.
Blood Vessels - Pan-endothelial	CD31	Sheep	R&D Systems	AF806	1:50, 1:500, 1: 1000	iFix & iFr-F	**Fixation variability:** Weak staining in iFix samples. **Sample variability**: May stain macrophages.
Blood Vessels - Pan-endothelial	CD31	Goat	R&D Systems	AF3628	1:100, 1:200	iFix & iFr-F	Some non-specific staining appearing in neurons .
Blood Vessels - Veins & capillaries	Aquaporin 1	Mouse	Santa Cruz	sc-25287	1:50	iFr-F	Not tested in iFix samples.
Blood Vessels - Veins & capillaries	Caveolin 1 (D46G3)	Rabbit	Cell Signaling	3267	1:500, 1:800	iFr-F	Not tested in iFix samples.
Blood Vessels - Veins & capillaries	CD34	Mouse	DAKO	M7165	1:50	iFr-F	Predominant Blood vessel staining, dim fibroblast signal.
Blood Vessels - Veins & capillaries	PLVAP	Mouse	Abcam	ab81719	1:200	iFr-F	**Fixation variability:** Weak staining in iFix samples.
Blood Vessels - Arteries & capillaries	CLDN5	Rabbit	Invitrogen	34-1600	1:50	iFix & iFr-F	High non-specific staining in neurons. **Fixation variability:** Weak staining in iFix samples.
Smooth Muscle Cells	ACTA2 (alpha SMA)	Mouse	Santa Cruz	sc-32251 AF647	1:500	iFix & iFr-F	
Pericytes	NG2	Rabbit-Biotin Conjugated	Abcam	AB5320B	1:100	iFix & iFr-F	Also highly present in SGCs and other cells
Fibroblasts	EGFR	Rabbit	Invitrogen	PA1-1100	1:100	iFix & iFr-F	Some neuronal staining, specially high in neuronal nuclei.
Fibroblasts	Glut-1 (SLC2A1)	Rabbit	EMD Milipore	07-1401	1:500	iFix & iFr-F	
Fibroblasts, neurons	P75NTR / NGFR	Rabbit	Abcam	ab52987	1:200	iFix	Not tested in iFr-F samples; it is also a neuronal marker.
Fibroblasts & glial cells	Vimentin	Goat	R&D Systems	AF2105	1:100	iFix & iFr-F	Express at variable degree in most non-neuronal cells.
Neural crest-Schwann cells & Satellite Glial Cells	S100beta	Rabbit	Abcam	ab52642	1:500	iFix	Also present in some neurons.
Neural crest-Schwann cells & Satellite Glial Cells	SOX10	Goat	R&D Systems	AF2864-SP	1:200	iFix & iFr-F	
Neural crest-Schwann cells & Satellite Glial Cells	SOX10	Mouse	Santa Cruz	Sc-365692	1:200	iFix & iFr-F	
Myelinating Schwann cells	MBP	Rat	Abcam	AB7349	1:200	iFix & iFr-F	
Satellite Glial Cells	Connexin 43	Rabbit	Sigma	C6219-25UL	1:200	iFr-F	Not tested in iFix samples.
Satellite Glial Cells	FABP7	Rabbit	Invitrogen	PA5-24949	1:100	iFix	**Fixation variability:** Loss of specific SGC signal and high neuronal background in iFr-F samples.
Satellite Glial Cells	FABP7	Goat	R&D Systems	AF3166	1:200	iFix	Unspecific fiber and small neuron labeling. **Fixation variability:** Loss of specific SGC signal in iFr-F samples.
Satellite Glial Cells	FASN	Rabbit	Abcam	ab128870	1:100, 1:500, 1:5000(TSA)	iFix & iFr-F	**Sample variability:** May present high signal/noise ratio (solvable with TSA).
Satellite Glial Cells	Kir 4.1	Rabbit	Milipore	AB5818	1:500, 1:1000	iFr-F	Not tested in iFix samples.
Satellite Glial Cells	Kir 4.1	Rabbit	Alomone	APC-035	1:200	iFr-F	Not tested in iFix samples.
Satellite Glial Cells - Subset	GFAP	Rabbit	DAKO	Z0334	1:1000	iFix & iFr-F	Present in a subset of glia cells and other non-neuronal cells.
Macrophages - pan-marker	IBA1	Chicken	Synaptic Systems	234009	1:500	iFix & iFr-F	**Fixation variability:** May not stain nuclear region in iFr-F samples.
Macrophages - pan-marker	IBA1	Rabbit	Wako	019-19741	1:200	iFix & iFr-F	**Fixation variability:** May not stain nuclear region in iFr-F samples.
Macrophages	CD32	Goat	R&D Systems	AF1330	1:50	iFix & iFr-F	
Macrophages and antigen presenting cells	HLA-Dr	Rabbit	Abcam	ab103998	1:50	iFix & iFr-F	
Macrophage - Perivascular macrophages	CD163	Mouse	Novus Biologicals	NB110-40686	1:500	iFix & iFr-F	
Macrophage subset	FOLR2	Mouse	Abcam	327002	1:500	iFix & iFr-F	**Fixation variability**: May stain dim in iFix samples
Macrophage subset	MRC1	Mouse	Thermo	MA5-44147	1:50	iFr-F	Not tested in iFix samples.
Macrophage subset	VSIG4	Mouse	BioTechne	MAB46463-SP	1:50	iFix & iFr-F	Appears to stain all macrophages.
Macrophages - Perineuronal macrophages	CX3CR1	Rat	Nordic Biosite	341602	1:50	iFix & iFr-F	**Fixation variability**: Weaker in iFix samples.
B-Cells	CD19	Rabbit	Abcam	ab134114	1:50, 1:500	iFix	Not tested in iFr-F samples.
T-Cells	CD3	Rabbit	DAKO	A0452	1:200	iFix & iFr-F	
Monocytes & other immune cells	S100A4	Mouse	Atlas Antibodies	AMAb90599	1:3000	iFix & iFr-F	Bright staining of monocytes and dimmer staining in some T-cells.
Mast Cells	FCeR1alpha	mouse	Invitrogen	12-5899-42	1:50	iFix & iFr-F	Dim staining, difficult to distinguish from background.
Mast Cells	KIT / C-KIT / CD177	Mouse	BD	333233	1:100	iFix & iFr-F	Also in FCER1A- cells.
Neutrophils	CD15	Mouse	DAKO	GA062	1:1 (Sold as solution ready to stain)	iFix & iFr-F	**Sample variability**: May present different cell numbers.
Neutrophils	Neutrophil Elastase	Rabbit	Abcam	AB131260-1001	1:50	iFix & iFr-F	Also present in cells with no trilobular nuclei. Sample variability: May present different cell numbers.
Melanocytes	MelanA	Sheep	R&D Systems	AF8008	1:200	iFix & iFr-F	
Cell structure - F-Actin	Phalloidin	Amanita phalloides	Abcam	AB176753	1:2000	iFix & iFr-F	
Mitochondrial activity	TSPO	Rabbit	Abcam	ab109497	1:500	iFix & iFr-F	
Cell Proliferation	KI67	Rat	Invitrogen	14-5698-82	1:100	iFix & iFr-F	**Sample variability:** May present different staining levels.
Cell senescence	P16	Mouse	Invitrogen	MA5-17054	1:500	iFix & iFr-F	**Sample variability:** May present different staining levels, mostly glial cells.

Donor	Age	Sex	Fixation time-point	Cause of Death
1	40	M	iFix & iFr-F	Cerebral hemorrhage
2	55	M	iFix & iFr-F	Cranial trauma / Anoxia
3	61	M	iFix & iFr-F	Suicide (CO Anoxia)
4	33	F	iFix & iFr-F	Suicide (Hanging)
5	47	F	iFix & iFr-F	Vein thrombosis at the transverse sinus
6	72	F	iFix & iFr-F	Cerebral hemorrhage (Car accident)
7	35	M	iFix	Suicide (Hanging, anoxia)
8	60	M	iFix	Trauma (Close head injury)
9	45	F	iFix	Brain hemorrhage
10	54	F	iFix	Stroke
11	56	F	iFix	Brain death (Cerebral venous sinus thrombosis)
12	69	M	iFr-F & iFr-FOS	Brain hemorrhage
13	27	F	iFr-F & iFr-FOS	Suicide (Hanging)
14	52	F	iFr-F & iFr-FOS	Brain hemorrhage
15	53	F	iFr-F & iFr-FOS	Cranial trauma
16	38	F	iFr-F & iFr-FOS	Brain hemorrhage
17	47	M	iFr-FOS	Brain hemorrhage

iFix: Immediately fixed at tissue collection; iFr-F: Immediately frozen, fixed before cryosectioning; iFr-FOS: Immediately frozen, fixed on slide